Simultaneous measurement of nucleotide occupancy and mechanical

displacement in myosin-V, a processive molecular motor.

連続運動分子モーター ミオシン 5 の化学サイクルと

力学サイクルの同時計測

Soft Nanomachine group, Laboratories for Nanobiology

Graduate School of Frontier Biosciences

Osaka University

Tomotaka Komori

論 文 内 容 の 要 旨

〔 題 名 〕Simultaneous measurement of nucleotide occupancy and mechanical displacement in myosin-V, a processive molecular motor.
（邦題：連続運動分子モーター　ミオシン 5 の化学サイクルと力学サイクルの同時計測)

学 位 申 請 者　　　E0116831　小森智貴　印

　ミオシンは筋収縮や小胞輸送において中心的な働きを担う ATP 駆動型分子モーターである。本研究では小胞輸送を主に担うミオシン 5 に着目して私は研究を行った。筋収縮を担うミオシン 2 がアクチンフィラメントに沿って連続変位を生み出さないのに対して、ミオシン 5 はアクチンフィラメント上で連続変位を生み出す分子モーターである。生化学、構造解析及び一分子計測が行われ様々な連続運動モデルが提唱されたが、未だにミオシン 5 が連続変位を生み出す機構は完全には解明されていない。これは連続運動ミオシンにおける ATP 加水分解サイクルと変位発生過程の対応関係が未だ解明されていないことに大きく起因する。そこで本研究では、ミオシン 5 による ATP 加水分解サイクルと変位発生過程の対応関係を一分子レベルで直接かつ同時に計測することで明らかにすることを試みた。

　まず私はミオシン 5 の ATP 加水分解サイクルと変位発生過程の同時計測を可能とする計測系構築を行った。ミオシン 5 への ATP 結合及び加水分解産物である ADP 解離は、蛍光性 ATP アナログ(2'-O-Cy3-EDA-ATP)及び全反射型蛍光顕微鏡を用いて可視化することにした。一方で、変位発生はレーザートラップを用いて検出することにした。変位発生過程はレーザートラップにより捕捉されたビーズの位置変化として検出される。そして ATP 加水分解サイクルは、ミオシン存在位置での蛍光強度変化として検出される。これら 2 つの計測系を 1 つの顕微鏡光学系内に組み込むことにより、両者の同時計測を可能とした。さらに新規に構築した計測系を用いて、2 量体形成部位を欠損させた単頭ミオシン 5 の ATP 加水分解サイクルと変位発生過程の同時計測を行った。今回の計測では「ATP 結合とミオシン解離」及び「ADP 解離と変位発生」の 2 つの対応関係に着目して解析した。ATP が結合するとすぐにミオシン 5 はアクチンフィラメントから解離した。続いてミオシン 5 は再びアクチンフィラメントと相互作用して変位発生を行う。ADP は変位発生時には解離せず、平均 69 ミリ秒の時間遅れを持ってミオシン 5 から解離した。これらの結果は、ATP 結合はミオシン 5 内部での瞬時の構造変化を引き起こしてミオシン 5 をアクチンフィラメントから解離させる一方で、ADP 解離過程はミオシン 5 の変位発生には関与せずに、変位発生から時間遅れを伴った遅い過程で ADP が解離することを示唆している。連続運動しないミオシン 2 はこのような長い ADP 状態を持たないことが報告されており、連続運動を示すミオシンにのみに見られる特徴的な過程である。

　生化学計測より、ADP 状態のミオシンはアクチンフィラメントに対して強い結合状態をとることが知られている。その為、今回観察された変位発生後の長い ADP 結合状態を持つことで、ミオシン 5 は安定してアクチンフィラメントに結合でき、結果として連続運動が可能であると予測される。本研究により ADP 解離は、変位発生そのものに直接寄与する過程ではないことが明らかとなった。ADP 解離はミオシンの運動特性を決定する制御因子として働く過程ではないだろうか。また、連続運動を示すミオシンファミリーはほぼ同様の機構で動作すると考えられている為、今回得られた結果は連続運動を示すミオシン広く適用できると期待できる。

Abstract

Myosin-V is an actin-based processive molecular motor driven by the chemical energy derived from ATP hydrolysis. Although the chemo-mechanical coupling in processive movement has been investigated by separate structural, mechanical and biochemical studies, no experiment has been able to directly test the conclusions from these works. Therefore the relationship between ATP-turnover cycle and force generation, and in extention, processive movement remains unclear. Currently, the most direct method to measure chemo-mechanical coupling in processive motors is to simultaneously observe ATP-turnovers and displacement at the single molecule level, which is the method I apply here.

At first, I developed a simultaneous measurement system for the mechanical and chemical activity of myosin-V in order to directly elucidate chemo-mechanical coupling. ATP-turnover cycles were visualized using the fluorescent ATP analog 2'-O-Cy3-EDA-ATP and total internal reflection fluorescence (TIRF) microscopy, while force generation was detected using dual optical traps. In this system, ATP-turnover cycles were detected by observing the fluorescence appearance and disappearance, while force generation was detected by measuring trapped bead displacement. My specific interests in the ATP-turnover cycle were the relationships between ATP-binding and myosin-V detachment and between ADP-release and force-generation. ATP-binding was found to cause immediate myosin-V detachment from the actin filament, while ADP was released 69 ms after force generation and displacement along the actin filament, providing direct evidence for a slow ADP-release. In a previous study, it was reported that ADP-release in nonprocessive myosin-II occurs before or around force generation. My findings show a very different property in processive motor myosin-V.

As proposed by several studies, this slow ADP-release probably ensures processivity by prolonging the strong actomyosin state in the ATP-turnover cycle. Because many other other processive motors are thought to function like myosin-V, these results are likely to have broader implications. In summary, my results suggest that ADP-release does not correlate with force generation. Instead, it is likely to be an important regulator for mechanical properties like processivity.

INDEX

Chapter I

Introduction

1.1. Preface

In a cell, many enzymes utilize the energy released from nucleotide hydrolysis. For example, molecular motors like myosin, kinesin and dynein converts ATP-hydrolysis energy into mechanical displacements along cytoskeletons like actin filaments and microtubules. GTP is another nucleotide involved in several cellular functions. GTPase Dynamin is responsible for endocytosis in the eukaryotic cell and produces an essential mechanical force for vesicle fission. Ras utilizes GTP-hydrolysis to transmit signals from a ligand to initiate a signaling cascade. In general, nucleotides are fundamental energy sources for organisms, with ATP being the prevailingly "energy currency". Despite the knowledge that the hydrolysis of nucleotides leads to mechanical work, there still remains a great deal of uncertainty regarding the relationship between the output work, like mechanical displacement and cell signaling, and nucleotide hydrolysis turnover cycles. Identifying the key steps in hydrolysis that leads to output work tremendous insight on biological energy transduction mechanisms. Studies that investigate such transduction mechanisms usually focus on molecular motors like myosin, kinesin or F_1F_o-ATPase since the mechanical displacement or rotation (the output by molecular motors) can be determined with high accuracy and high time resolution.

1.2. General introduction about myosin family

Myosin is an actin filament interacting ATP driven molecular motor. Although many myosin types exist, they share a general structure that includes an N-terminus head or

5

motor domain, a light chain binding neck domain and a class conserved C-terminus tail domain, where remarkable variations in domain organization exist among known myosin classes (Fig 1.1). It is the motor domain that is considered to be mainly responsible for myosin motility. Although there modest differences in head domains between myosin types (e.g. two unique insertions in myosin VI, which is considered responsible for minus end directed motility; and a unique insertion in myosin IXb loop2, which is considered responsible for single headed processive movement (Coluccio, 2008; Foth et al., 2006)), the motor domain's core sequence, which includes the ATP-binding domain, ATPase activity and actin binding domain called Loop 2, is highly conserved in all myosin classes (Fig. 1.2A).

Sequential structural changes in the head domain of myosin-II, Va, VI during an ATP-hydrolysis cycle have been postulated according to crystal structures and electron microscopy images that used several ATP analogues (ADP, AMPPNP, ADP-Vi, ADP-BeF) (Fig. 1.2B for that of myosin-Va). However, structure studies alone cannot clarify the relationship between these structural changes and states in the ATP-hydrolysis cycles. Furthermore, it remains unclear whether these myosin structures bound to ATP analogues are representative of the true ATP-hydrolysis cycle.

In fact, several experimental results are inconsistent with the conclusions made from structure studies. In 1998, Ishijima et al demonstrated that muscle type myosin-II can generate a force even after ADP-release, which disagrees with the prevailed assumption that myosin generates force upon Pi-release (Ishijima et al., 1998) (Fig 1.3A, B). In 1999, Kitamura et al showed the several substeps during a single force generation

coupled with a single ATP-hydrolysis cycle (Kitamura et al., 1999) (Fig 1.3C, D). This result meant that myosin-II generates force by diffusing along an actin filament using biased Brownian motion, challenging the postulation that myosin-II generates force by changing the angle of its lever arm domain in a single process. Recently, M. Nishikawa et al. showed using single molecule imaging techniques that single headed myosin-IXb can move processively along an actin filament (Nishikawa et al., 2006) (Fig. 1.4). In their work, the lever arm domain of myosin-IXb was not fixed to any base. Therefore, the swing motion of the lever arm domain could not contribute to the force generated by myosin-IXb. Nishikawa et al. have also proposed that myosin-II generates variable step sizes depending on the ATP concentration by analyzing the variance change of the velocity, a feature not share with processive myosin-Va (Nishikawa et al., 2008).

This last observation suggests that the chemomechanical coupling mechanism is not universal in myosin. Here I investigate the chemomechanical coupling in processive myosin to clarify processivity and, upon comparing with myosin-II studies, establish whether all myosins utilize a common coupling mechanisim. Currently, the most effective and informative method to measure chemomechanical coupling in processive motors is to simultaneously observe ATP-turnover cycle and force generation at the single molecule level, which is what I do here.

1.3. General description about myosin-Va

Before introducing my own study, it is important to introduce some general properties about myosin-Va. Myosin-Va was first purified from brain (Espindola et al., 1992;

Larson et al., 1990) and was subsequently determined to be a novel myosin (Espreafico et al., 1992). It is a dimeric protein. The heavy chain has a motor domain at the N-terminus, having high homology with the motor domains of other myosin family members. A six light chain binding domain (IQ motifs) follows the motor domain. This IQ region is called the "neck" or "lever arm" while the motor domain is called the "head". The neck is followed by a long predicted coiled-coil region. Finally, the C-terminus region has a globular tail domain (GTD). In a cell, a cargo like vesicle binds to myosin-Va via this GTD. Myosin-Va has many physiological responsibilities including pigment granules transport along an actin filament. GTD also play a role in regulating myosin-Va motility by binding to the ATP-binding region of the motor domain, a process dependent on Ca^{2+} concentration (Thirumurugan et al., 2006). To remove this regulation, GTD was genetically truncated in our measurement. Optical trapping nanometry has revealed that a single, two headed myosin-Va moves processively along an actin filament (Rief et al., 2000), while single molecule imaging using TIRF microscopy has directly demonstrated the processive movement of GFP labeled myosin-Va along an actin filament (Sakamoto et al., 2000). Numerous chemical and mechanical measurements (De La Cruz et al., 1999; Purcell et al., 2002; Purcell et al., 2005; Tanaka et al., 2002; Trybus et al., 1999; Uemura et al., 2004; Veigel et al., 2005; Veigel et al., 2002; Yildiz et al., 2003) have been performed, finding that myosin-Va has a large 36 nm step size, and high ATPase activity and ATP affinity compared with other unconventional myosins. Therefore, myosin-Va is ideal for processive motor studies. Recently, by observing ATP-turnover cycles and stepping

motions simultaneously using TIRF microscopy, it was revealed that a single ATP-turnover cycle couples with a single stepping motion (Sakamoto et al., 2008). However, poor time resolution meant the sequential relationship could not be identified. Here, I clarify part of the sequential relationship between the chemical and mechanical cycles (in particular, that between ATP-binding and myosin detachment, and ADP-release and force generation) by measuring the ATP-turnover cycle and mechanical cycle directly and simultaneously.
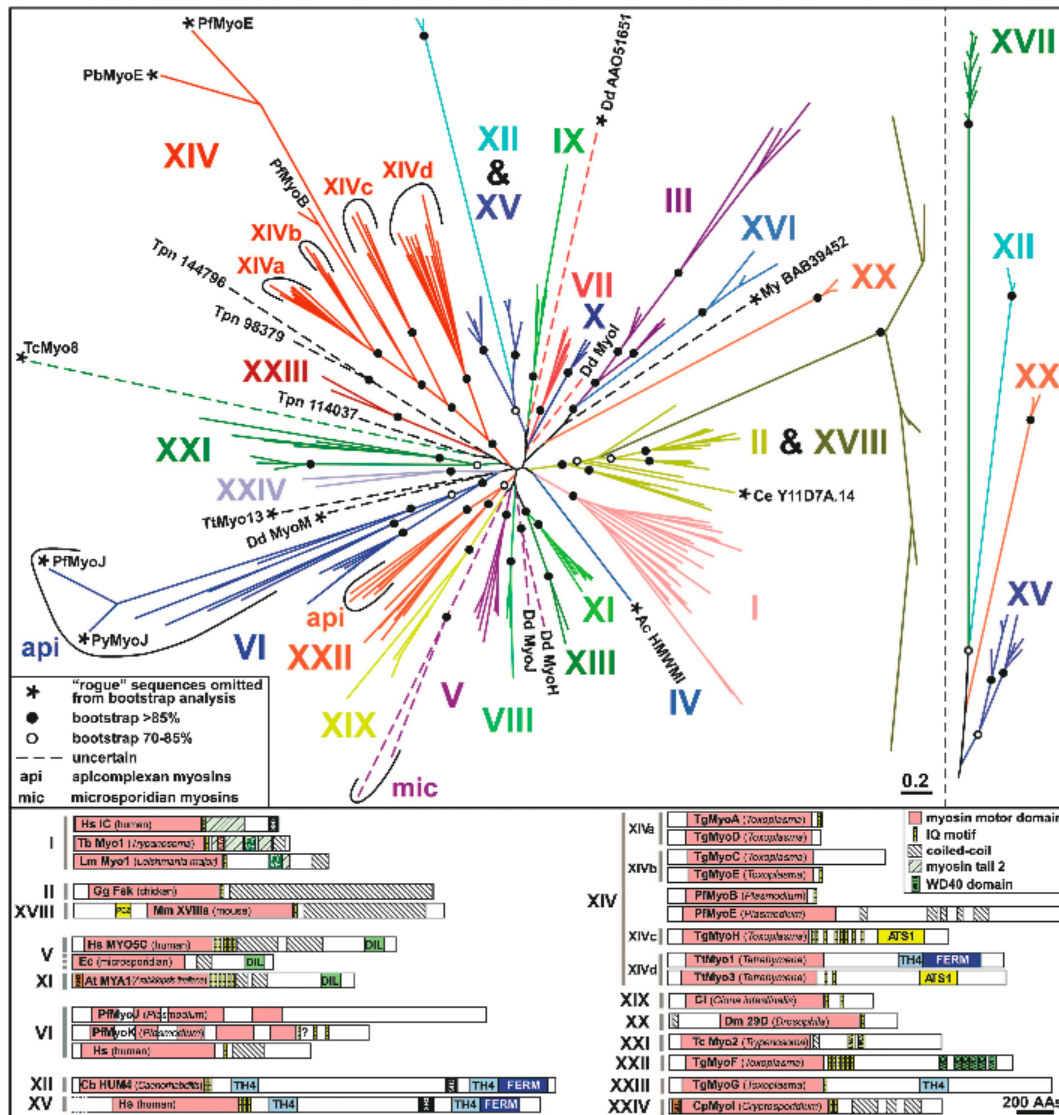
Figure 1.1 The diversity of myosin family.

(This figure was excerpted from B.J. Foth et al. PNAS (2006) Vol.103, pp 3681-6)

(A)
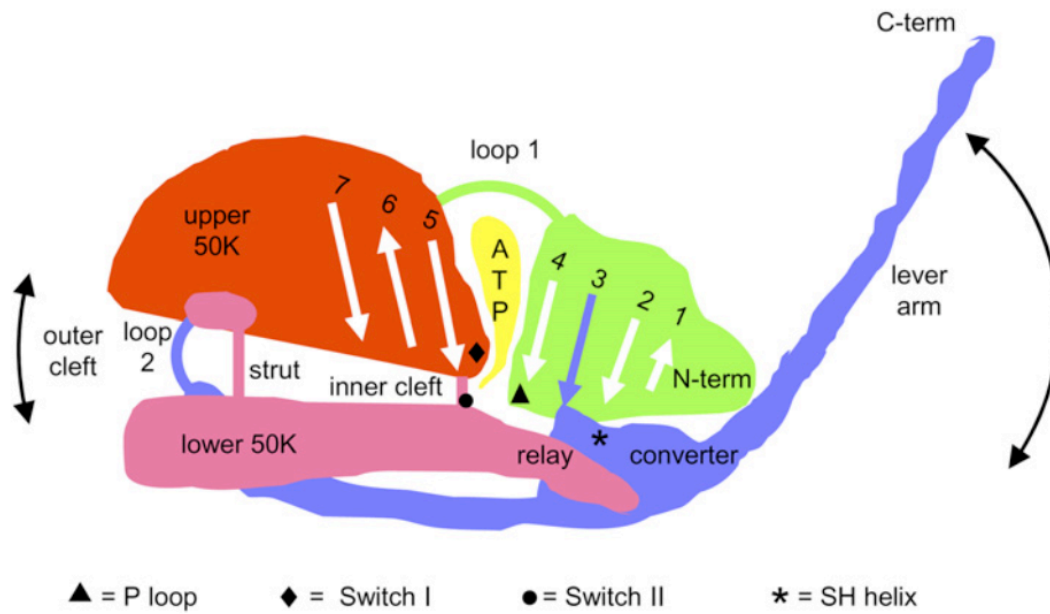
(B)

Figure 1.2

(Figure1.2A, B were excerpted from C. R. Bagshaw Structure (2007) vol. 15, pp 511-2, while Figure 1.2C, D from P. J. Coureux et al. EMBO J. (2004) vol. 23, pp 4527-37)
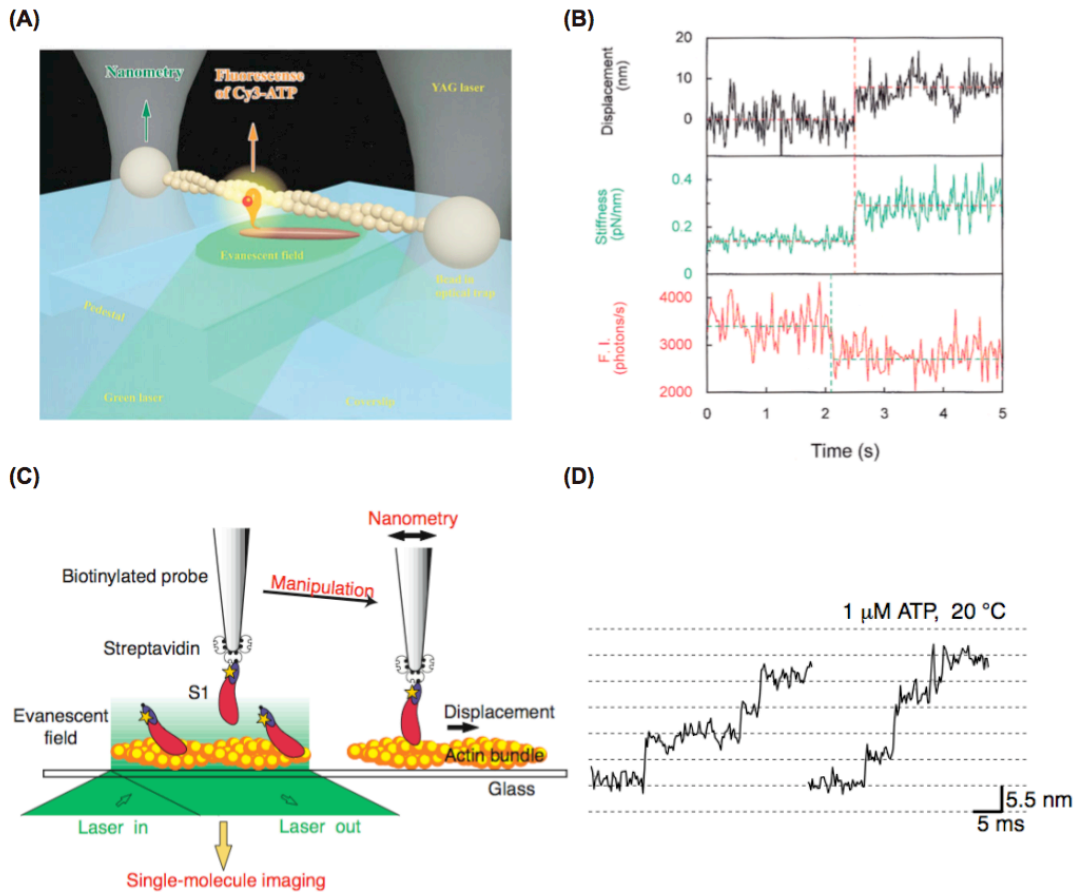
Figure 1.3 (A) experimental setup for muscle type myosin-II (B) typical relationship between ATP-turnover cycle and force generation. (C) the image of glass microneedle experiment. (D) 5.5 nm substeps during single ATP turnover coupled displacement.

(Fig 1.3A, B were excerpted from A. Ishijima et al. Cell (1998) Vol.92, pp 161-71, while Fig 1.3C, D from K. Kitamura et al. Nature (1999) Vol. 397, pp129-34)
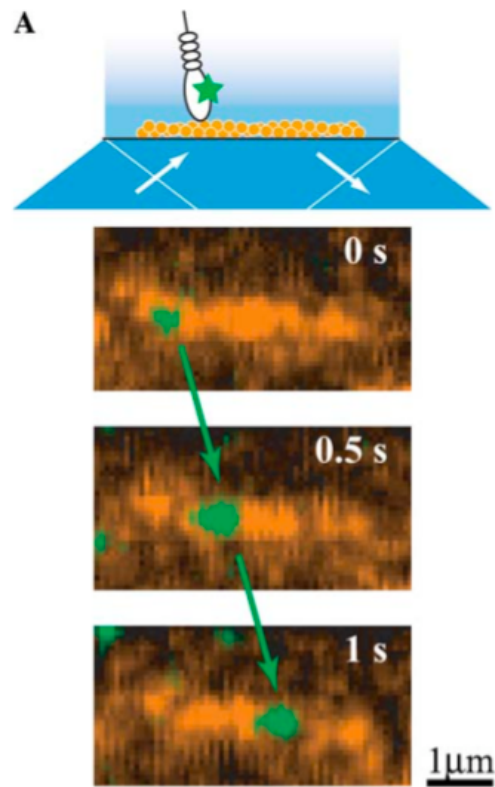
Figure 1.4 Single molecule imaging of single-heade myosin-IX processive movement.

(This figure was excerpted from M. Nishikawa et al. BBRC (2006) Vol.343, pp 1159-64)

(A)
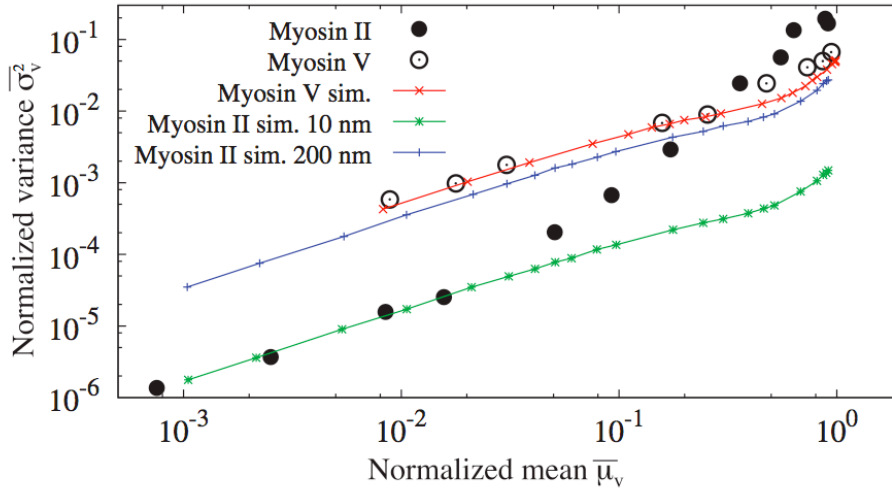
(B)
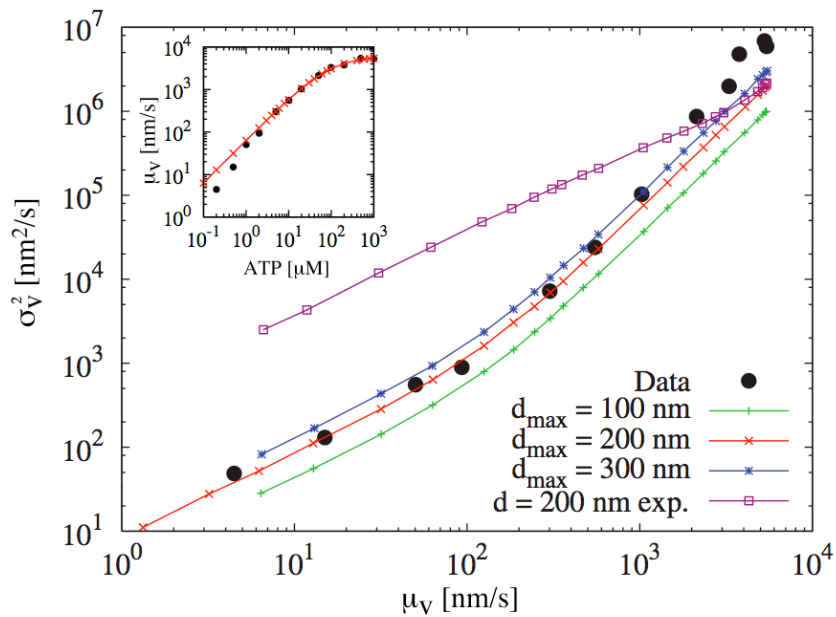
Figure 1.5 (A) relationship between mean velocity and variance in various type myosin (B) Comparison with Nishikawa et al. proposed model to the experimental data of myosin-II. Solid lines show the simulated relationship of their model. Red line of d_{max}=200 nm was well fit to the experimental data, meaning that myosin-II can generate 200 nm large step size during single ATP-turnover cycle.

(This figure was excerpted from M. Nishikawa et al. PRL (2008) Vol.101, pp 128103)

Chapter II

Measurement system for simultaneous observation of myosin-V chemical and mechanical events

2.1. Introduction

The development of single molecule detection techniques has allowed the elementary mechanical and chemical processes of various ATP driven motor proteins like myosin, an actin based motor, to be monitored. Both fluorescence imaging and manipulation techniques, which make up the basis for single molecule measurements, have been employed to study myosin motility. Total internal reflection fluorescence microscopy (TIRFM) is one such imaging technique capable of visualizing the chemical and mechanical activities of single motor molecules (Funatsu et al., 1995; Vale et al., 1996). Individual turnovers of ATPase activity in myosin have been monitored by observing the association and dissociation cycles of fluorescent ATP analogues (Funatsu et al., 1995; Tokunaga et al., 1997). In parallel, manipulation techniques, like the glass microneedle and optical trap, allow the movements of single actin filaments and myosin molecules to be observed with nanometer accuracy (Kishino and Yanagida, 1988; Ishijima et al., 1991; Finer et al., 1994). By combining TIRFM and the optical trap, chemical and mechanical events have been observed simultaneously. Simultaneous observation allows several chemo-mechanical parameters to be directly related including ATP hydrolysis and motor steps and, by extension, force generation (Ishijima et al., 1998). This has been observed in myosin-II, which is a non-processive myosin found in muscle. That study provided the first direct evidence for chemo-mechanical coupling and also showed that the energy stored after the release of the ATP hydrolysis products is used for the mechanical events. However, it remains unclear whether the chemo-mechanical coupling seen in myosin-II is universal for all myosins (Nishikawa

et al., 2008).

There exist at least 24 classes of myosins (Foth et al., 2006) (Fig 1.1). Myosin-Va (henceforth denoted as myosin-V) is the most commonly studied processive motor (Mehta et al., 1999; Rief et al., 2000; Sakamoto et al., 2000; Tanaka et al., 2002; Komori et al., 2007). Understanding the chemo-mechanical coupling in this myosin should clarify processivity and, upon comparing with myosin-II studies, establish whether all myosins utilize a common coupling mechanism. Although past data have already led to hypotheses for myosin-V chemo-mechanical coupling (De La Cruz et al., 1999; Coureux et al., 2003; Coureux et al., 2004; Uemura et al., 2004; Purcell et al., 2005; Veigel et al., 2005), no direct experimental data have been obtained by simultaneously measuring the chemical (ATP-turnover) and mechanical (displacement) events at the single molecule level. Recently, ATP-turnover cycles during myosin-V processive movement were visualized (Sakamoto et al., 2008). However, the limited time resolution prevented them from revealing the ADP-release and force-generation relationship.

Myosin-V experiments cannot be done the exact same way as they were for myosin-II. This is because myosin-V possesses significantly different traits from myosin-II. For example, myosin-V has a lower ATP-turnover rate and higher Km value than myosin-II (Harada et al., 1987; De La Cruz et al., 1999). This reduces the frequency of detecting myosin-V displacements as compared to myosin-II at the same nucleotide concentration. Also, there are several differences in the C-terminal structure between myosin-II and myosin-V (Sellers, 1999). This means that protocols have to be adjusted depending on

the myosin type. This is especially true when fixing myosin onto a glass surface, which is necessary to conduct single molecule experiments.

In this chapter, we explain how we overcame these problems and developed a simultaneous measurement system suitable for mechanical and chemical assays of a typical myosin-V in order to directly elucidate the chemo-mechanical coupling in processive motors.

2.2. Optical setup for simultaneous observation

2.2.1. Imaging and Photon Counting

An inverted fluorescence microscope (TE2000, Nikon, Japan) and other optics were set on a vibration-free table (TDI-189LA, HELTZ, Japan) in a soundproof room and air-conditioned room (Fig 2.1 and 2.2A) to minimize vibration and thermal drift. The stage could be manipulated by a three-axis manipulator (3-Dimensional Motorized Stage, MP-285, SUTTER INSTRUMENT). An oil immersion objective lens (60×Plan Apo TIRF NA=1.45, NIKON, Japan) and the sample stage were fixed on a Z-axis highly stable stage (model KS-N, Nikon Japan). All of the light paths were enclosed within plastic boxes to avoid the influence of stray light and air fluctuations (Fig 2.2B).

Cy5-labeled actin filaments were observed using epifluorescence microscopy. A beam from a He-Ne laser for Cy5 (05-LHP-925, MELLES GRIOT; 30 mW; λ= 632.8 nm), a beam of a frequency-doubled Nd:YAG green laser for Cy3 (COMPASS 315M-100, COHERENT; power 100 mW; λ=532 nm) and a sapphire laser for GFP (SAPOHIRE488-20; 20 mW; COHERENT; λ=488 nm) were expanded by 5.3 times (He-Ne laser) or 6.7 times (Nd:YAG green laser) using the laser beam expander consisted of concave lens and convex lens (BE1 for Nd;YAG green laser and BE2 for He-Ne laser in Fig 2.1) to adjust the excited area by beam by changing the diameters of lasers. Next these beams passed through half-lambda plate (λ/2 plate) to rotate the direction of polarity and change the ratio of p-wave and s-wave. P-wave of beams passed through polarizing beam splitter (PBS1 in Fig 2.1) and s-wave was reflected by

polarizing beam splitter (PBS1 in Fig 2.1). Transmitted p-wave was for epifluorescence microscopy and reflected s-wave was for total internal reflection fluorescence microscopy (TIRFM). P-wave of beams were passed through Neutral Density (ND) filter (ND1 in Fig 2.1) to adjust laser power and convex lens (L1 in Fig 2.1, f=450 mm). L1 was used to focus the beam at the back focal plane of the objective lens, achieving the parallel beam at sample plane. Finally the beam was directed to the objective lens by a dichroic mirror (D1 in Fig 2.1, FF562-Di01 for Cy3, FF660-Di01 for Cy5, FF495-Di01 for GFP, Semrock).

Single molecules of GFP bound myosin-V and Cy3-nucleotide (ATP or ADP) were observed with prism-type TIRFM. S-wave of the beam were reflected by polarized beam splitter (BS1 in Fig 2.1) and passed through a fresnel quarter-wave plate ($\lambda/4$ plate) to be converted into circularly polarized beam, laser beam expander to adjust the excited area by beam and ND filter (ND2 in Fig 2.1) to adjust laser power. The incident light then focused on a silica slide that is positioned parallel to the longitudinal axis of striped pedestals, through a cubic fused silica prism 2 μm wide and 1 μm deep. The gap between the prism and a fused silica slide was filled with pure glycerol specifically for fluorescence microscopy (Merck). The incident angle at the quartz-to-solution interface was 75° to normal while the critical angle was 66° between glass and water. The beam was focused onto an area 40×160 μm^2 on the specimen plane by a convex lens (L2 in Fig 2.1, f = 80 mm). This size of area was a little larger than the field of microscope. Infrared light used for optical trapping nanometry (see next section) was rejected from these detectors with two successive 750 nm long cut filters (only single filter was not

17

enough to reject the infrared light for optical trapping and the light from halogen lump for the bright field imaging) and barrier filters (LC2, SVX750, Asahi Spectra; BF1, FF495-Em02 for GFP, FF562-Em02 for Cy3 or FF660-Em02 for Cy5, Semrock, Inc.). The fluorescent image was focused using the microscope tube lens (L3, f =200 mm) and then converted into parallel light using a convex lens (L4, f = 50 mm).

 For simultaneous observation, the optical paths to the image intensifier (II, C8600, Hamamatsu Photonics) coupled to a CCD (CCD1, MC681SPD-R0B0, Texas Instruments) and the APD (SPCM-AQR-16, Perkin Elmer optoelectronics) were separated by a dichroic mirror (D6, Asahi Spectra, Japan). Fluorescent images with wavelengths over 625 nm (Cy5-phalloidin labeled actin filaments) were passed through the dichroic mirror and focused on the II coupled CCD camera using a convex lens (L5, f = 200 mm). Fluorescent images with wavelengths under 625 nm (Cy3-nucleotides) were reflected and focused onto a pinhole (PH, 50 μm diameter, Sigma Koki, Japan) using a convex lens (L6, f = 50 mm). Fluorescence from the specimen area was limited to a 0.9 μm diameter using this pinhole and focused on the APD using a convex lens (L7, f = 50 mm). Finally, photons from Cy3 modified nucleotides were detected using the APD. The number of photons was converted to a voltage every 10 ms using a data acquisition PCI board (National Instruments). The output was recorded on a PC using a digital data recorder (ADINSTRUMENTS). The position of the APD detecting area on the sample plane was checked using yellow-green fluorescent microspheres (Invitrogen) every 2 to 3 days. Except during simultaneous observations, in order to acquire

fluorescent images of the fluorescent ATP analogues, rhodamine-phallodiin actin filaments and GFP, the images were intensified by the II and focused onto the CCD directly (CCD2) using the microscope tube lens (L3).

2.2.2 Optical Tweezers and Nanometry

The two optical traps were generated by an infrared YAG laser (T10-8S, Spectraphisics, CA; power, 600 mW in max; $\lambda = 1064$ nm) reflected by a dichroic mirror (D3 in Fig 2.1). The laser passes through half lambda plate. Next p-wave passed through polarizing beam splitter (PBS2 in Fig 2.1). The reflected s-wave was scattered by a beam diffuser (Sigma Koki, Japan). These half lambda plate and polarizing beam splitter played role as the optical attenuator to adjust the power of infrared YAG laser. The passed laser was expanded by 3 times using laser beam expander consisted of concave lens and convex lens (BE4 in Fig 2.1), and passed through half-lambda plate to adjust the ratio of p-wave and s-wave. P-wave passed through two polarizing beam splitters (PBS3 and PBS4 in Fig 2.1). This position of beam remained fixed. S-wave was reflected by polarizing beam splitter (PBS3 in Fig 2.1). This position of beam was adjusted by two orthogonal galvano scanners (Model 6210 Galvanometer optical scanners, CAMBRIDGE TECHNOLOGY, INC.) controlled by custom software written in LabVIEW. The laser followed by two orthogonal galvano scanners passes through half lambda plate to be reflected by polarizing beam splitter (PBS4 in Fig 2.1). After the recombination the laser beam were expanded by 4 times using laser beam expander

consisted of two plano convex lens (BE5 in Fig 2.1) and passed through a quarter-wave plate. Next the two beams were passed through a dichroic mirror with a separation wavelength of 950 nm (D2 in Fig 2.1, Asahi Spectra Co., Ltd) and directed to an objective lens by a dichroic mirror with separation wavelength of 750 nm (D3 in Fig 2.1, Asahi Spectra Co., Ltd).

The bead displacements were measured with nanometer accuracy as follows. Microbeads were illuminated with infrared light originated from a halogen lamp that has passed through a 780 nm long-pass filter (LP1 and SCF1 in Fig 2.1, Asahi Spectra Co., Ltd, Japan) and 1050nm super cold filter (Asahi Spectra Co., Ltd, Japan). The infrared light was directed to a quadrant photodiode detector by the dichroic mirrors with a separation wavelength of 750 nm and 970 nm (D3 and D2 in Fig 2.1, Sigma Koki). The 750 nm shortcut filter and 950 nm long cut filter or the 750 nm longcut filter (SC1, LC1 and LC2 in Figure2, Asahi Spectra Co., Ltd, Japan) was used to eliminate the light from a visible laser and an infrared YAG laser. The image of the bead passed through imaging convex lens (L4 in figure2, f = 200 mm) and pellicle beam splitter (PB1 in Fig 2.1, BP108, R/T Ratio: 8/92 for 400 – 2400 nm, Thorlabs). 8% of the image is reflected and focused on CCD (CCD2 in figure2, WAT-525EX, Watec Co., LTD.). The transmitted 92% of the image passed through concave lens (L5 in Fig 2.1, f = -20 mm) to be magnified 500 times and pellicle beam splitter (PB2 in Fig 2.1, BP108, R/T Ratio: 8/92 for 400 – 2400 nm, Thorlabs). The transmitted image was projected onto the center of a quadrant photodiode detector (QPD in Fig 2.1, S994-13, Hamamatsu Photonics). The reflected imaged was focused on CCD (CCD3 in Fig 2.1, TM-524N,

Takenaka system, Japan). The differential outputs of the quadrant photodiode were amplified by an order-made differential amplifier (OP711A, Sentech, Japan) and recorded on PC using a digital data recorder. CCD2 was utilized to capture the image of bright field and CCD3 was utilized to capture the image of magnified bead, which was projected on quadrant photodiode detector.

In these simultaneous measurements, the displacements of the beads in the orthogonal direction could be determined while the fluorescence intensity from the Cy3-nucleotides was monitored simultaneously.

2.3. Materials and methods

2.3.1. Protein preparation

2.3.1.1. Myosin purification

Recombinant human myosin-Va HMM (henceforth denoted as myosin-V HMM) (Fig 2.3A, B) and human myosin-Va S1 IQ6 (henceforth denoted as myosin-V S1) (Fig 2.4A, B) were expressed and purified as described (Okada et al., 2007; Komori et al., 2008). Briefly, myosin V HMM has a FLAG-tag and GFP fused at its N-terminus; a motor domain; six-light-chain binding motifs; a coiled-coil domain truncated at Thr-1238; and a Myc-tag fused at its C-terminus. For myosin-V S1, the coiled-coil domain was removed at Glu-926. These constructs were coexpressed with calmodulin in Sf9 cells and then purified using FLAG M2 affinity gel (Sigma-Aldrich). The sample concentration was estimated by the Bradford method.

Recombinant calmodulin from Xenopus oocytes was expressed in Escherichia coli according to a previous method with some modifications (Ikebe et al., 1998).

2.3.1.2. Actin purification and fluorescent labeling of actin filament.

Actin was obtained from rabbit skeletal muscle and purified as described (Spudich and Watt, 1971). To visualize and attach the actin filaments to the beads, actin filaments were fluorescently labeled and biotinylated. The fluorescent phalloidin labeled biotinylated actin filaments were obtained by mixing rabbit skeletal actin and biotinylated-actin at a molar ratio of 19:1 (total [actin]=4 μM) in F buffer (0.1 M KCl,

10 mM HEPES-KOH (pH 7.8)) and 4 μM fluorescent phalloidin.

The biotinylated actin (Cytoskleton, Inc.), Rhodamine-phalloidin (Fluka) and Alexa633-phalloidin (Invitrogen) were purchased. Cy5-phalloidin and Cy3-phalloidin were synthesized from Cy5-NHS ester or Cy3-NHS ester (GE Healthcare Life Sciences) and amino-phalloidin (Alexis Biochemicals). Briefly, Cy5-NHS ester or Cy3-NHS ester and amino-phalloidin were mixed at a molar ratio of 1:1 in 20 mM CHES pH 9.0 and then incubated for 30 min at 30 °C. The reaction mixture was purified using HPLC reverse phase chromatography on Novapack C18 (Waters). First, the reaction mixture was applied to Novapak C18. Next, the column was washed using 30 ml of 10 mM KPi and 15%(v/v) ACN for Cy3-phalloidin or 10 mM KPi and 20%(v/v) ACN for Cy5-phalloidin at 1.5 ml/min flow rate. Then, the column was washed using 90 ml of MilliQ to remove phosphate from the column. Finally, 80% ACN diluted using milliQ was applied to extract the fluorescent phalloidin. The extracted fraction was dried using a rotary evapolater and then solved using about 200 μl MilliQ. The concentration of the fluorescent phalloidin solution was determined according to the absorption of the fluorescent dye. Next, the fluorescent phallodin solution was dried again and solved using 10 mM Hepes-KOH pH 7.0 and 100 mM KCl solution to adjust the fluorescent phalloidin concentration to 20 μM.

Fluorescent maleimide labeled actin was prepared by linking Cy5-maleimide (GE Healthcare Life Sciences), DyLight647-maleimide (PIERCE) or ATTO655-maleimide (ATTO-Tec, Germany) to Cys374 of actin as described (Ishijima et al., 1998). Fluorescent labeled actin filaments were obtained by mixing 2 μM native actin and 2

23

μM fluorescent labeled actin in F buffer and 4 μM phalloidin.

2.3.2. Fluorescent ATP analogues

EDA-ATP (2'(3')-*O*-[*N*-(2-aminoethyl)carbamoyl]ATP) and HDA-ATP (2'(3')-*O*-[*N*-(2-aminohexyl)carbamoyl]ATP) (Fig 2.5A,B), the precursors of 2'(3')-*O*-Cy3-EDA-ATP and 2'(3')-*O*-Cy3-HDA-ATP, respectively, were synthesized and purified as described previously (Jameson and Eccleston, 1997). Cy3-3'amino-3'-deoxy-ATP, 2'(3')-*O*-Cy3-EDA-ATP and 2'(3')-*O*-Cy3-HDA-ATP (Fig2.6A,B,C,D) were synthesized using 3'-Amino-3'-deoxy-ATP (TriLink Biotechnologies), EDA-ATP or HDA-ATP and Cy3-NHS-ester (GE Healthcare Life Sciences), respectively. The reaction mixture was purified using an FPLC anion exchange chromatography on a DEAE cellulose column (DE52, Whatman). The purity was greater than 99%, as determined by HPLC reverse phase chromatography on Novapack C18 (Waters) according to Oiwa's method (Oiwa et al., 2000). The isomers of Cy3-ATP (2'-*O*- and 3'-*O*-Cy3-EDA-ATP) (Fig 2.6A,B) were then separated as described (Oiwa et al., 2000). The purities of the isomers were greater than 98%.

ATTO550-EDA-ATP, ATTO520-EDA-ATP, ATTO520 g-(6-Aminohexyl)-ATP (Fig 2.7A,B,C), N^6-(6-Amino)hexyl-ATP and 8-[(6-amino)hexyl]-amino-ATP (Fig 2.8A,B) were purchased from Jena bioscience (Germany).

24

2.3.3. *In vitro* motility assay

Actin gliding movement over myosin immobilized on the glass surface was observed as previously reported (Kron and Spudich, 1986; Harada et al., 1987) with some modification. A flow chamber with a volume of 10 μl was made by placing a small coverslip (18×18 mm, No.1 Thickness, Matsunami, Japan) onto a larger one (24×60 mm, No.1 Thickness, Matsunami, Japan) using double sided adhesive tape (50 μm thickness). Coverslips were cleaned by washing in detergent (dcn90, AR BROWN CO., LTD.) and 99.5% m/m acetone before use. Detergent and acetone were chosen because myosin-V fixed onto KOH-treated glasses coated with nitrocellulose (Collodion in amyl acetate sterile 12620-50, Electron Microscopy Sciences or Collodion 032-03885, Wako, Japan) could not move actin filaments. Myosin-V HMM was first adsorbed to an ultra pure nitrocellulose (Collodion in amyl acetate sterile, Electron Microscopy Sciences) coated coverslip (24×60 mm) by introducing 0.2 μM myosin-V HMM in assay buffer (AB: 25 mM HEPES-KOH pH 7.4, 30 mM KCl, 5 mM $MgCl_2$, 1 mM EGTA) with 0.1 mg/ml calmodulin. After the incubation and wash using 100 μl AB, 0.4 μg/ml of fluorescent labeled actin filaments in AB was flowed into the chamber. Rhodamine-phalloidin labeled actin filaments were used for ATP and Alexa633-phalloidin labeled actin filaments for fluorescent ATP analogues because of the fluorescence spectral overlap between rhodamine and fluorescent ATP analogues, Following incubation and wash using 100 μl AB, 20 μl of AB including various concentrations of nucleotide, 0.1 mg/ml calmodulin and an oxygen scavenging system

(4.5 mg/ml glucose, 36 μg/ml catalase, 216 μg/ml glucose oxidase and 1% v/v β–mercaptoethanol) were added to the flow chamber. The movement of actin filaments were observed under epifluorescence microscopy or objective TIRFM for ATP and objective TIRFM for fluorescent ATP analogues to minimize the background caused by fluorescent ATP analogues).

2.3.4. Single molecule imaging

 A microchamber with a volume of 10 μl was made by placing a coverslip (18×18 mm, No.1 Thickness, Matsunami, Japan) onto a quartz glass using polyester spacers (50 μm thickness, TORAY, Japan) and fastening them with a paper clip. 1.5 nM myosin-V S1 was fixed on the quartz glass surface in a nonspecific manner. Next, AB containing 100 nM 2'-*O*-Cy3-EDA-ATP was added to the flow chamber. The Polystyrene spacers were removed and the chamber was sealed with nail polish. Single ATP-turnovers by myosin-V S1 were observed using prism type TIRFM at a sampling rate of 1 Hz.

 To exclude the possibility that 2'-*O*-Cy3-EDA-ATP non-specffically bound to myosin-V, 100 nM ATP and 2 mM vanadate was added to myosin-V and followed by 2'(3')-*O*-Cy3-EDA-ATP. After 2 min incubation and wash using 1 ml AB including 2 mM vanadate, AB containing 100 nM 2'-*O*-Cy3-EDA-ATP was flowed through the chamber and the chamber was sealed.

2.3.5. Single molecule mechanical assay

We performed single molecule mechanical assays using chemically etched glass (Ishijima et al., 1998; Tanaka et al., 1998) with some modification. Chemically etched quartz glass (striped pattern with 20 μm interval of mean 1 μm wide and 2 μm deep pedestal) was custom-made at the Institute of Microchemical Technology, Japan (http://www.i-mt.co.jp). The flow chamber was made as described in the previous section. Chemically etched quartz glass and coverslips were cleaned by washing in detergent and 99.5% m/m acetone before use. Myosin-V S1 was adsorbed to an ultra pure nitrocellulose coated etched glass via monoclonal anti-Myc antibody (Medical and Biological Laboratories Co., Ltd., Japan). After treatment with antibody (0.01 mg/ml), the glass surface was coated with 1 mg/ml bovine serum albumin (BSA) in AB. 10 pM myosin-V S1 in AB with 0.1 mg/ml calmodulin was added to the flow chamber. Next, the glass surface was coated with 1 mg/ml α-casein in AB modified with 0.5% Pluronic F-127 (Invitrogen) to prevent nonspecific binding of neutravidin coated beads (diameter: 1 μm, Invitrogen) and washed using 3 ml AB to completely remove the excess α-casein. Biotinylated and fluorescent labeled actin filaments and neutravidin coated beads in 20 μl of AB mixed with 1 μM concentration of nucleotide, 0.1 mg/ml calmodulin, the oxygen scavenging system and polystyrene beads (diameter: 4.5 μm, Polysciecnce, Inc.) were added to the flow chamber. Polystyrene spacers were removed and excess solution in the sample chamber was absorbed using a wipe paper. As a result, the chamber thickness was 4.5 μm, equal to the polystyrene bead diameter. Finally, the

chamber was sealed with nail polish. The displacements of myosin-V S1 were determined as previously described (Molloy et al., 1995).

2.3.6. Measuring photobleaching rate

The flow chamber was made as described above. 150 nM myosin-V S1 was fixed onto the glass surface as described in section 2.3.4, saturating the glass surface with myosin-V. 100 μl of AB mixed with 100 nM 2'(3')-*O*-Cy3-EDA-ATP or 2'-*O*-Cy3-EDA-ATP and 2 mM vanadate was added into the flow chamber. After a 2 min incubation and wash using 1 ml AB including 2 mM vanadate, followed by 20 μl of AB including 2 mM vanadate and the oxygen scavenging system. Finally, the chamber was sealed with nail polish and the experiment was performed. Cy3-nucleotide was excited using prism-type TIRFM as done for the simultaneous observation experiments. The fluorescent images of Cy3-nucleotide were captured by CCD. The time dependent, fluorescence intensity decay in a 10 μm × 10 μm region was acquired from the images using custom software written in LabVIEW7.1 (National Instruments). The photobleaching rates were determined by fitting these decay intensities using a single exponential decay function.

Furthermore, to evaluate the effect of Cy3 photobleaching by a 1064 nm infrared laser, Cy3 photobleaching by a 1064 nm infrared laser was determined using Cy3-phalloidin labeled actin filaments. An over 15 μm long Cy3-phalloidin labeled actin filament was

captured using an optical trap. After 2 min of excitation by a 532 nm laser for epifluorescent illumination, the fluorescent image of the photobleached actin filament was captured by an II coupled CCD and recorded on a PC. The fluorescence intensities along the actin filament from the center of the optical trap were measured using ImageJ (http://www.rsb.info.nih.gov/ij/).

2.3.7. Simultaneous observation of chemical and mechanical events

Protein L (ACTIgen) was adhered nonspecifically to the etched glass of the flow chamber, made as described in section 2.3.4, by applying 1 mg/ml Protein L in AB. The glass surface was blocked with 1 mg/ml BSA and anti-Myc antibody (0.01 mg/ml) was added. Then 10 pM myosin V S1 in AB with 0.1 mg/ml calmodulin was flowed into the chamber. Next, the glass surface was coated with an additional flow of 1 mg/ml α-casein including 0.5% v/v Pluronic F-127 and washed using 3 ml AB. Biotinylated and fluorescent labeled actin filaments and neutravidin coated beads in AB modified with 1 μM ATP, 100 nM 2'-O-Cy3-EDA-ATP, 0.1 mg/ml calmodulin, the oxygen scavenging system and polystyrene beads as described in section 2.3.4. were added to the flow chamber. Finally the chamber was sealed with nail polish. All experiments were performed at room temperature (23 °C). The experiment was performed as described in Fig. 2.9.

2.4. Results and discussion

2.4.1. Functional properties of fluorescent ATP analogues

Individual ATP-turnover cycles by myosin have previously been visualized using fluorescent ATP analogues as the substrate (Funatsu et al., 1995; Iwane et al., 1997; Tokunaga et al., 1997). In solution, fluorescent ATP analogues diffuse too quickly to be detected as single spots. However, we can observe single spots when the fluorescent analogue is bound to the ATP binding domain of myosin during ATP hydrolysis. By observing the binding of fluorescent ATP and its dissociation after hydrolysis, ATP turnover can be monitored. Therefore, functional fluorescent ATP analogues for myosin-V were needed to visualize myosin-V ATP turnovers.

Ten ATP analogues were prepared and their functional properties were determined using *in vitro* motility assay (Table. 1), single molecule TIRFM and single molecule mechanical assays. For the analogues 2'(3')-*O*-Cy3-EDA-ATP, 2' -*O*-Cy3-EDA-ATP, 2'-*O*-Cy3-EDA-ATP and 2'(3')-*O*-Cy3-HDA-ATP, the actin gliding velocity was a function of ATP concentration following Michaelis-Menten kinetics, which yielded a max velocity and a Km value. The max velocity for these ATP analogues was the same as ATP but the Km was greater, indicating that modification of the Cy3 dye at the ATP ribose ring decrease myosin ATPase mainly by lowering ATP affinity to myosin-V (Table. 1). The differences in affinity are probably caused by differences in steric hindrance depending on the linker length.

For the analogues Cy3-3'amino-3'-deoxy-ATP, ATTO520-EDA-ATP and

ATTO550-EDA-ATP, actin gliding was not observed. Single molecule fluorescence imaging of these ATP analogues on myosin-V using TIRFM showed that they did not bind to myosin-V, explaining the lack of actin gliding. It is likely that steric hindrance makes myosin-V inaccessible, because the linker length between the ribose ring and chromophore required to bind to the myosin ATP binding domain is too short (all three were modified at the ribose ring and had linker lengths shorter than 2'(3')-*O*-Cy3-EDA-ATP).

Cy3-N^6-(6-Amino)hexylamino-ATP, which is modified at the adenine ring, can also act as a myosin-II substrate (Funatsu et al., 1995). However, N^6-(6-Amino)hexyl-ATP and 8-[(6-amino)hexyl]-amino-ATP, which are precursors of fluorescent ATP analogues modified at the adenine ring, show no activity with myosin-V. ATTO520 g-(6-Aminohexyl)-ATP, modified at the 5' phosphate group, also shows no activity. As a result, 2'-*O*-Cy3-EDA-ATP (henceforth denoted as Cy3-ATP), because it had the same max velocity as ATP and the highest affinity for myosin-V among all analogues, was the fluorescent ATP analogue of choice.

Furthermore, we studied the effects of the Cy3 molecule on individual ATP turnovers and myosin-V step size. Using TIRFM, we successfully observed single Cy3-ATP turnovers at the myosin-V S1 position (Fig. 2.10A). The appearance and the disappearance of Cy3-fluorescence were observed as indicated by the rising and falling phases of fluorescence intensity. The myosin-V S1 position was determined by following the fluorescence imaging of the attached GFP. The off-rate of Cy3-fluorescence bound to the glass surface was 0.02 s^{-1} (Fig. 2.10B). This value is

31

consistent with ATP-turnover rate of 0.03 s^{-1} reported using a biochemical assay (De La Cruz et al., 1999). Therefore, the appearance of Cy3-nucleotide fluorescence is probably due to the Cy3-ATP binding to the ATP binding domain of myosin-V. Hence the disappearance of Cy3-nucleotide is probably due to Cy3-ADP dissociation from the same ATP binding domain.

Moreover, to clarify whether these turnovers were due to non-specific binding of Cy3-ATP to myosin-V, two additional experiments were performed. First, we observed the fluorescent images of Cy3-ATP when the ATP binding domain was blocked by a stable ADP-vanadate stable complex (Goodno, 1979) according to the method described in section 2.3.6. (detail analysis was described section 2.3.4.3.). Second, we observed fluorescent images of Cy3-ATP in the presence of excess ATP (10 mM ATP against 25 nM Cy3-ATP). In both cases, ATP-turnover by myosin-V was not observed. The competitive binding with ATP suggests that Cy3-ATP binds to the ATP binding domain of myosin-V and the appearance of fluorescence on the surface suggests specific binding to the active site of myosin-V.

Lastly, we examined the effects of Cy3-ATP on the mechanical properties of myosin-V S1 (Figure 2.11). In ATP, we measured a stroke size of 20 ± 14 nm (mean ± s.d.; n=190), consistent with previous reports (Purcell et al., 2002; Veigel et al., 2002), while stroke size for Cy3-ATP was 20 ± 16 nm (mean ± s.d.; n=238) showing that Cy3-ATP did not affect myosin-V S1 stroke size. Furthermore, the dwell time during displacement was 1.3 ± 0.06 s in 1 μM ATP (mean ± s.e.m.; n=182) but 1.6 ± 0.05 s in 1 μM Cy3-ATP

(mean ± s.e.m.; n=238). This difference in dwell time is probably caused by the difference in the affinity for ATP and Cy3-ATP by myosin-V.

2.4.2. Photostability of Cy3-ATP

To eliminate the possibility that the results are compromised by photobleaching of Cy3-nucleotides before Cy3-ADP dissociation, the photobleaching rate of Cy3-nucleotides was measured when Cy3-ATP was bound to a glass surface and when Cy3-ADP formed a stable complex with myosin-V and excess vanadate (2 mM) (half life of ~3 days in the case of myosin-II-ADP (Goodno, 1979; Oiwa et al., 2003)). In the presence of the oxygen scavenging system including 1% v/v (143 mM) β-mercaptoethanol, the photobleaching rate of Cy3-nucleotides bound to a myosin-V head in the presence of vanadate was 0.006 s^{-1} under simultaneous observation experimental conditions, while the photobleaching rate of 2', 3'-Cy3-nucleotides was 0.005 s^{-1}.

Dithiothreitol (DTT) is a stronger reducing agent than β-mercaptoethanol. Therefore, in some cases, a high concentration of DTT was used instead of β-mercaptoethanol in the oxygen scavenging system. The photobleaching rate of 2', 3'-Cy3ATP in the presence of 50 mM, 5 mM and 1 mM DTT was 0.008 s^{-1}, 0.02 s^{-1} and 0.03 s^{-1}, respectively. However, *in vitro* motility assay demonstrated that for 5 mM and 50 mM DTT little or no actin gliding events were observed, while for 1% v/v β-mercaptoethanol and 1 mM DTT actin gliding events were observed. Concentrations

>5 mM DTT probably disrupted antibody recognition of the antigen leading to detachment of myosin-V from the glass surface. Thus, 1% β-mercaptoethanol, which allows the highest Cy3-nucleotide photostability among all reducing agents and did not impact antigen recognition, was preferred for the oxygen scavenging system.

In previous simultaneous observation experiments, the binding time of the fluorescent ATP analogue is assumed to approximate the time a myosin-II head bound to a nucleotide spends dissociated from an actin filament (Ishijima et al., 1998). For myosin-V, a similar assumption was made. Our optical trap studies found that the association rate constant for myosin-V to actin was approximately 1.72 s^{-1} (data not shown). Actually, the average total duration of Cy3-nucleotide binding to myosin-V, meaning the duration between the fluorescence intensity rising and falling phases (Fig. 2.18 lower trace and Fig. 3.2 lower trace) was 0.63 s (data not shown) (refer next chapter). Using this value and the 0.006 s^{-1} photobleaching rate of Cy3-nucleotides, the probability that photobleaching occurred prior to nucleotide release is ~0.3 % confirming that the observed decrease in fluorescence intensity was due to the dissociation of bound Cy3-nucleotides.

It has been reported that the photobleaching rate of Cy3 dye is enhanced by simultaneously exposing the molecules to the optical trap laser (λ=1064 nm) and the fluorescence excitation laser (λ=532 nm), even though there is no significant absorbance at the wavelength of the trapping laser (Brau et al., 2006; van Dijk et al., 2004). We quantified this effect to eliminate the possibility that artifacts and not ATP-turnover rates were measured. The fluorescent intensity of Cy3-phalloidin labeled

34

actin filaments was measured against the distance from the center of the optical trap (indicated by white arrows in Fig. 2.12A). The effect of the trapping laser on the photobleaching rate of Cy3-dye was calculated by applying a Gaussian function with a standard deviation of $\sigma = 1.3$ μm (Fig. 2.12B). In fact, the photobleaching rate of Cy3-nucleotide binding to myosin-V 4 μm from the center of the optical trap was 0.024 s^{-1} with 1064 nm laser illumination and 0.027 s^{-1} without illumination (we should note that the Cy3-excitation intensity was less in the simultaneous observation condition). It can be seen that the influence of the trapping laser on the photobleaching of Cy3-nucleotides binding to myosin-V at 4 μm ($>3\sigma$) from the optical trap was negligible.

As a consequence, we measured displacements and ATP-turnovers of myosin-V S1 fixed at more than 4 μm from the centers of the optical traps.

2.4.3. Construction of the measurement system for simultaneous observation experiments of myosin-V

2.4.3.1. Fluorescent labeling of actin filaments

In the simultaneous observation experiment of chemical and mechanical events, one must visualize the fluorescent ATP and the actin filament. In this section, we describe the florescence properties of five fluorescent dyes as labels for actin filaments (Alexa633-phalloidin, DyLight647-maleimide, ATTO655-maleimide, Cy5-maleimide and Cy5-phallodin).

Although Alexa633-phalloidin labeled actin filament were used in *in vitro* motility assays, it could not be applied to simultaneous observation experiments because the fluorescence of Alexa633-phalloidin labeled actin filaments could pass the dichroic mirror and barrier filter for Cy3 when excited by the green laser (λ=532 nm). Therefore Alexa633-phalloidin is not suitable for the simultaneous observation experiments.

Cy5-maleimide and DyLight647-maleimide labeled actin filaments showed unusual rapid photobleaching within several seconds when excited by the 633 nm laser and the 1064 nm infrared laser simultaneously (Fig. 2.13A,B for Cy5-maleimide; data not shown for DyLight647-maleimide). In contrast, Cy5-phalloidin and ATTO655-maleimide labeled actin filaments showed high stability upon simultaneous excitation (Fig. 2.13C,D for Cy5-phalloidin; data not shown for ATTO655-maleimide) with Cy5-phalloidin's stability being greater. For these reasons, Cy5-phalloidin was selected as the actin filament label.

2.4.3.2. Suitable nucleotide concentrations for simultaneous observation experiments

When the concentration of the fluorescent ATP analogue increases to more than 100 nM, the fluorescent spots on the surface become obscured because of the increased background fluorescence due to fluorescent ATP analogue molecules free in solution. At 100 nM Cy3-ATP, we were able to observe fluorescent images with a signal to noise ratio of 2.5.

However, Cy3-ATP has a weaker affinity for myosin than ATP. At 100 nM Cy3-ATP, the dwell time was estimated to be 40 s, longer than the dwell time for 100nM ATP (De La Cruz et al., 1999). Using this information with the 0.007 s^{-1} unbinding rate for myosin-V from actin filament in nucleotide free rigor condition means that about 13% of myosin-V detachments were the result of nucleotide uncoupled events. Furthermore, this concentration compromises our ability to detect the relationship between ATP hydrolysis and force generation.

To overcome these problems, 1 μM unmodified ATP was added to the Cy3-ATP concentration (Nishizaka et al., 2004) . This means we could not view all ATP-turnover events. However, one can still correlate the chemical reactions with the mechanical events. In this condition, the mean dwell time of a step is estimated as about 1 s. Thus only < 0.7% of the myosin-V detachment event were events uncoupled from nucleotide binding.

2.4.3.3. Evaluating the effectiveness of measuring myosin-V fixed to a pedestal

Though nitrocellulose is commonly used to fix active myosin and antibody on a glass surface, non-specific binding of Cy3-ATP to the glass surface makes nitrocellulose unsuitable to observe ATP-turnovers. Instead, we selected Protein L, which has immunoglobulin binding domains to fix the antibody to the glass surface and still retain myosin activity (Pal et al., 2005; Post et al., 2002). Protein L is absorbed to the glass surface in a non-specific manner.

After coating with protein L, BSA was used to block non-specific binding of antibodies and myosin-V to the glass surface. Following myosin-V attachment, α-casein was used to block the nonspecific binding of neutravidin coated beads because BSA alone is insufficient. Because α-casein masks the immunoglobulin binding domain of Protein L, it was added after BSA.

We should note that in general, casein is not utilized as a blocker in avidin-biotin systems because casein is a milk-related protein and endogenous biotin in milk remains even after purification. On the other hand, casein is a strong blocker against neutravidin beads and, as stated, BSA is not a suitable substitute. To remove excess casein and biotin, the flow chamber was washed completely using 3 ml of AB before simultaneous observations were made.

2.4.3.4. Non-specific binding of Cy3-ATP to glass surface

Myosin-V S1 was successfully fixed on glass surface using above method. Here, I remove the possibility that non-specific binding of Cy3-ATP affect the result of

simultaneous observation. It is impossible to completely remove non-specific binding of Cy3-ATP to some protein coated glass surface. To evaluate the non-specific binding of Cy3-ATP at 100 nM concentration, I measured non-specific binding of Cy3-ATP to α-casein including 0.5%(v/v) Pluronic F-127, Protein L and anti-Myc antibody, meaning the same condition described in previous section except for myosin-V S1. As a result, in our condition, there is a little non-specific binding except for shot bindings within 100 ms (Fig 2.14A, B). Actually, the off-rate of non-specific Cy3-ATP binding was 10 ± 0.2 s^{-1} (mean $\pm$ s.e.m.; n= 293) (Fig 2.15A). This value is much shorter than the duration between the fluorescence intensity rising and falling phases (0.63 s) (refer next chapter).

Furthermore, to remove the possibility that Cy3-ATP non-specifically binds to myosin-V itself, I measured the off-rate of non-specific Cy3-ATP binding in the existence of ADP-Vi blocked myosin-V S1.The off-rate of non-specific Cy3-ATP binding in the existence of ADP-Vi blocked myosin-V S1 was 8.1 ± 0.6 s^{-1} (mean $\pm$ s.e.m.; n= 155) (Fig 2.15B), meaning that the non-specific Cy3-ATP binding to myosin-V itself have not to be cared. However, strictly speaking, we can never remove the possibility of non-specific binding completely in this condition. Only way to remove the possibility as possible is to acquire a lot of data and analyze them statistically.

2.4.3.5. Fluorescent images observed on a thin pedestal

In myosin-II studies, myosin-II was fixed on a 7 μm wide pedestal (Ishijima et al., 1998). Applying this to myosin-V experiments meant we had to search along the

vertical and horizontal axes of the pedestal to detect the myosin position. This proved laborious because ATP-turnovers were detected by the APD, which had a detection region of only 0.9 μm diameter. Instead, myosin-V was fixed on a 1 μm width pedestal. Furthermore, by taking advantage of the etched glass, we did not have to search along the vertical axis of the pedestal to detect the myosin-V position, simplifying detection.

It was confirmed with 488 nm and 532 nm laser light that evanescent fields were generated on this thin pedestal as shown in Fig. 2.16A. Cy3-ATP (ADP) binding to myosin-V fixed on the pedestal were observed using a CCD camera (Fig. 2.16B) and the APD (Fig. 3.2 lower trace).

2.4.3.6. APD and QPD signal response

In the simultaneous observation, the timing difference between the signal from APD and that from QPD was measured. Thus, we must verify that there is no signal response difference between these two detectors in our experimental setup. To check this, we measured the rising signal response when a step input from the same light source was introduced to these two detectors simultaneously. Signals from the APD and the QPD were measured at a 1 kHz sampling rate, which is ten times higher than the 100 Hz sampling rate of the ATP-turnover cycle and 100 Hz low-pass filter rate for displacement traces. As shown in Figure 2.17A,B, there was no significant difference in the signal response between these two detectors within the experimental sampling rate of 100 Hz. Thus, we concluded that the signal difference between the APD and the QPD was negligible.

40

2.4.3.7. Myosin-V simultaneous observation experiments

The improvements and developments described in this study enabled us to measure ATP-turnovers and displacements of myosin-V simultaneously. Overall, the simultaneous observation was performed using Cy3-ATP, single headed myosin-V fixed using Protein L and antibodies, 1 μm wide chemically etched glass and Cy5-phalloidin labeled actin filaments (Fig. 2.9). 10 pM myosin-V S1 was flowed into the flow chamber and resulted in a density on the glass surface of 2.8×10^{-2} molecules/μm^2. From the system geometry, we estimated that the sampled area in the optical trap nanometry was 0.08 μm^2 on a 1 μm width pedestal. Therefore, assuming that the molecular number of interaction obeys Poisson distribution, there were 2.2×10^{-3} molecules per surface platform tested. Thus, we can expect the probability that observed mechanical events were driven by a single molecule is 99.8 %. The detected area by APD was 0.63 μm^2. The probability that observed chemical events derived from a single molecule is 98.3 %. Therefore, one can safely assume that in simultaneous observation, the mechanical record is coming from the same molecule as the ATP-analog binding.

As a result, the relationship between the chemical events and mechanical events of myosin-V was directly observed (Fig. 2.18). The upper trace shows a time course of displacements caused by myosin-V S1 in the presence of 1 μM ATP and 100 nM Cy3-ATP. The rising phase shows myosin-V S1 head attachment to an actin filament followed by rapid force generation. The dropping phase shows the myosin-V S1

detachment from the actin filament. The lower trace shows the time trajectory of the fluorescent change in Cy3-nucleotides. The increase and decrease in the fluorescence intensity were caused by the association and dissociation of single Cy3-nucleotides to the ATP binding domain of myosin heads. The intensity increase likely represents the binding of Cy3-ATP to myosin while the decrease likely represents the release of hydrolyzed Cy3-ADP.

Consequently, we can identify the coupling between ATP-binding and myosin-V detachment from the actin filament. Additionally, the coupling between ADP-release from myosin-V and force generation can be studied. This relationship is especially important in the processive movement of myosin-V (De La Cruz et al., 1999; Purcell et al., 2005; Veigel et al., 2005). In the next chapter, how chemical events couple with mechanical ones is focused.

	Max velocity (μm/s)		Km (μM)
ATP [a]	0.22 ± 0.04		37 ± 9
Cy3-3'amino-3'-deoxy-ATP [a, b]		No activity	
2'-*O*-, 3'-*O*-Cy3-EDA-ATP [a]	0.23 ± 0.06		133 ± 49
2'-*O*-Cy3-EDA-ATP [a]	0.18 ± 0.04		64 ± 20
3'-*O*-Cy3-EDA-ATP [a]	0.23 ± 0.07		173 ± 78
2'-*O*-, 3'-*O*-Cy3-HDA-ATP [a]	0.25 ± 0.04		209 ± 103
ATTO520-EDA-ATP [a, b]		No activity	
ATTO550-EDA-ATP [a, b]		No activity	
N6-(6-amino)hexyl-ATP [a]		No activity	
8-[(6-amino)hexyl]-amino-ATP [a]		No activity	
ATTO-520-g-(6-aminohexyl)-ATP [a, b]		No activity	

Table 1. Functional properties of fluorewscent ATP analogs.

[a] Evaluated using *in vitro* motility assay.
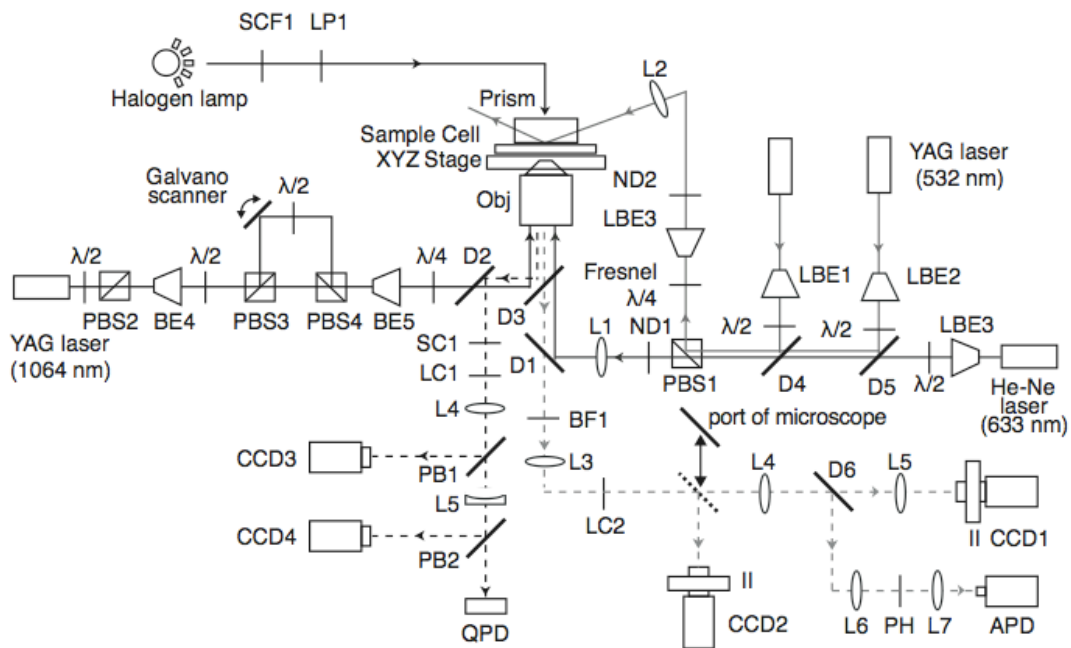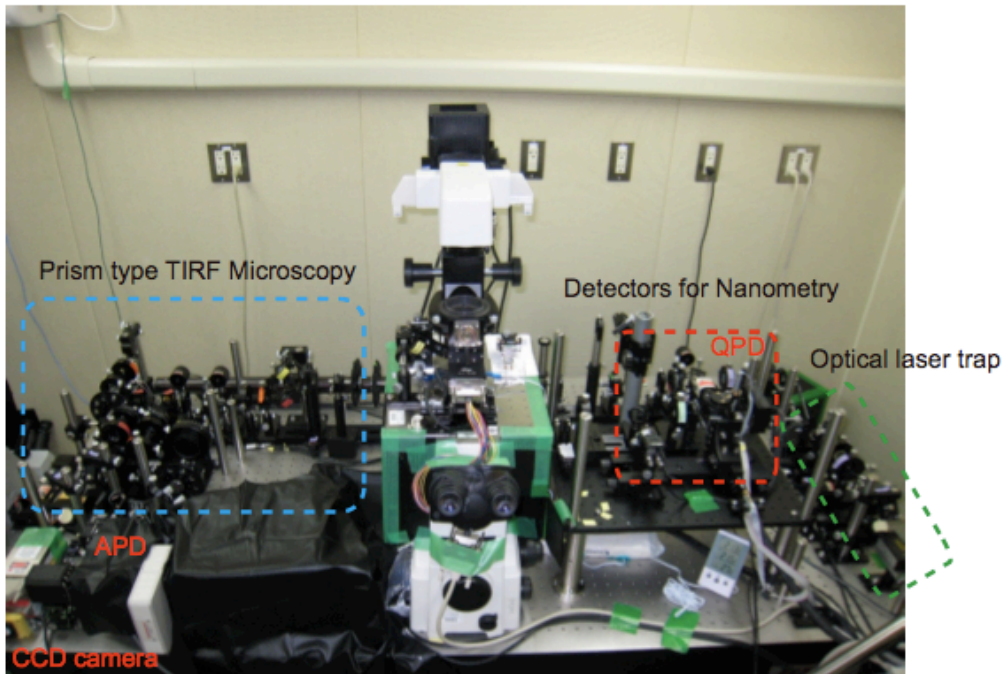[b] Evaluated using single molecule imaging.

Figure 2.1. the optical setup for the simultaneous observation.

A microscope for simultaneous measurement of ATP turnover and mechanical events. APD, BE, BF, BP, CCD, D, II, L, BE, LC, LP, ND, Obj, PB, PBS, PH, QPD, SCF mean avalanche photodiode, laser beam expander, barrier filter, band pass filter, Charge Coupled Device camera, dichroic mirror, image intensifier, lens, longcut filter, longpass filter, Neutral Density filter, objective lens, pellicle beam splitter, polarizing beam splitter, pinhole, quadrant photodiode detector and super cold filter, respectively. See "Imaging and Photon Counting" and "Optical Tweezers and Nanometry" for details.

(Most of the optical setups was constructed by T. Ariga, Ph. D. (present address: Tokyo University), APD detection part was constructed by T.K.)
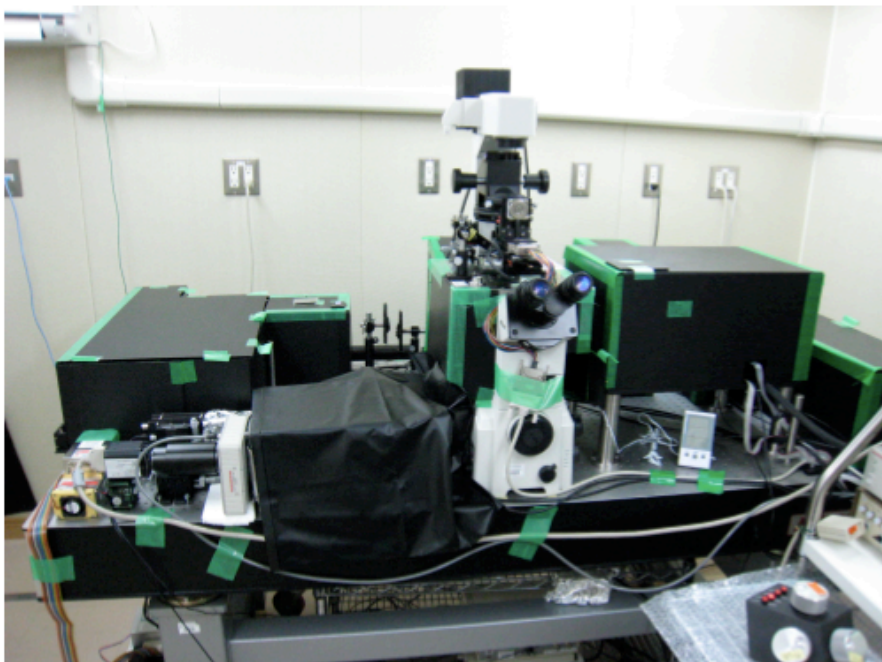
(A)

(B)

Figure 2.2 (A) a picture of optical pathways for simultaneous observation. (B) enclosed optical pathways to prevent air fluctuation.

(A)

Flag-EGFP-hMyosin 5a(1238)HMM-Myc (1527aa)

177,233Da

Flag MDWKDDDDKR SMNSKAYVD

EGFP
MVSKGEELFT GVVPILVELD GDVNGHKFSV SGEGEGDATY GKLTLKFICT TGKLPVPWPT LVTTLTYGVQ CFSRYPDHMK QHDFFKSAMP EGYVQERTIF
FKDDGNYKTR AEVKFEGDTL VNRIELKGID FKEDGNILGH KLEYNYNSHN VYIMADKQKN GIKVNFKIRH NIEDGSVQLA DHYQQNTPIG DGPVLLPDNH
YLSTQSALSK DPNEKRDHMV LLEFVTAAGI TLGMDELYKS GLRSAALDRP TRPA

Myosin head-like(1-765)
MAASELYTKF ARVWIPDPEE VWKSAELLKD YKPGDKVLLL HLEEGKDLEY HLDPKTKELP HLRNPDILVG ENDLTALSYL HEPAVLHNLR VRFIDSKLIY
TYCGIVLVAI NPYEQLPIYG EDIINAYSGQ NMGDMDPHIF AVAEEAYKQM ARDERNQSII VS GESGAGKT VSAKYAMRYF ATVSGSASEA NVEEKVLASN
  P-Loop
  ATP binding(163-170)
PIMESIGNAK TTRNDNSSRF GKYIEIGFDK RYRIIGANMR TYLLEKSRVV FQAEEERNYH IFYQLCASAK LPEFKMLRLG NADNFNYTKQ GGSPVIEGVD
  Swich I (214-221)
DAKEMAHTRQ ACTLLGISES HQMGIFRILA GILHLGNVGF TSRDADSCTI PPKHEPLCIF CDLMGVDYEE MCHWLCHRKL ATATETYIKP ISKLQATNAR
DALAKHIYAK LFNWIVDNVN QALHSAVKQH SFIGVLDIYG FETFEINSFE QFCINYANEK LQQQFNMHVF KLEQEEYMKE QIPWTLIDFY DNQPCINLIE
  Swich II (437-447)
SKLGILDLLD EECKMPKGTD DTWAQKLYNT HLNKCALFEK PRLSNKAFII QHFADKVEYQ CEGFLEKNKD TVFEEQIKVL KSSKFKMLPE LFQDDEKAIS
PTSATSSGRT PLTRTPAKPT KGRPGQMAKE HKKTVGHQFR NSLHLLMETL NATTPHYVRC IKPNDFKFPF TFDEKRAVQQ LRACGVLETI RISAAGFPSR
  Actin binding(643-655)
WTYQEFFSRY RVLMKQKDVL SDRKQTCKNV LEKLILDKDK YQFGKTKIFF RAGQVAYLEK LRADKLRAAC IRIQKTIRGW LLRKKYLRMR KAAITMQRYV
  IQ1   IQ2
RGYQARCYAK FLRRTKAATI IQKYWRMYVV RRRYKIRRAA TIVLQSYLRG FLARNRYRKI LREHKAVIIQ KRVRGWLART HYKRSMHAII YLQCCFRRMM
  IQ3   IQ4   IQ5   IQ6
AKRELKKLKI EARSVERYKK LHIGMENKIM QLQRKVDEQN KDYKCLVEKL TNLEGIYNSE TEKLRSDLER LQLSEEEAKV ATGRVLSLQE EIAKLRKDLE
QTRSEKKCIE EHADRYKQET EQLVSNLKEE NTLLKQEKEA LNHRIVQQAK EMTETMEKKL VEETKQLELD LNDERLRYQN LLNEFSRLEE RYDDLKEEMT
LMVHVPKPGH KRTDSTHSSN ESEYIFSSEI AEMEDIPSRT EEPSEKKVPL DMSLFLKLQK RVTELEQEKQ VMQDELDRKE EQVLRSKAKE EERPQIRGAE
LEYESLKRQE LESENKKLKN ELNELRKALS EKSAPEVTRA EEQKLISEEDLLRK
                                    1238   Myc-Tag

Neck or Regulatory domain(768-907)
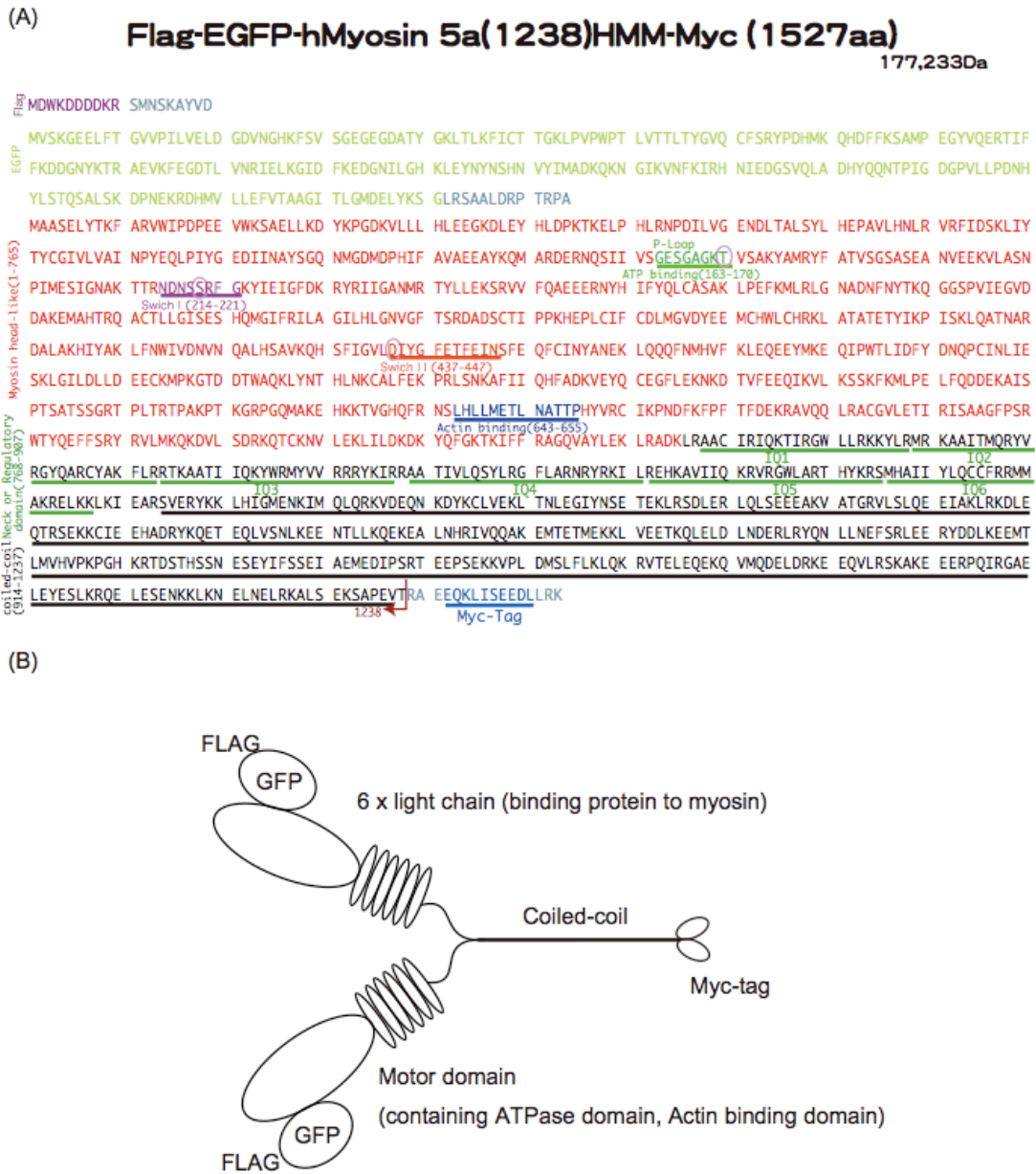coiled-coil (Neck or Regulatory domain)(914-1237)

(B)

Figure 2.3 two headed myosin-Va HMM.

(A) Amino acid sequence of two headed myosin-Va HMM (B) schematic drawing of two headed myosin-Va HMM

(this myosin mutant was constructed by A.H. Iwane, Ph. D.)

(A)

Flag-GFP-hMyosin 5a (926)IQ6-S1-myc (1216aa)

140,375Da

Flag MDYKDDDDKR SMNSKAYVDM VSKGEELFTG VVPILVELDG DVNGHKFSVS GEGEGDATYG KLTLKFICTT GKLPVPWPTL VTTLTYGVQC FSRYPDHMK(

EGFP HDFFKSAMPE GYVQERTIFF KDDGNYKTRA EVKFEGDTLV NRIELKGIDF KEDGNILGHK LEYNYNSHNV YIMADKQKNG IKVNFKIRHN IEDGSVQLAD
HYQQNTPIGD GPVLLPDNHY LSTQSALSKD PNEKRDHMVL LEFVTAAGIT LGMDELYKSG LRSAALDRPT RPA

MAASELYTKF ARVWIPDPEE VWKSAELLKD YKPGDKVLLL HLEEGKDLEY HLDPKTKELP HLRNPDILVG ENDLTALSYL HEPAVLHNLR VRFIDSKLIY

Myosin head-like(1-765) TYCGIVLVAI NPYEQLPIYG EDIINAYSGQ NMGDMDPHIF AVAEEAYKQM ARDERNQSII VSGESGAGKT VSAKYAMRYF ATVSGSASEA NVEEKVLASN
ATP binding(163-170)
PIMESIGNAK TTRNDNSSRF GKYIEIGFDK RYRIIGANMR TYLLEKSRVV FQAEEERNYH IFYQLCASAK LPEFKMLRLG NADNFNYTKQ GGSPVIEGVD
DAKEMAHTRQ ACTLLGISES HQMGIFRILA GILHLGNVGF TSRDADSCTI PPKHEPLCIF CDLMGVDYEE MCHWLCHRKL ATATETYIKP ISKLQATNAF
DALAKHIYAK LFNWIVDNVN QALHSAVKQH SFIGVLDIYG FETFEINSFE QFCINYANEK LQQQFNMHVF KLEQEEYMKE QIPWTLIDFY DNQPCINLIE
SKLGILDLLD EECKMPKGTD DTWAQKLYNT HLNKCALFEK PRLSNKAFII QHFADKVEYQ CEGFLEKNKD TVFEEQIKVL KSSKFKMLPE LFQDDEKAIS
PTSATSSGRT PLTRTPAKPT KGRPGQMAKE HKKTVGHQFR NSLHLLMETL NATTPHYVRC IKPNDFKFPF TFDEKRAVQQ LRACGVLETI RISAAGFPSF
Actin binding(643-655)

Neck or Regulatory domain(768-907) WTYQEFFSRY RVLMKQKDVL SDRKQTCKNV LEKLILDKDK YQFGKTKIFF RAGQVAYLEK LRADKLRAAC IRIQKTIRGW LLRKKYLRMR KAAITMORYV
RGYQARCYAK FLRRTKAATI IQKYWRMYVV RRRYKIRRAA TIVLQSYLRG FLARNRYRKI LREHKAVIIQ KRVRGWLART HYKRSMHAII YLQCCFRRMM
IQ1 IQ2
AKRELKKLKI EARSVERYKK LHIGMEFQAE EQKLISEEDL LRK IQ4 IQ5 IQ6
IQ3
926← Myc-Tag

(B)
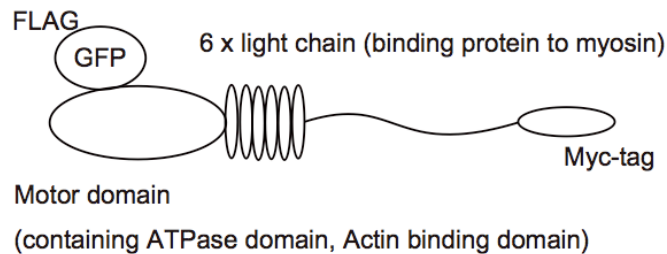
Figure 2.4 single headed myosin-Va S1 IQ6.

(A) Amino acid sequence of single headed myosin-Va S1 IQ6 (B) schematic drawing of single headed myosin-Va S1 IQ6

(this myosin mutant was constructed by A.H. Iwane, Ph. D.)

(A) 2'-,3'-O-EDA-ATP   (B) 2'-,3'-O-HDA-ATP
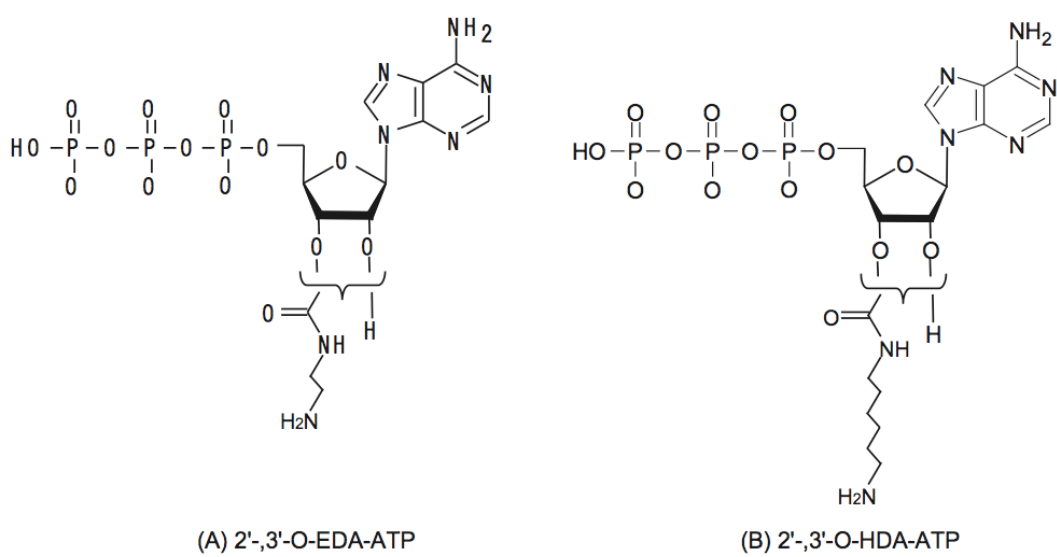
Figure 2.5 the ribose ring modified precursor of fluorescent ATP analogs
(A) 2',3'-*O*-EDA-ATP (B) 2',3'-*O* -HDA-ATP

(A) 2'-*O*-Cy3-EDA-ATP

(B) 3'-*O*-Cy3-EDA-ATP

(C) Cy3-NH-ATP

(D) 2', 3'-*O*-Cy3-HDA-ATP
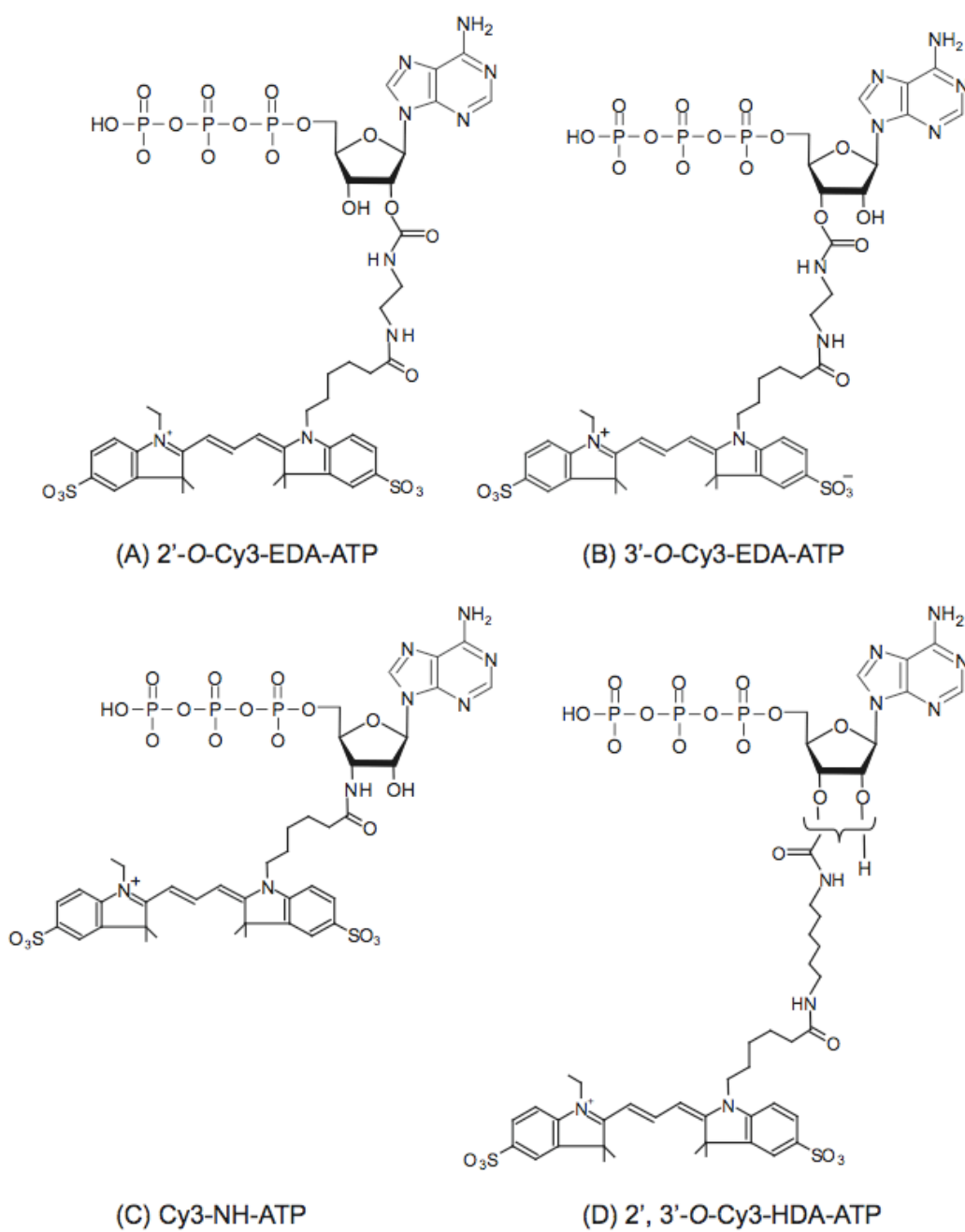
Figure 2.6 Cy3-dye labeled fluorescent ATP analogs

(A) 2',3;-ATTO 520-EDA-ATP

(B) 2',3;-ATTO 550-EDA-ATP

(C) ATTO520-g-(6-aminohexyl-ATP

Figure 2.7 ATTO-dye labeled fluorescent ATP analogs

(A) 8-[(6-amino)hexyl]-amino-ATP

(B) N^6-(6-amino)hexyl-ATP

Figure 2.8 the adenine ring modified precursor of fluorescent ATP analogs
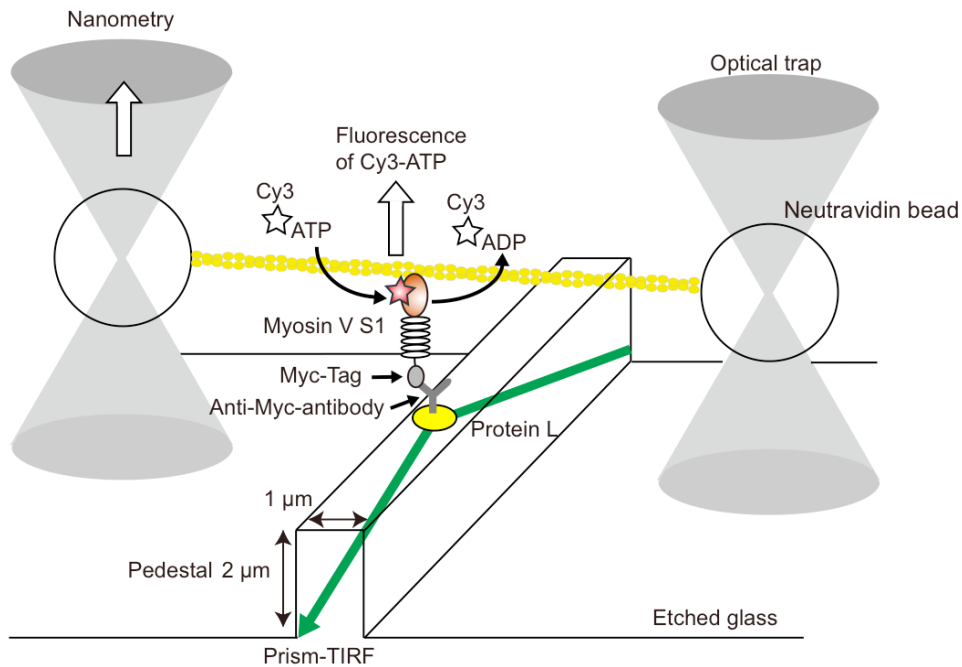
Figure 2.9. **Experimental setup for simultaneous observation of ATP-turnover cycles and force generation.**

Myosin-V S1 was immobilized on the pedestal of a glass slide. Myosin displacement was measured by tracking the change in position of one of the neutravidin coated polystyrene beads using a quadrant photodiode (QPD) at a sampling rate of 20 kHz for the simultaneous observation or 1 kHz to determine the response time of the experimental setup (see "measuring the timing between chemical events and mechanical events"). The ATP turnover was measured by monitoring the fluorescence from a Cy3-nucleotide that associated with and dissociated from the myosin head using TIRFM with a green laser (λ = 532 nm) and an avalanche photodiode (APD) at a sampling rate of 100 Hz for simultaneous observation or 1 kHz to determine the response time of the experimental setup. The output signals from the QPD and the APD were simultaneously recorded on a PC using a digital data recorder.

(the photon counting LabVIEW program was constructed by S. Nishikawa, Ph. D. and modified by T.K.)
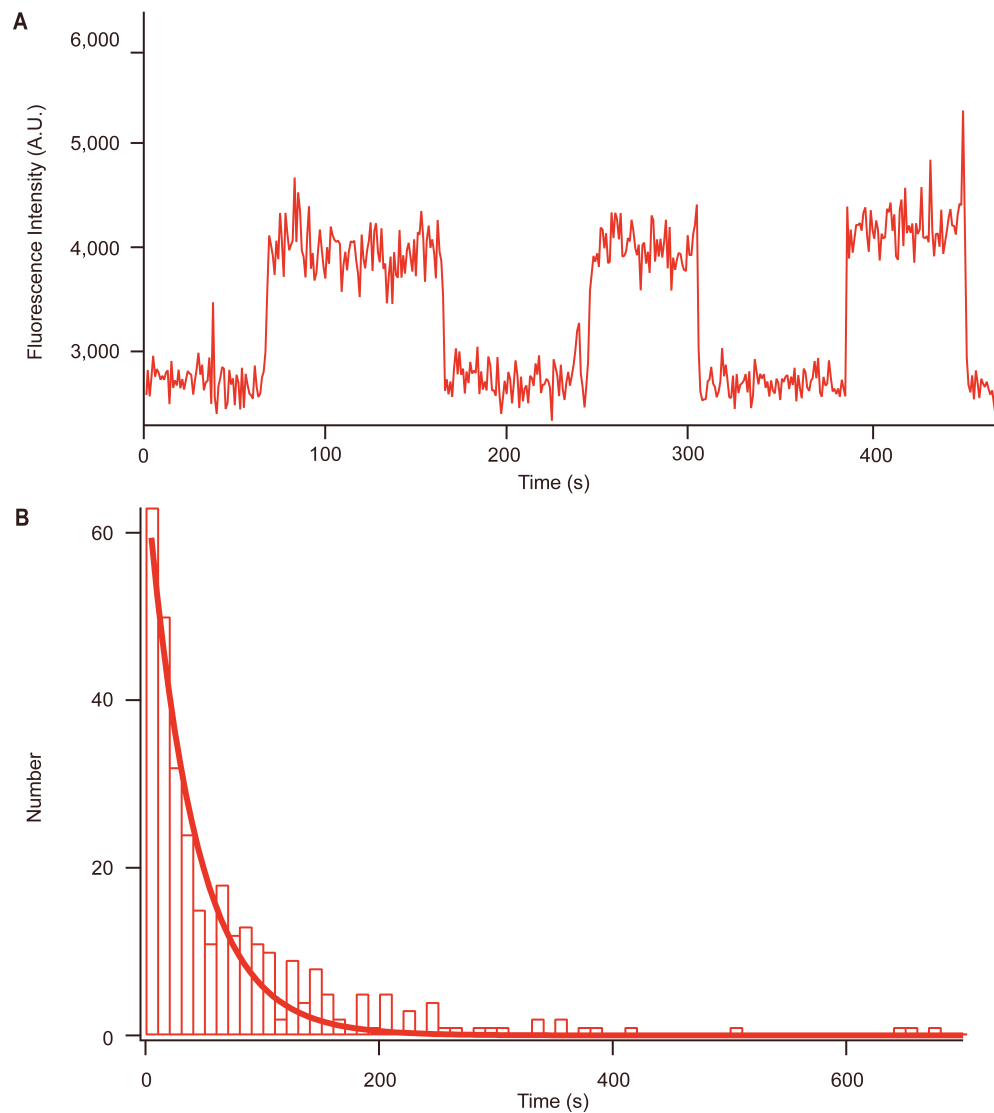
Figure 2.10 Individual Cy3-ATP turnovers by myosin-V S1

  (A) Using TIRFM and Cy3-ATP, the appearance and disappearance of Cy3-fluorescence were observed at the myosin-V S1 position according to a method previously described (Komori et al., 2008). The myosin-V position was determined by following the fluorescence spot of the attached GFP. Fluorescent images were observed using prism type TIRFM every 1 s for 15 min. Fluorescent images of individual ATP turnovers were converted into time trajectories of fluorescence intensities using ImageJ (http://www.rsb.info.nih.gov/ij/). **(B)** The interval between the appearance and the disappearance of Cy3-fluorescence was well fit to a single exponential decay function with a rate constant of 0.02 ± 0.001 s^{-1} (mean ± s.e.m.: n=323).
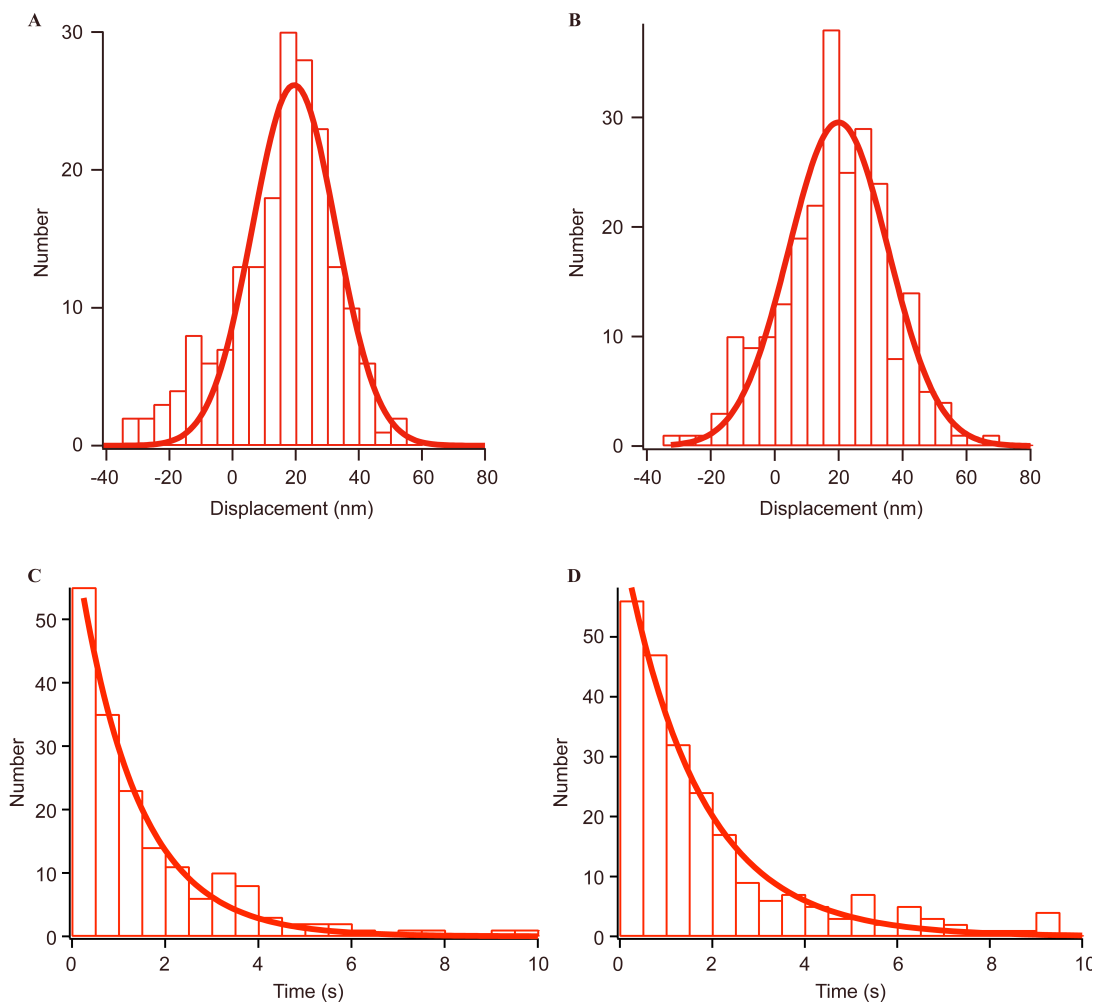
Figure 2.11 The effect of Cy3-ATP on myosin-V S1 stroke size and dwell time

  (A) Myosin-V S1 stroke size was determined in 1 μM ATP according to a method previously described (Komori et al., 2008; Molloy et al., 1995). Stroke size distribution for 1 μM ATP was well fit to a Gaussian function with a mean ± s.d. of 20 ± 14 nm (n=190). **(B)** Stroke size distribution for 1 μM Cy3-ATP. A 20 ± 16 nm stroke size (mean ± s.d.: n=238) was determined as described above. **(C)** The dwell time during displacement for 1 μM ATP. The solid line indicates a single exponential decay fit. **(D)** The dwell time during displacement for 1 μM Cy3-ATP.

(A)

(B)
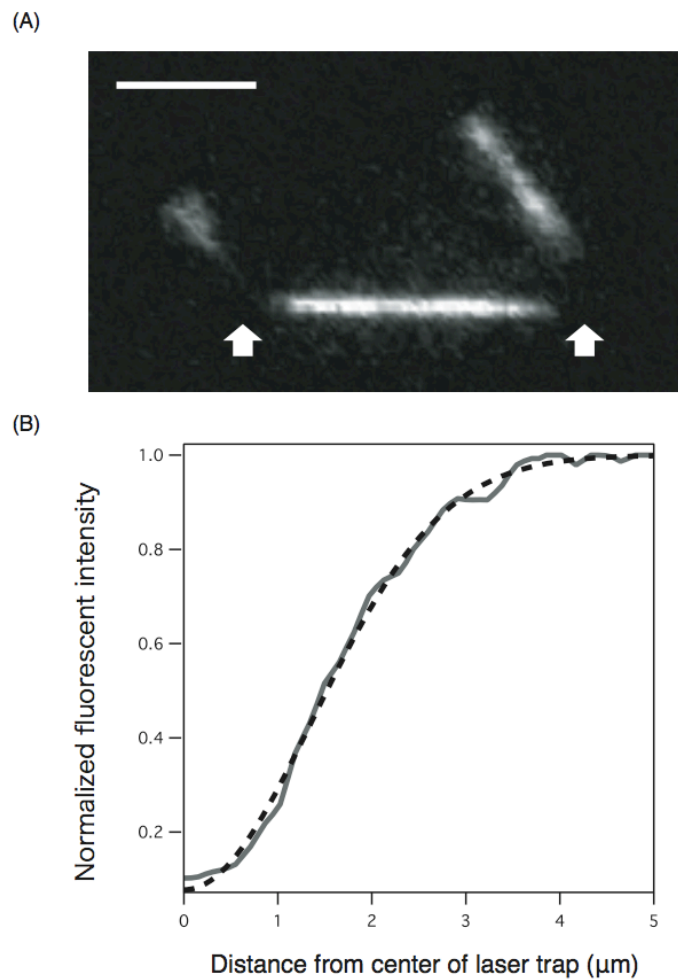
Figure 2.12 Cy3 photobleaching by a 1064 nm trapping laser

(A) Photobleaching of Cy3-Phalloidin labeled actin filaments. A Cy3-phalloidin labeled actin filament was tethered using two optical traps under simultaneous excitation by a 532 nm laser and a 1064 nm laser. Over 15 μm long filaments were selected. The center of the optical traps are indicated by white arrows. Photobleaching by the 1064 nm laser occurred near the optical trap center. Scale bar, 5 μm. (B) Photobleaching of Cy3 dye enhanced by the 1064 nm infrared laser. The fluorescence intensity of Cy3-phalloidin was measured against the distance from the optical trap center to quantify the range of photobleaching caused by the 1064 nm infrared laser. Twenty-seven filaments were averaged. The fluorescent intensity decay was fit to a Gaussian function with a S. D. of 1.3 μm (dashed line).

(A)

(B)

(C)

(D)
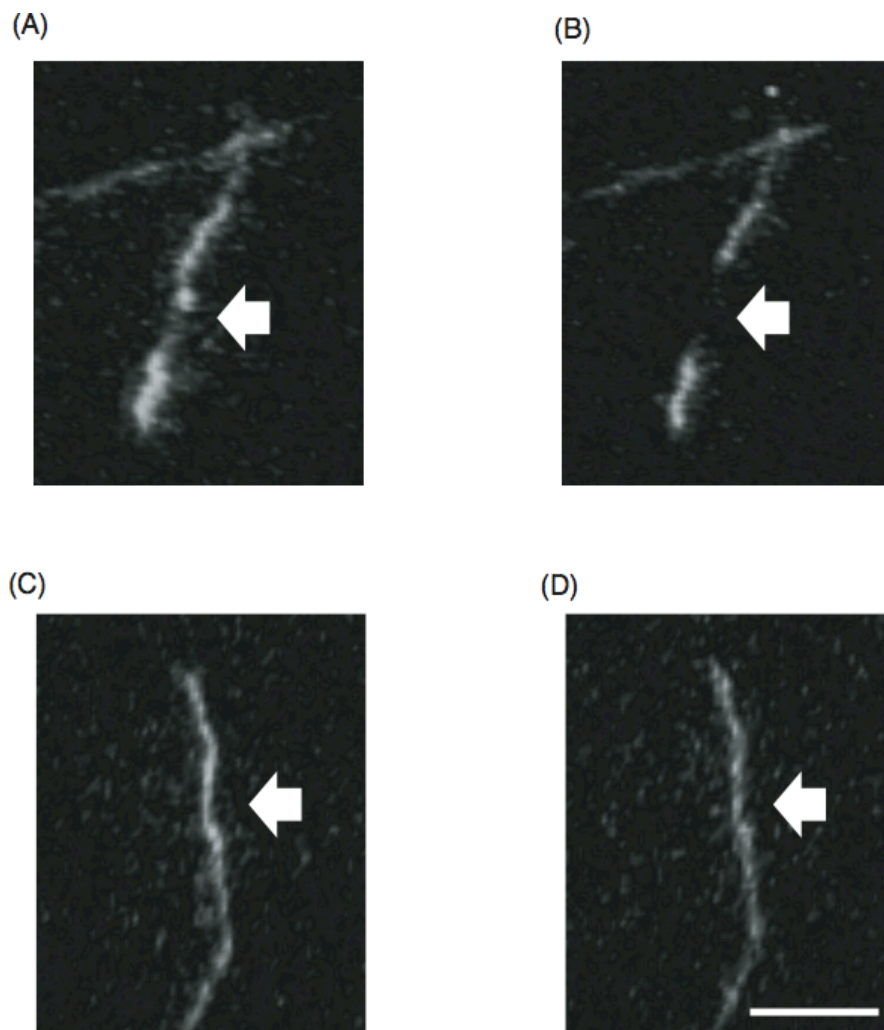
Figure 2.13 The effect of a trapping laser on Cy5-maleimide and Cy5-phalloidin labeled actin filaments

(A)(B) Cy5-maleimide labeled actin filament. Cy5-maleimide labeled actin filament fixed to a glass surface via rigor state muscle type myosin II and excited by both a 633 nm laser and a 1064 nm laser. The position of the optical traps is indicated by the white arrow. Images were taken immediately at (A) and 15 s after excitation at (B). (C)(D) Cy5-phalloidin labeled actin filament. Using the same method, a Cy5-phalloidin labeled actin filament was fixed and excited. Images were taken immediately at (C) and two minutes after excitation at (D). Scale bar, 5 μm.

(A)

(B)
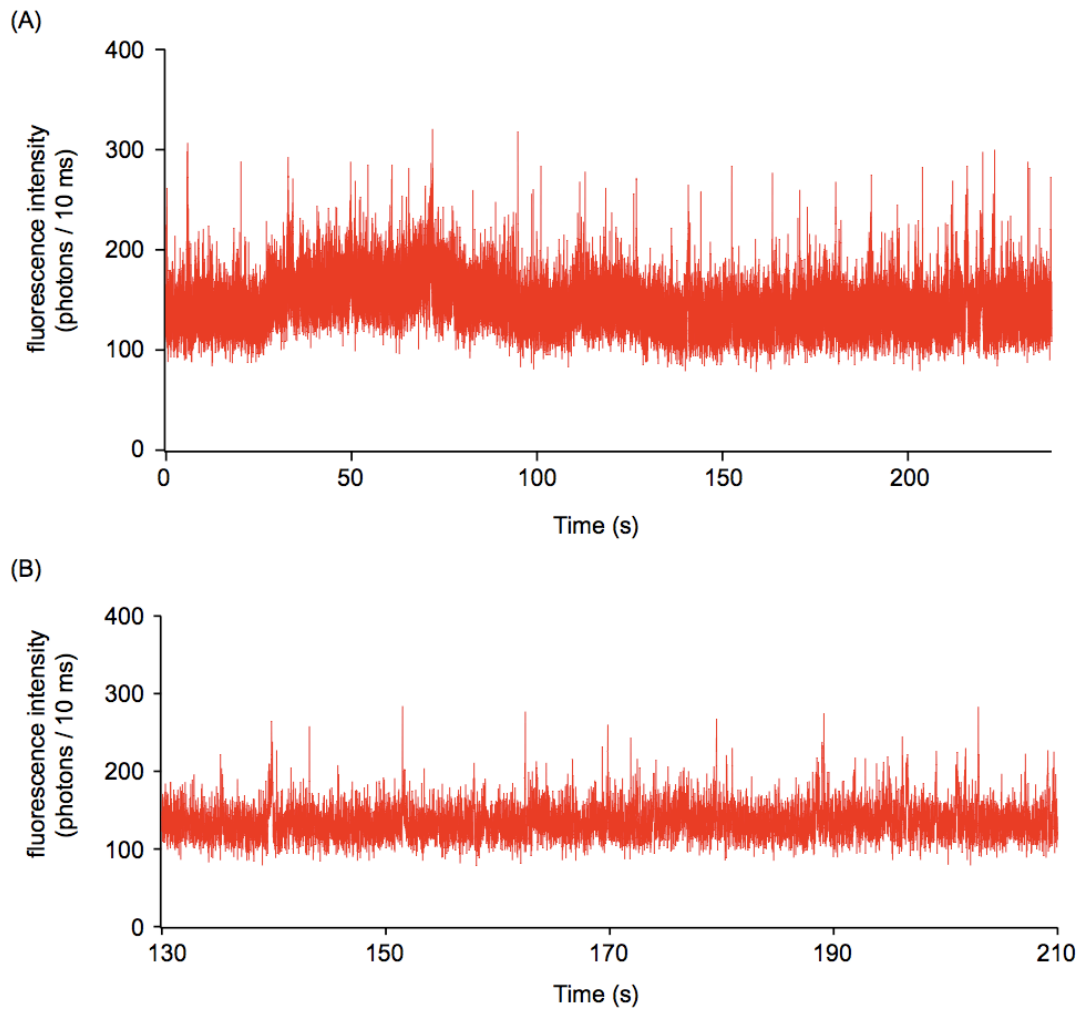
Figure 2.14 Non-specific binding of Cy3-ATP to glass surface.

(A) Non-specific binding of 100 nM Cy3-ATP to casein including 0.5%(v/v) Pluronic F-127, ProteinL and anti-Myc antibody coated glass surface. (B) the horizontal magnified trace of (A) (130 to 210 s range).
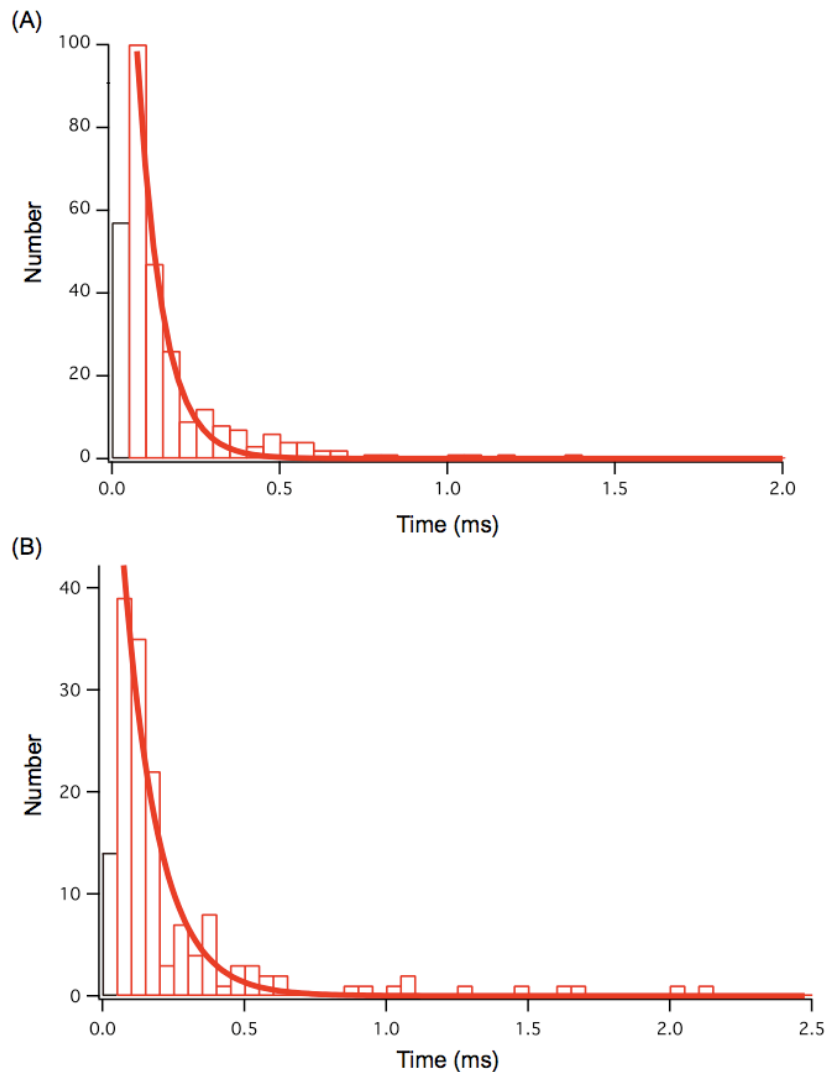
Figure 2.15 The off rate constant of non-specific bound Cy3-ATP.

(A) The non-specific binding time distribution of 100 nM Cy3-ATP to casein including 0.5%(v/v) Pluronic F-127, ProteinL and anti-Myc antibody coated glass surface. The solid line indicates a single exponential decay fit of 10 ± 0.2 s^{-1} (mean $\pm$ s.e.m.; n =293) .

(B) The non-specific binding time distribution of 100 nM Cy3-ATP to above proteins with ADP-Vi blocked myosin-V S1 coated glass surface. The solid line indicates a single exponential decay fit of 8.1 ± 0.6 s^{-1} (mean $\pm$ s.e.m.; n =155) .

(A) GFP-Myosin V S1
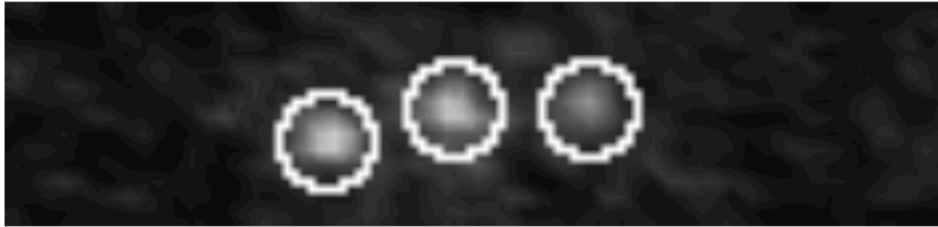
(B) Cy3-ATP

Figure 2.16 Single molecule imaging of Cy3 and GFP on the pedestal

(A) A fluorescent image of myosin V S1 fixed on the pedestal. (B) A fluorescent image of Cy3-nucleotides attached to a myosin V S1 indicated by white circles. Scale bar, 3 μm.
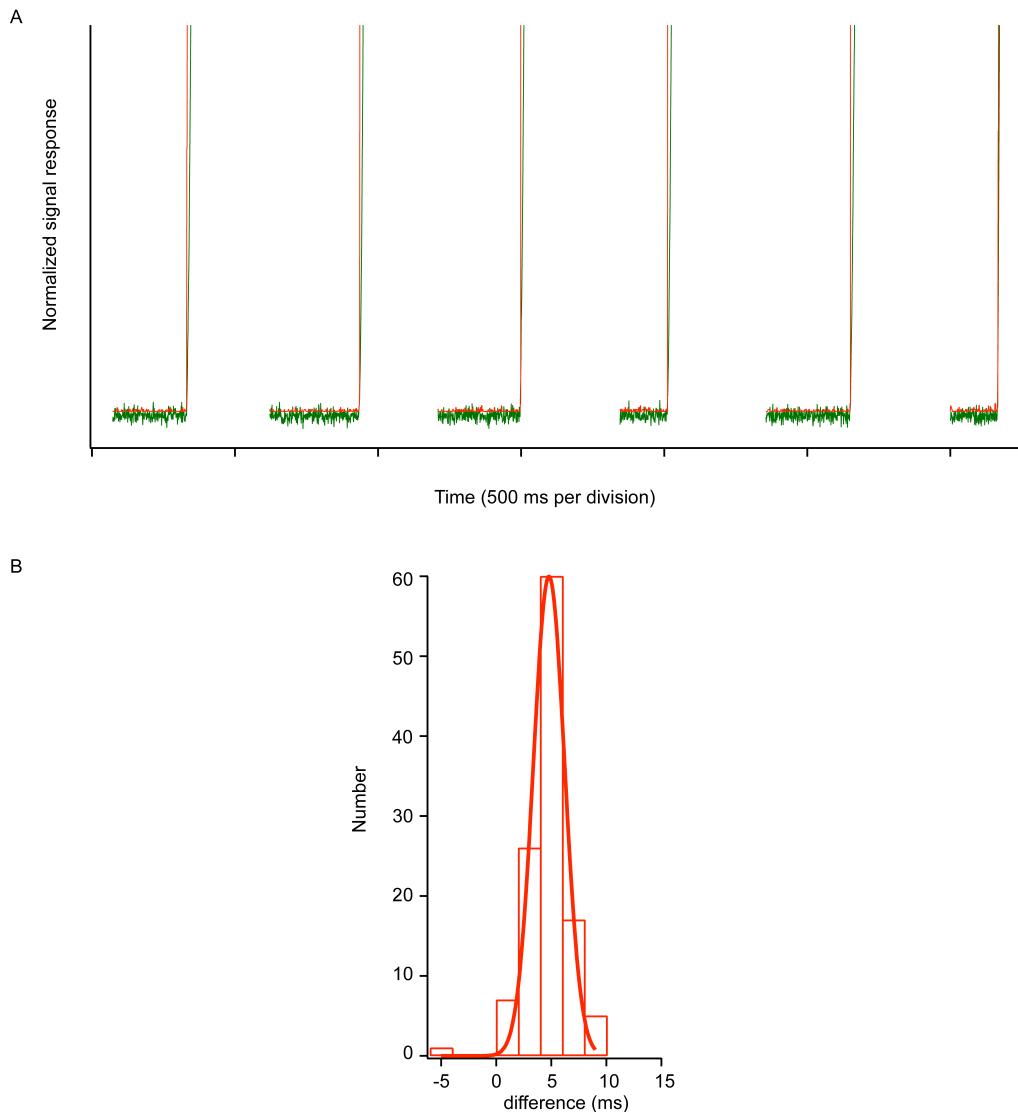
A

Time (500 ms per division)

B

difference (ms)

Figure 2.17 Signal response of APD and QPD

(A) The red trace shows signal output from APD, while the green trace shows signal output from QPD. Both signals were recorded at a 1 kHz sampling rate to compare the signal response difference between these two detectors. The vertical axis shows the relative relationship of the signal output from the two detectors. The horizontal axis shows the time scale (500 ms per division). **(B)** Histogram of the difference of response times. Positive values indicate that the QPD responded before the APD. The solid line indicates a Gaussian function fit with a mean ± s.d. of 4.8 ± 1.4 ms (n=116), meaning the QPD responded 4.8 ms before the APD. However, it is shorter than the data point intervals in 100 Hz sampling rate of the APD or 100 Hz low pass filter rate for displacement trace from the QPD.
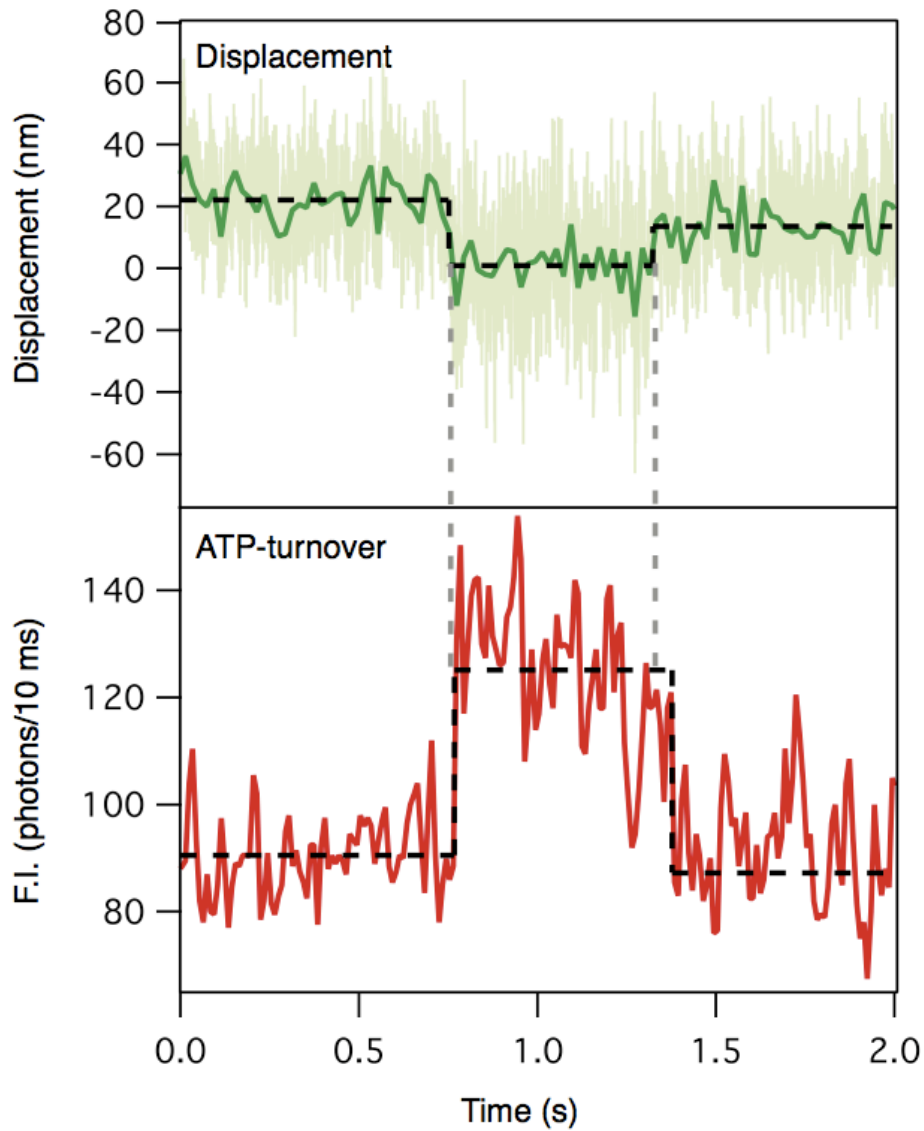
Figure 2.18 Time trajectory of the displacement of myosin V S1 and the ATP turnover

Displacement and ATP turnovers were measured at 100 nM Cy3-ATP with 1 μM ATP. The upper trace shows the time course of displacements. Raw data and 100 Hz bandwidth low-pass filtered data are superimposed. The lower trace shows changes in the fluorescence intensity of Cy3-nucleotide at the myosin V head. The data were filtered by a median filter of rank 2.

Chapter III

Simultaneous observation of single-headed myosin-V.

3.1. Introduction

Myosin-V is the most commonly studied processive motor (Mehta et al., 1999; Sakamoto et al., 2000; Yildiz et al., 2003). By forming a homodimer, myosin-V transports cargos over long distances requiring many ATP-turnover cycles without detaching from the actin-filament. During these cycles, ATP binds to myosin-V and is hydrolyzed to ADP, which is then released. Although ADP-release is thought to contribute to the myosin-V motility, there is no direct evidence affirming the relationship between ADP release and force generation (Oguchi et al., 2008; Purcell et al., 2005; Veigel et al., 2005). Measurments of ADP-release, Pi-release and Pyrene-actin fluorescence in biochemical studies have indicated a relationship between ADP-release and Pi-release or the weak to strong transition in the actomyosin binding state (De La Cruz et al., 1999; Forgacs et al., 2006; Rosenfeld and Sweeney, 2004). However, these studies could only speculate on the relationship between ADP-release and force generation or mechanical displacement between myosin and actin. Meanwhile, mechanical studies of myosin-V could observe the timing of the force generation, but they could not directly observe the ADP-release step (Purcell et al., 2005; Veigel et al., 2005). Therefore, there is no direct experimental observation of the relationship between ADP-release and force generation.

In this chapter, we attempted to clarify the timing of these events and resolve the role of ADP-release in myosin-V based motility.

3.2. Materials and method

3.2.1. Simultaneous observation of ATP-turnover cycles and myosin-V S1 displacement

Simultaneous measurement of ATP-turnover cycle and myosin-V displacement was performed according to the method described in the previous chapter.

3.2.2. Measuring the timing between chemical events and mechanical events

Displacement and ATP-turnover cycle were determined respectively using Matlab stepfinder routines kindly provided by J. Kerssemakers and M. Dogterom (Kerssemakers et al., 2006). The algorithm of this software was described in "Appendix 3". The difference between ATP-binding and myosin-V detachment was calculated by subtracting the time of ATP-binding from that of myosin-V detachment, while the difference between ADP-release and force generation was calculated by subtracting the time of force generation from that of ADP-release.

3.3. Results and discussion

3.3.1. Manipulation procedures for simultaneous observation

At first, a biotinylated and Cy5-phalloidin labeled actin filament was tethered between two trapped neutravidin coated polystyrene beads, each of 1 μm diameter by monitoring the fluorescent image illuminated using the blue laser (Fig 3.1). The actin dumbbells were stretched to 1 pN resulting in a net stiffness of 0.019 pN·nm^{-1}. In this condition, 0.02 to 0.88 pN (mean 0.34 pN) backwards force along the actin filament axis was applied to myosin-V S1 during the actomyosin interaction. To adjust the detected area of APD to the postion of myosin-V on the pedestal, the actin filament, tethered by two trapped beads, was moved on the detected area of APD with monitoring the fluorescent image by manipulating the controllable trapped bead. Next the detected area was moved on the pedestal by monitoring the bright field image by manipulating the stage (MP-285; Sutter instruments). Then, the excitation laser was exchange from the blue laser to the green laser to visualize Cy3-ATP and power off the CCD camera and II to remove the noise from the camera fun. Finally, the APD detected area was moved in order to find a single molecule myosin on the pedestal (1 μm width), indicated by non-processive steps (Fig. 3.2 upper trace) along the horizontal axis, by manipulating the stage. We do not have to search along the vertical axis of the pedestal, because the detected area of APD (0.9 μm) is almost same length as the vertical length of pedestal (0.8 – 1.0 μm). As the result, the relationship between the chemical event and

47

mechanical event of myosin-V was observed directly by using this developed measurement system (Fig. 3.2).

3.3.2. Simultaneous observation of myosin-V S1

Figure 3.2 (upper trace) shows the time course displacements by myosin-V S1 of a bead-actin-bead dumbell held in the optical trap. The rising and falling phases correspond to the force generation of myosin-V S1 and its detachment from the actin filament, respectively. Fig. 3.2 (bottom trace) shows the time course of the fluorescence intensity changes of the Cy3-nucleotide. Fluorescent-spots were observed coupled to the mechanical cycles (filled arrow). Since the fluorescent spots appeared at almost the same time as the falling-phase of the displacement, these events were attributed to Cy3-ATP-binding to myosin-V S1. The fluorescent spots disappeared following the subsequent rising phase of the displacement. Since force-generation is unlikely to be coupled to ATP release and Pi dissociates rapidly from acto-myosin-V-ADP-Pi (De La Cruz et al., 1999; Forgacs et al., 2008; Rosenfeld and Sweeney, 2004), the reduction of intensity was attributed to release of the Cy3-ADP from acto-myosin-V-Cy3-ADP. Some displacements (Fig. 3.2, white arrows) did not couple to detection of fluorescent-spots suggesting that these events likely accompanied binding of non-fluorescent ATP. The fraction of mechanical events coupled to Cy3-nucleotide binding was 2.5%. The ratio of ATP (1 μM) to Cy3-ATP (100 nM) in the medium and the lower affinity of Cy3-ATP for actomyosin-V (Table S1) accounts for the observed

proportion of Cy3-associated mechanical events. This result is consistent with a recent report showing 1:1 coupling between stepping of double-headed myosin-V and binding of deac-amino-ATP (Sakamoto et al., 2008).

3.3.3. The relatioship between myosin-V S1 detachment and ATP-binding.

ATP-binding to myosin-V S1 occurred concomitantly with the falling-phase of the displacement, indicating Cy3-ATP induced detachment of myosin-V S1 from actin (Figure 3.3A). The distribution of delay times between ATP-binding and myosin-V S1 detachment, which were determined respectively using a stepfinder MatLab routine kindly provided by Drs. J. Kerssemakers and M. Dogterom (Kerssemakers et al., 2006), was fitted by a Gausssian function with a mean ± s.d. of 6.0 ± 31 ms (n=61) (Figure 3.3B). The deviation indicates the limit of resolution for effectively detecting the event times (Ishijima et al., 1998). Thus, we conclude myosin-V S1 detachment occurred promptly upon ATP-binding.

3.3.4. The relatioship between myosin-V S1 force generation and ADP release.

ADP-release always occurred following force generation after a delay (Figure 3.4A). The delay time distribution was fitted by a single exponential function with a mean rate constant ± s.e.m. of 14 ± 1.1 s^{-1} (n=61), indicating ADP is released from myosin-V in a first-order process (Figure 3.4B). This value agrees with several biochemical studies

reporting an ADP-release rate from the actomyosin-V-ADP complex of 12 to 22 s^{-1} (De La Cruz et al., 1999; Trybus et al., 1999). The same studies also suggested that myosin-V spends the majority of it's ATPase cycle bound in the acto-myosin V-ADP state. Other studies have shown that ADP-release follows Pi-release (Forgacs et al., 2006; Forgacs et al., 2008; Rosenfeld and Sweeney, 2004). Thus the observed ADP release following force generation corresponds to the elementary ADP-release process from actomyosin-V-ADP, not the ADP-Pi complex. This is the first direct evidence of slow ADP-release following force generation. This 14 s^{-1} ADP-release delay following force generation was consistent with 76 ms dwell time (13 s^{-1} off rate) determined using optical trap nanometry at saturated ATP concentration (Fig 3.5), meaning that dwell time at saturated ATP concentration consists of ADP-release delay and there is no significant refractory period (the duration when next ATP cannot bind to acto-myosin-V) following ADP-release. Furthermore, since the ADP-bound state is considered to be a strong actomyosin state, the delay of ADP-release stabilizes actomyosin binding by prolonging the strongly bound state and thus probably improves myosin-V processivity.

Recently, the ADP-release rate was found to be strongly affected by applied force (Oguchi et al., 2008; Purcell et al., 2005; Veigel et al., 2005). According to the proposed relationship between ADP-release rate and force (Veigel et al., 2005), the zero-load ADP-release rate of 12-22 s^{-1} would decrease to 9-16 s^{-1} at 0.34 pN, the average force applied in our experiments (see above section). However, this force level is too small to make conclusions about the force dependence of ADP-release from the present

experiments. Experiments with higher forces are required. Aatually, no correlation was found between ADP-release delay and applied force in our applied fore range (Fig 3.6).

Interpretation of biochemical assays of ADP- and Pi-release and the weak-to-strong transition have assumed that force generation coincides with the release of Pi (De La Cruz et al., 1999). This assumption is based on crystal structure experiments that examined the linkage between rotation of the myosin lever arm and occupancy of the active site with various ATP-analogs (Coureux et al., 2004; Volkmann et al., 2005). Force generation and relative sliding of myosin and actin can only be measured by mechanical excperiments. In fact, optical trap studies of the dwell times of single myosin-V molecules have also suggested a slow and delayed ADP-release (Purcell et al., 2005; Veigel et al., 2005), consistent with the present experiments. Our report is the first study to directly reveal the relationship between ADP-release and force generation or filament sliding in myosin V (Fig 3.7).

3.3.5. ADP-release coupled displacement was not found.

Conformational changes in the myosin-V head in response to the presence and absence of ADP have been observed in crystal structures (Coureux et al., 2004; Coureux et al., 2003; Volkmann et al., 2005). Another study has reported the ADP-release coupled displacement (Veigel et al., 2005). We selected 17 events which have over 100 ms

ADP-relase delay to test whether an additional displacement couples to the conformational change caused by ADP-release, since under 100 ms delay is not sufficient to compare the relationship between displacement around ADP-release. Using Kerssemaker's algorithm (Kerssemakers et al., 2006), we investigated whether each of the 17 events contain an additional displacement near the moment of ADP-release. No such events were found, however, because the standard deviation of the single molecule displacement trace is 6.6 nm, this analysis might be insufficient to detect small displacement (~ 5 nm) coupled with ADP-release as previously reported (Veigel et al., 2005).

3.3.6. The expectation from ADP-release delay distribution.

ADP-release delay following forece-generation distributed in a single-exponential decay function, meaning that ADP-release delay occured in a single process after forece-generaiton. This distribution also meant that some chemical process existed around force-generation and ADP-release occurred in a single process after this expected chemical event. Accoding to the biochemical assay result (De La Cruz et al., 1999), the primary chemical event before ADP-release was Pi-release. Therefore, this single exponential distribution may mean that Pi-release occurred around force genration and ADP-release occurred in a single process after Pi-release around force generaion. However, to confirm this hypothesis statistically, more data points are required.

3.3.7. Comparison with the previous study of muscle type myosin-II

In a previous study using non-processive myosin-II, our group observed ADP-release before force generation (Ishijima et al., 1998). The Cy3-ATP turnover rate of myosin-II without actin activation was 0.14-0.2 s^{-1} (Oiwa et al., 2000; Tokunaga et al., 1997) and the interval between mechanical displacements was approximately 8 s (Ishijima et al., 1998). Therefore, over half of the myosins released ADP before rebinding to actin filament. Yet myosin-II still generated a force. This observation suggested that myosin II stored the energy in a protein conformation between ADP dissociation and actin binding. Cy3-ATP-turnover rate of myosin-V without actin activation was 0.02 s^{-1} (Figure S3b), which is ten times longer than that of myosin-II, and the interval between displacements in the present study was approximately 0.6 s (data not shown). In this condition, only ~1% of ADP-release occurs before myosin-V rebinds to the actin filament, and most of the mechanical events are directly coupled to ATP-turnover. Differences in ADP affinity between myosin types are likely to explain differences in the relationship between ADP-release and force generation.

In summary, this study provides direct evidence of slow ADP-release following force generation in myosin-V. Because many other processive motors are thought to function like myosin-V except for myosin-IX (O'Connell et al., 2007), these results are likely to have broader implications. Similar results were not observed in the non-processsive

motor myosin-II (Ishijima et al., 1998), in which multiple myosin molecules assemble to form a filament and move actin-filaments together. In such an assembled system, slow ADP-release from a myosin molecule could potentially interfere with the motion generated by other molecules and disrupt motility. Thus, ADP-release is likely to be tuned to specialized functions within the myosin family.
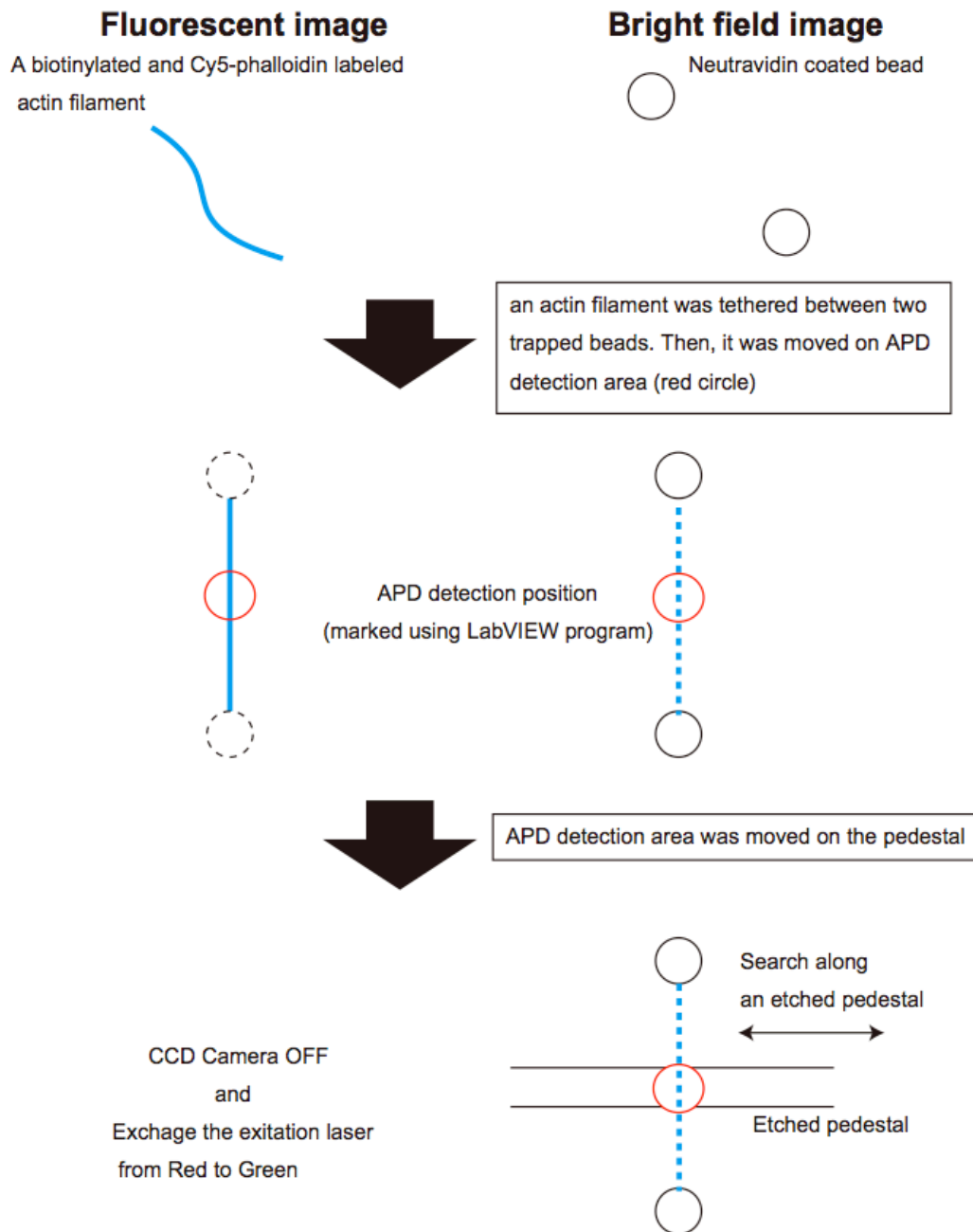
Figure 3.1 Experimental procedures for simultaneous observation.

(LabVIEW program was constructed by T. Ariga, Ph. D. and modified by T.K.)
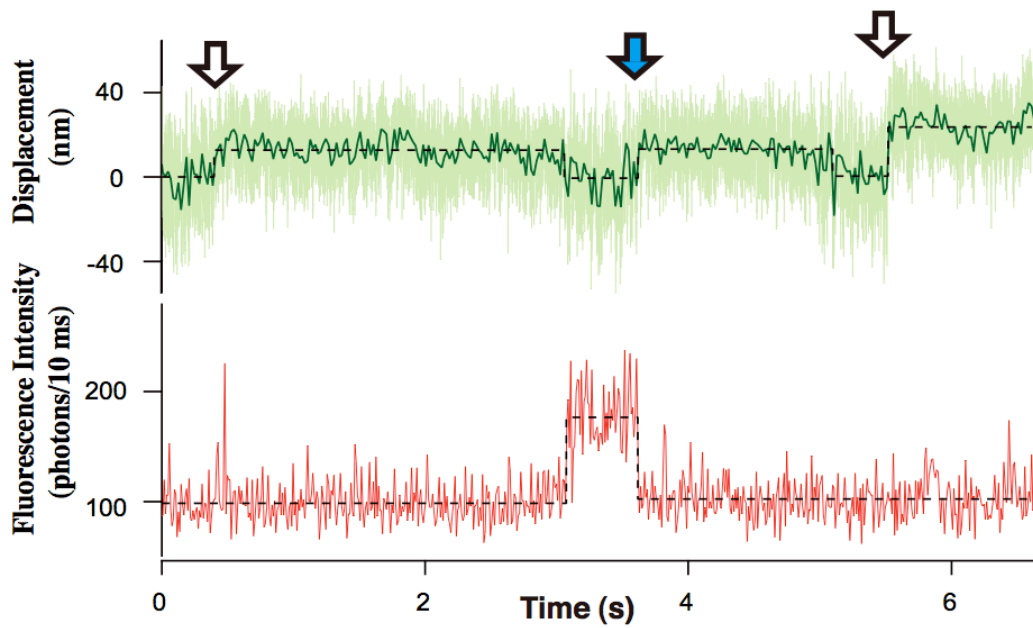
Figure 3.2 Simultaneous observation of ATP-turnover cycles and force generation by myosin-V S1.

The upper trace shows the time course of the trapped bead displacements. Raw data and data passed through a 100 Hz low pass filter are superimposed. The bottom trace shows the fluorescence intensity change of a Cy3-nucleotide located at the myosin-V position. White arrows show mechanical events coupled to binding of non-fluorescent ATP. The blue arrow shows an event coupled to binding of Cy3-ATP.
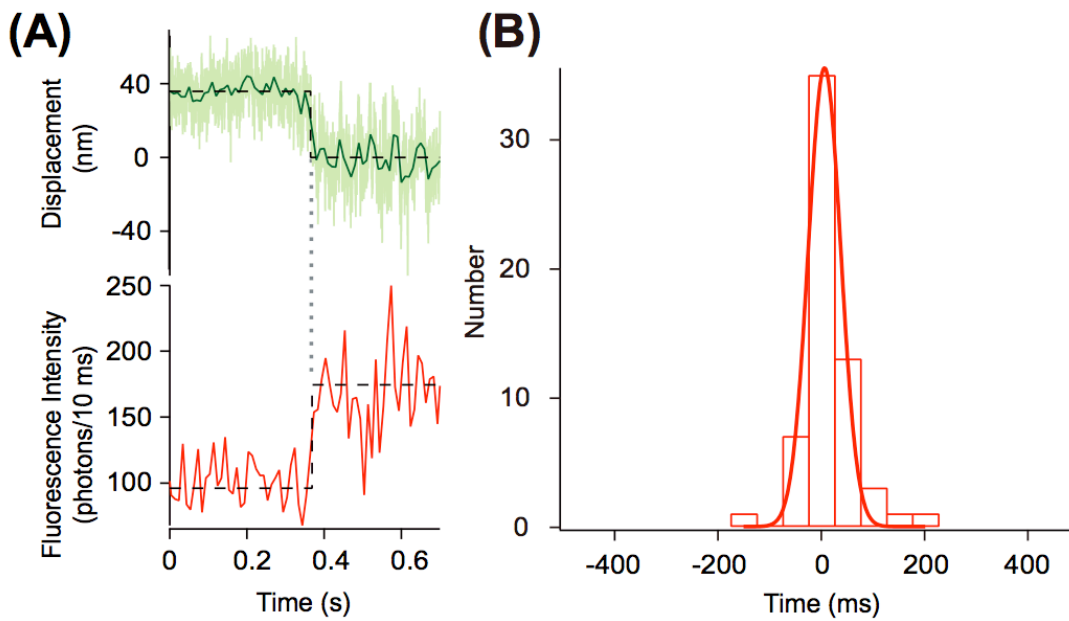
Figure 3.3 The relationship between ATP-binding and myosin-V S1 detachment.

(A) The time course of myosin-V detachment (upper-trace) and Cy3-ATP-binding (bottom-trace). (B) A histogram of the time delay between detachment of myosin-V and binding of Cy3-ATP. Positive time indicates ATP-binding before detachment. The solid line indicates a Gaussian function fit.
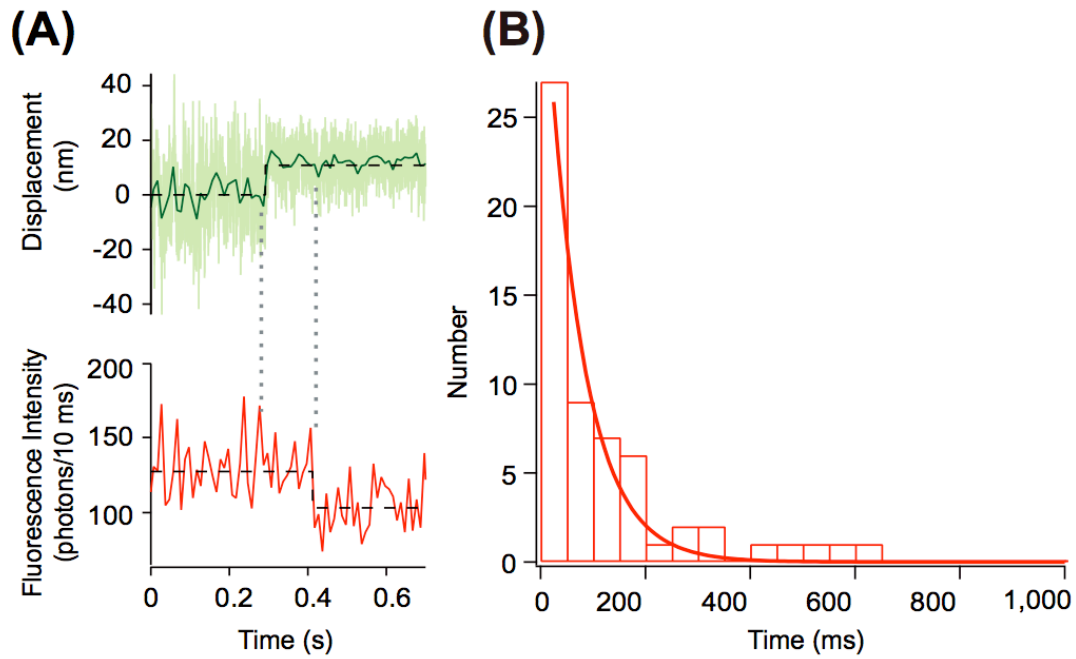
Figure 3.4 The relationship between ADP-release and force generation.

(A) Cy3-ADP-release occurred with a delay after force generation. (B) Histogram showing the delay of Cy3-ADP-release following force generation. Two outliers over 1 s were omitted. The solid line indicates a single exponential function fit.
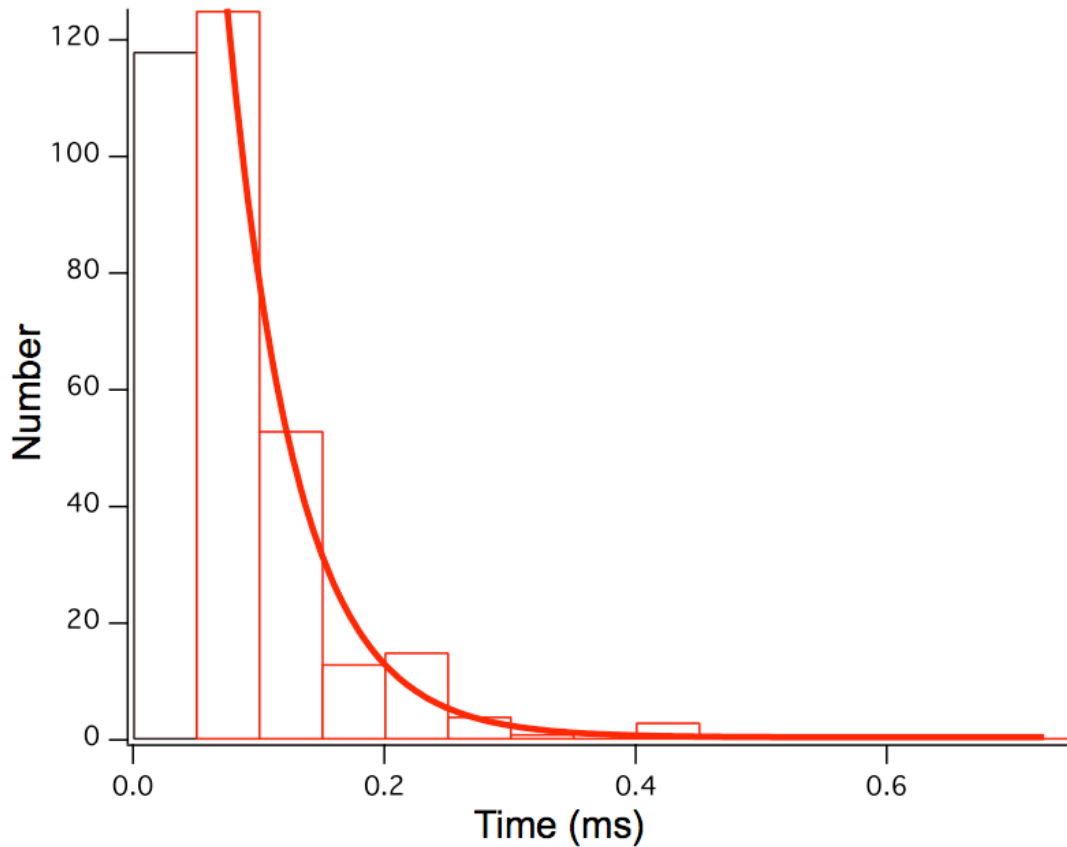
Figure 3.5 Dwell time of myosin-V S1 at saturated ATP concentration.

The dwell time during displacement for 2 mM ATP. The solid line indicates a single exponential function fit of 13 ± 0.2 s^{-1} (mean ± s.e.m.; n=332).
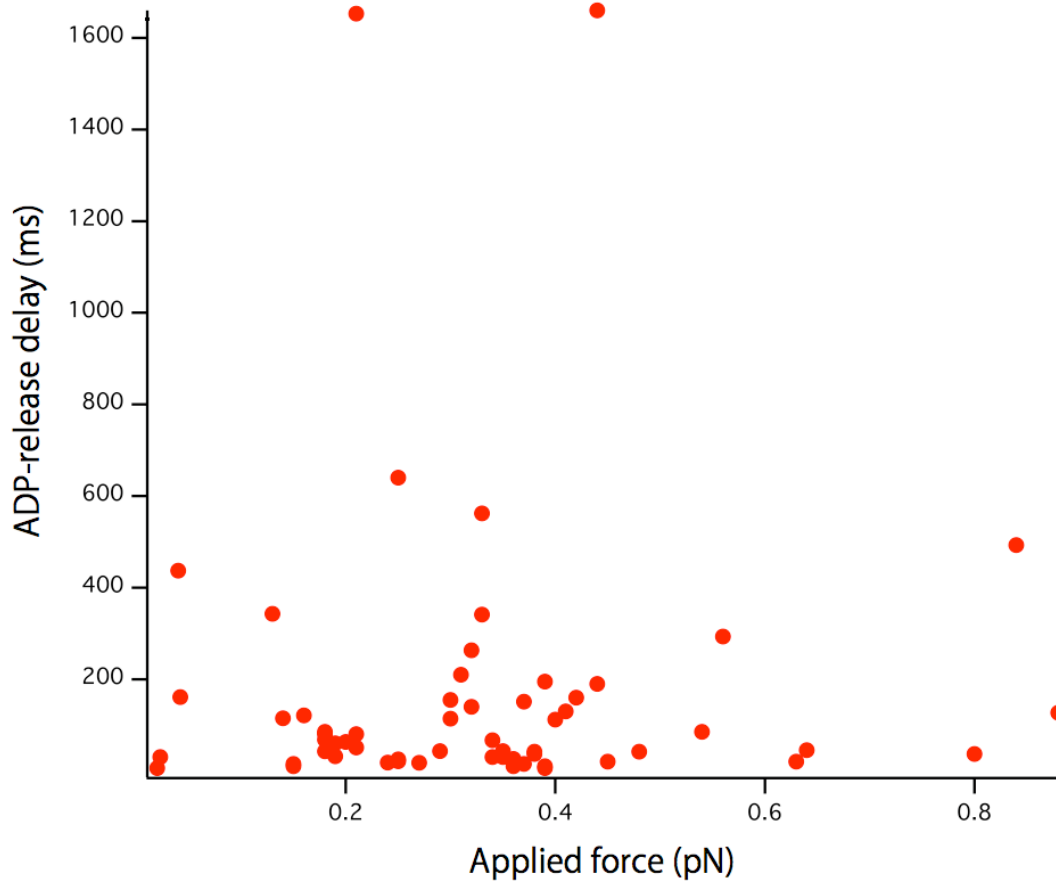
Figure 3.6 The relationship between ADP-release delay and applied force.

ADP-release delay following force generation were plotted against applied force by optical trap. No obvious correlation between them was found, meaning that in this force range, ADP-release delay were not affected by applied force.

Proposed Scheme
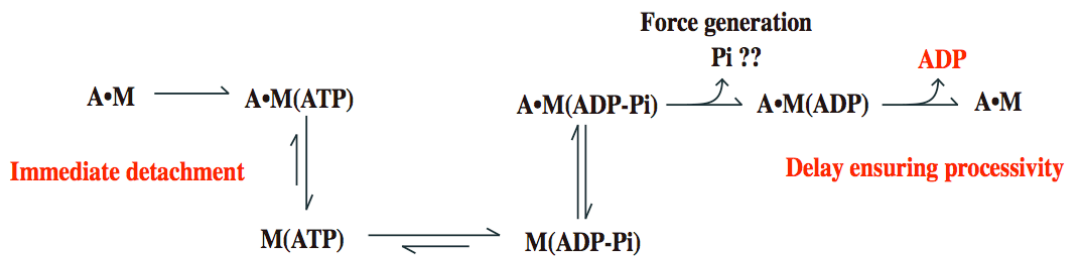
Figure 3.7 chemo-mechanocoupling scheme proposed according to the result of simultaneous observation.

This processis postulated by separate structural, mechanical and biochemical studies. The mechanical process indicated by red is determined by the simultaneous observation result. Here, A, M, Pi mean actin, myosin, inorganic phosphate, respectively.

Acknowledgement

Appendix

Appendix 1: Simultaneous observation of double headed myosin-V.

Myosin-V can move processively along an actin filament as a constructed dimer. Therefore, to clarify the relationship in processive motors between ADP-turnover cycles and force-generation, I used double headed myosin-V (myosin-V HMM). Myosin-V also generates a backward step during processive movement. However, it remains unclear whether the ATP-turnover cycle couples to these backward steps. Thus, I have performed simultaneous observation of myosin-V HMM. This study is still a work in progress. However, some conclusions have already been made.

1, ATP-turnover cycles coupled to the forward step

In the case of a forward step, myosin-V HMM produced a step after the fluorescent nucleotide Cy3-ATP bound to myosin-V HMM (Fig S1.1). A fluorescent spot disappeared after steps, indicating that Cy3-ADP was released with a delay.

2, ATP-turnover cycles coupled to the backward step

Myosin-V HMM produced a backward step when the fluorescent nucleotide, probably ATP, bound to myosin-V HMM (Fig S1.2A ,B). Myosin-V HMM then took its next forward after ADP-release.

3, Current statement

According to these and other's results, I propose the following relationship between

chemo-mechanical coupling and forward steps (Fig S1.3) and backward steps (Fig S1.4).

In a forward step, Cy3-ATP binds to the rear head (green head in Fig S1.3) causing rear head detachment and a forward step (Fig S1.3(a)). Then, Cy3-ATP is hydrolyzed to Cy3-ADP (Fig S1.3(b)). Following successive forward steps, the Cy3-ADP bound head becomes the rear head again (Fig S1.3(c)). Finally, Cy3-ADP is released from the rear head with a delay.

In a backward step, Cy3-ATP binds to the leading head (green head) causing the leading head to detach and step backward (Fig S1.4 (a)). Next, Cy3-ATP is hydrolyzed to Cy3-ADP (Fig S1.4 (b)). Then, Cy3-ADP is released from the rear head with a delay. Finally, after Cy3-ADP release, ATP (unlabeled) binding causes the rear head (green head) to detach and take a forward step.

To confirm these models, more data must be collected and analyzed statistically to verify rate constants like the ADP-release rate and the ATP-binding rate.
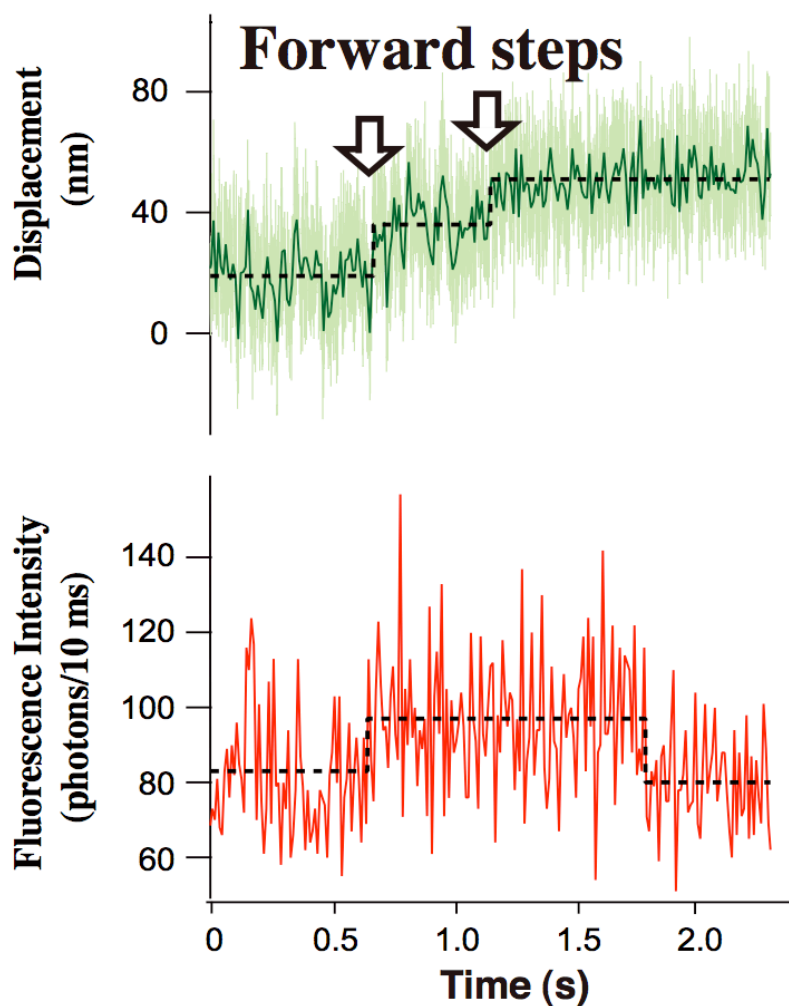
Figure S1.1 ATP-turnover cycle coupled to a forward step of myosin-V HMM.

The upper trace shows the time course of the trapped bead displacements. Raw data and data passed through a 100 Hz low pass filter are superimposed. The bottom trace shows the fluorescence intensity change of a Cy3-nucleotide located at the myosin-V position. White arrows show mechanical events coupled to binding of non-fluorescent ATP. The blue arrow shows an event coupled to binding of Cy3-ATP.

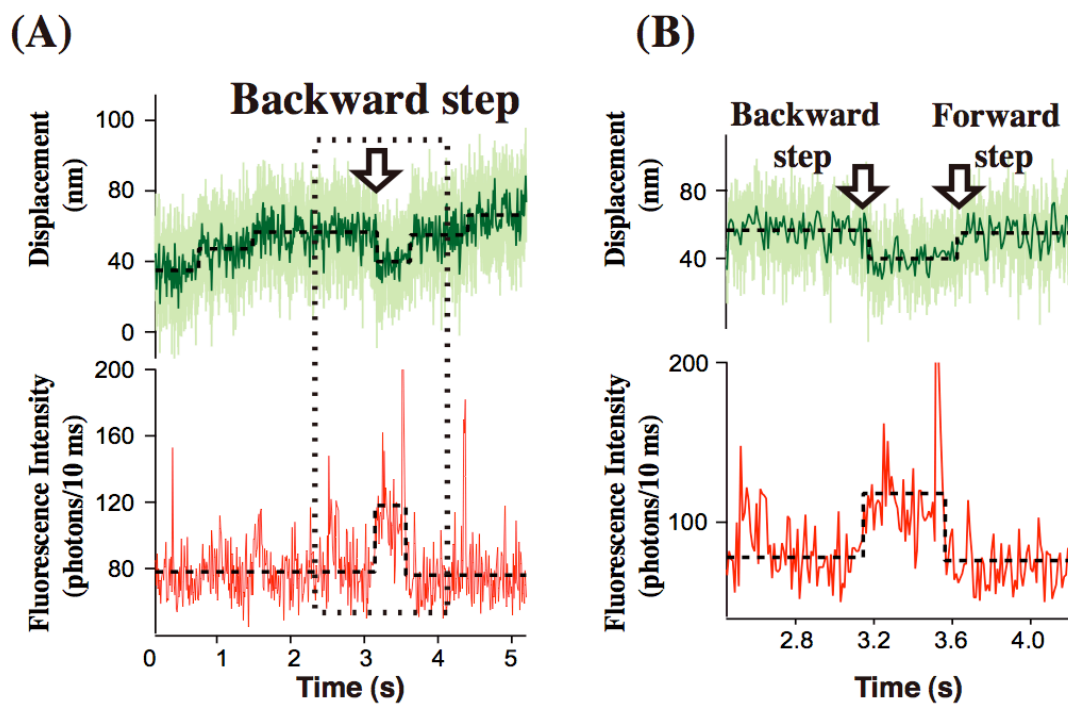**Figure S1.2 ATP-turnover cycle coupled to a backward step of myosin-V HMM.**

(A) the time coarse of myosin-V HMM backward step during processive movement. (B) the magnified image of chemomechanical coupling of a backward step.
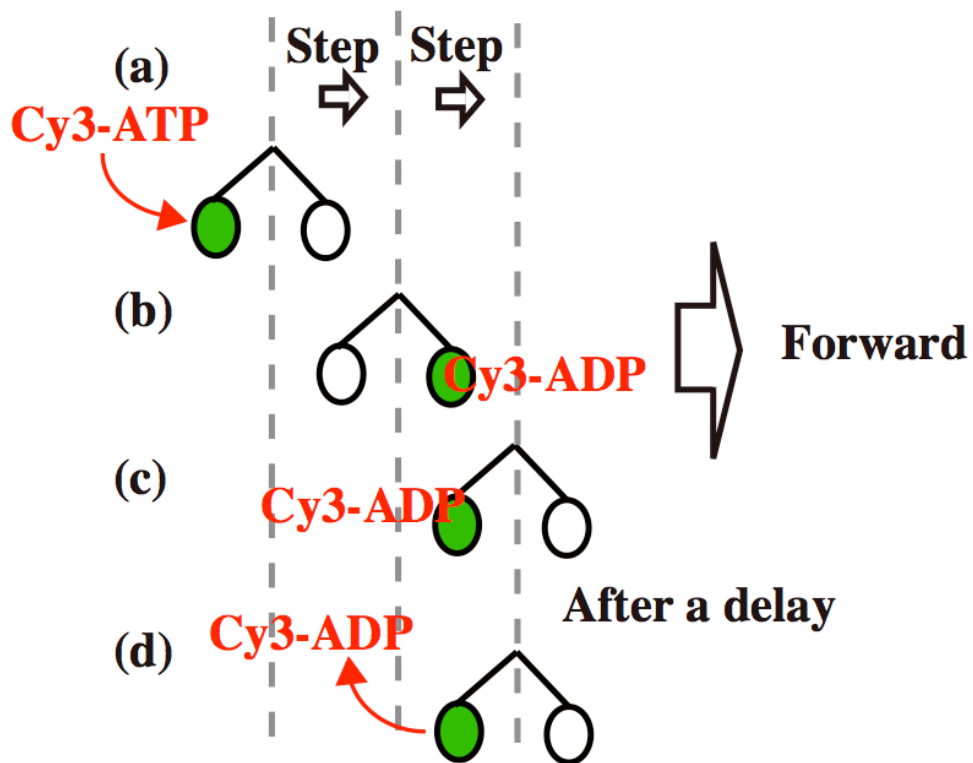
Figure S1.3 Current model about the chemomechanical coupling during a forward step.
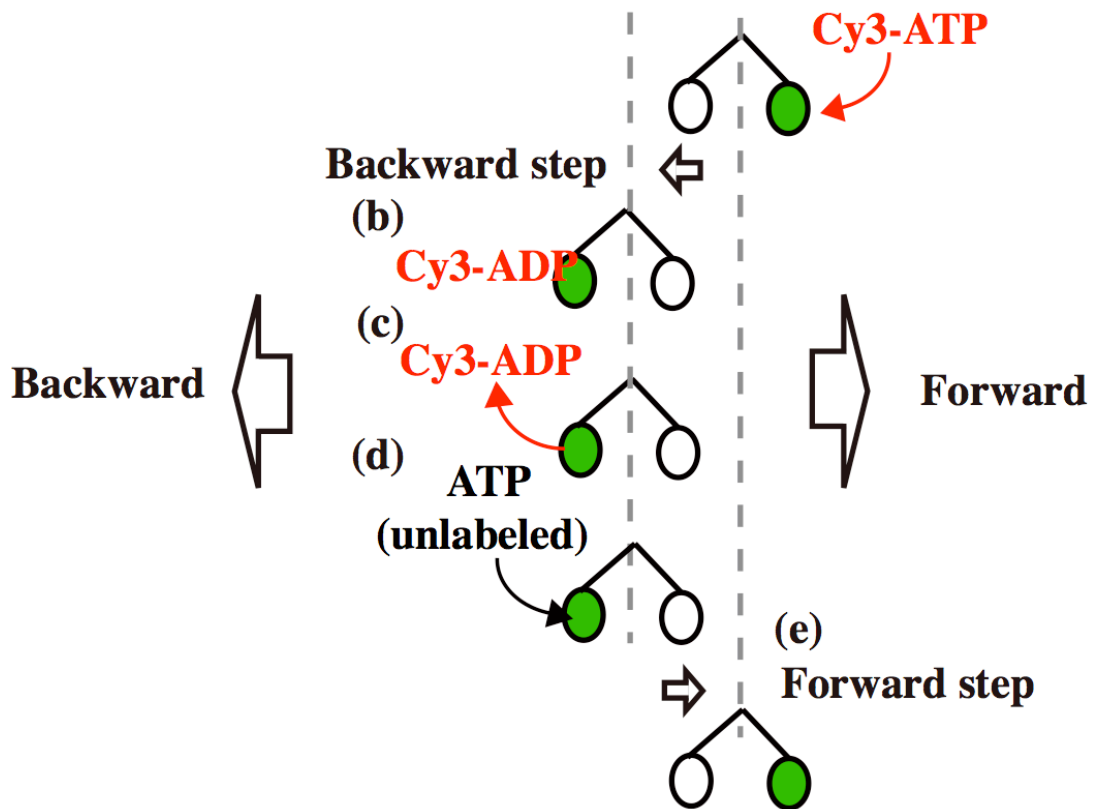
Figure S1.4 Current model about the chemomechanical coupling during a backward step.

Appendix 2: the calibration method of the step size.

In optical trap nanometry, the displacement of a trapped bead (ΔX_{bead}) is detected. Since myosin, tethered actin filament and bound biotin-avidin binding each have elastic properties, the actual displacement of myosin (ΔX_{myosin}) is greater by $\Delta X_{protein}$ than that measured (Fig S2.1). Here, the relationship between these three displacement is described by

$$\Delta X_{myo\sin} = \Delta X_{bead} + \Delta X_{preotein}$$

To determine the actual displacement of myosin, the displacement of the bead must be calibrated using its stiffness (spring constant) (Molloy et al. 1995).

Here, the spring constant of laser trap is defined as K_{trap}, while that of the myosin, actin filament and biotin-avidin binding complex is defined as $K_{protein}$. Then, by assuming that these springs act as springs in series, the relationship between these three spring constants is described as below.

$$K_{system} = K_{trap} + K_{protein}$$

Furthermore, each force applied to the trapped bead at each side is equal, described below.

$$K_{trap}\Delta X_{bead} = K_{protein}\Delta X_{protein}$$

Finally, by using the above relationships, ΔX_{myosin} is described as

$$\Delta X_{myo\sin} = \Delta X_{bead}\left(\frac{K_{system}}{K_{system} - K_{trap}} \right).$$

The total spring constant, K_{system}, is determined by using the Law of Equipartition of Energy by monitoring the trapped bead motion.

$$K_{system} = \frac{K_b T}{\left\langle x_{system}^2 \right\rangle}$$

Here, $<x^2>$ is the variance of the trapped bead; Kb is the Boltzmann constant; and T is the absolute temperature. K_{trap} is also determined by monitoring the trapped bead motion without myosin interaction.

$$K_{trap} = \frac{K_b T}{\left\langle x_{trap}^2 \right\rangle}$$

Therefore, by calculating K_{system} and K_{trap} using the variance of the trapped bead, the actual displacement of myosin (ΔX_{myosin}) can be estimated.

However, under a high load condition, the displacement of myosin may be underestimated even if the bead displacement is calibrated (Purcell et al., 2002). To avoid this possibility, I utilized a feedback system. In such a measurement system, the bead displacements are equivalent to myosin displacements.
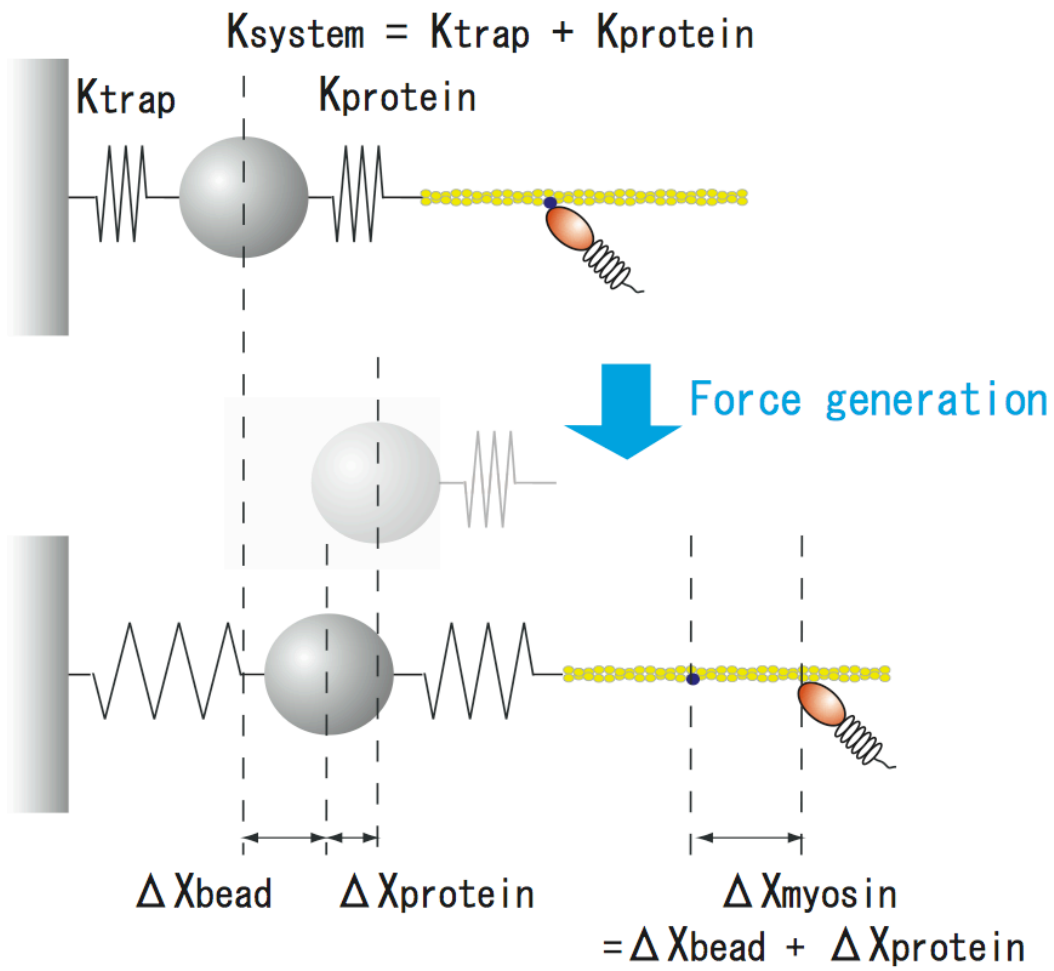
Figure S2.1 Calibration of bead displacement according to the stiffness change.

Appendix 3: the algorithm of the step finder software

We used MatLab software prepared by Dr. J. Kerssemakers (Nature (2006) Vol.442, pp 709-12).

Briefly, this algorithm starts by fitting a single, large step to the data. The size and location of this first step is determined by a Chi-squared calculation. Subsequent steps are found by fitting new steps to the plateaus of the previous ones (Fig S3.1a). This eventually leads to a series of best fits that differ only by one step. Fits with a very low number of steps are likely to underestimate the real number of steps in the data, whereas small steps that are added in the final iterations will merely be fitting noise and are thus overfitting the data. To evaluate the step number, each best fit in the series is compared to a "counter fit " that has an equal number of steps as the original one but with additional steps located between the steps found by the best fit (Fig S3.1b). Kerssemakers defined the step-indicator S as the ratio between the Chi-squared of the counter fit and the Chi-squared of the best fit. When the number of steps in the best fit is very close to the real number of steps in the data, the value of S will be large (Fig S3.1c). The reason is described below.

1) If the best fit is at its optimal iteration, all significant steps will have been included in the analysis. On the other hand, all step locations found with the counter fit are significantly misplaced, meaning the quality of the best fit and counter fit differ strongly. As a result, S is large.

2) In the case of severe underfitting, when many true steps are excluded, the quality of the counter fit will not differ much from the best fit.

3) In the case of severe overfiting, both counter fit and best fit are likely to include noise such that the quality of the fits will be similar.

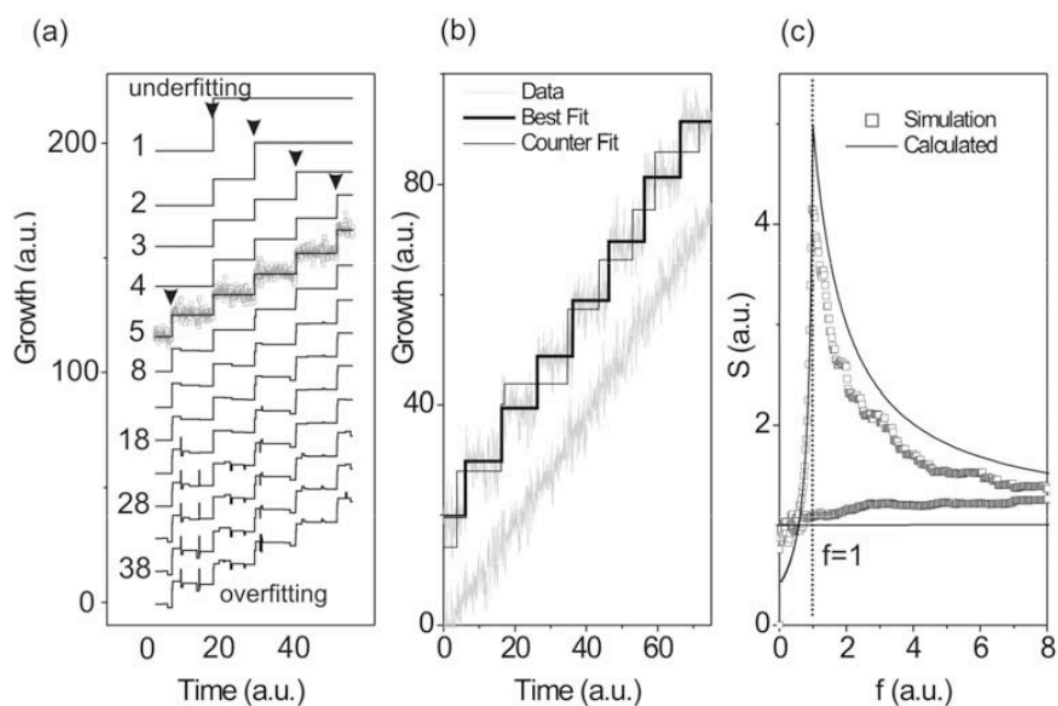(please see Kerssemakers *et al.* Nature (2006) Vol.442, pp 709-12)

Figure S3.1 Step fitting procedure.

(a) Iterations of the step-fitting algorithm on a simulated noisy track of stepped data (step size 10 nm, RMS noise 2.5 nm). Curves are shifted vertically for clarity. The arrowheads point to every new step that is added to the fit. Underfitting means that significant steps in the data are not yet located, while overfitting means that merely noise is fitted. (b) A "best" fit (thick line) to noisy steps (step size 10 nm, RMS noise 2.5 nm) together with a "counter" fit (thin line, see text). The quality of these two fits differs strongly for a stepped signal, while for linear noisy growth (lower curve), the location of any step is arbitrary and the quality is equal. (c) Simulation result and calculation of the quality ratio S of best fit and counter fit, plotted vs. the relative number of fitted steps f. Upper curves are for a noisy stepped signal. Lower curves are for a noisy linear signal. S only peaks sharply if there are steps present, and if the correct number of steps is fitted (f=1).

(This figure was excerpted from Kerssemakers et al. Nature (2006) Vol.442, pp 709-12)

Appendix 4: Future direction and outlook (actin filament)

Actin is a globular protein, about 42-kDa, found in eukaryotic cells. Analogously, an actin-like protein (ParM) was found in bacterium (Moller-Jenesen et al. 2002). It is also one of the most highly conserved proteins in all organisms and participates in many important cellular functions like motility and cell signaling. Although actin is highly conserved, its partner, myosin is not, with particular diversity at the actin-binding region. Actin's high conservation suggests its structure has essential properties for several cell functions including myosin motility. Therefore, it is reasonable to assume that the fundamental mechanism of motility can be found in the actin structure or actin filament dynamics. Previously, our group has proposed that the actin filament creates an energy potential slope due to its spiral structure, which myosin slides (Kitamura et al. 1999). In the future, I would like to modulate this potential by constructing various actin mutants with different myosin affinities (Fig S4.1).

At no load, myosin-V may diffuse freely to its final destination without utilizing the actin filament potential slope (Fig S4.2). This was recently proposed from dark field illumination and gold nano particle studies (Dunn et al. 2007). According to this theory, when chimera actin filaments containing wild type actin (WT-actin) and mutant actin (MT-actin), which has low myosin affinity, is utilized, the step size at no load does not change but its deviation is broader compared to WT-actin filament alone since myosin may not bind to its preferred position on MT-actin. However, at high load, 1 to 2 pN, the pivoting leading head was bended to backward because of the high external force (Fig

S4.3). In such conditions, myosin-V cannot reach its final destination if it only uses free diffusion to move. To compensate myosin needs another mechanism to move. I propose that it slides along the actin filament. If this idea is correct, myosin displacement along a chimera actin filament under high load condition will decrease, while that along a WT-actin filament will not change since the differences in affinity mean myosin on MT-actin will not remain bound to the actin long enough for long displacements (Fig S4.4b).
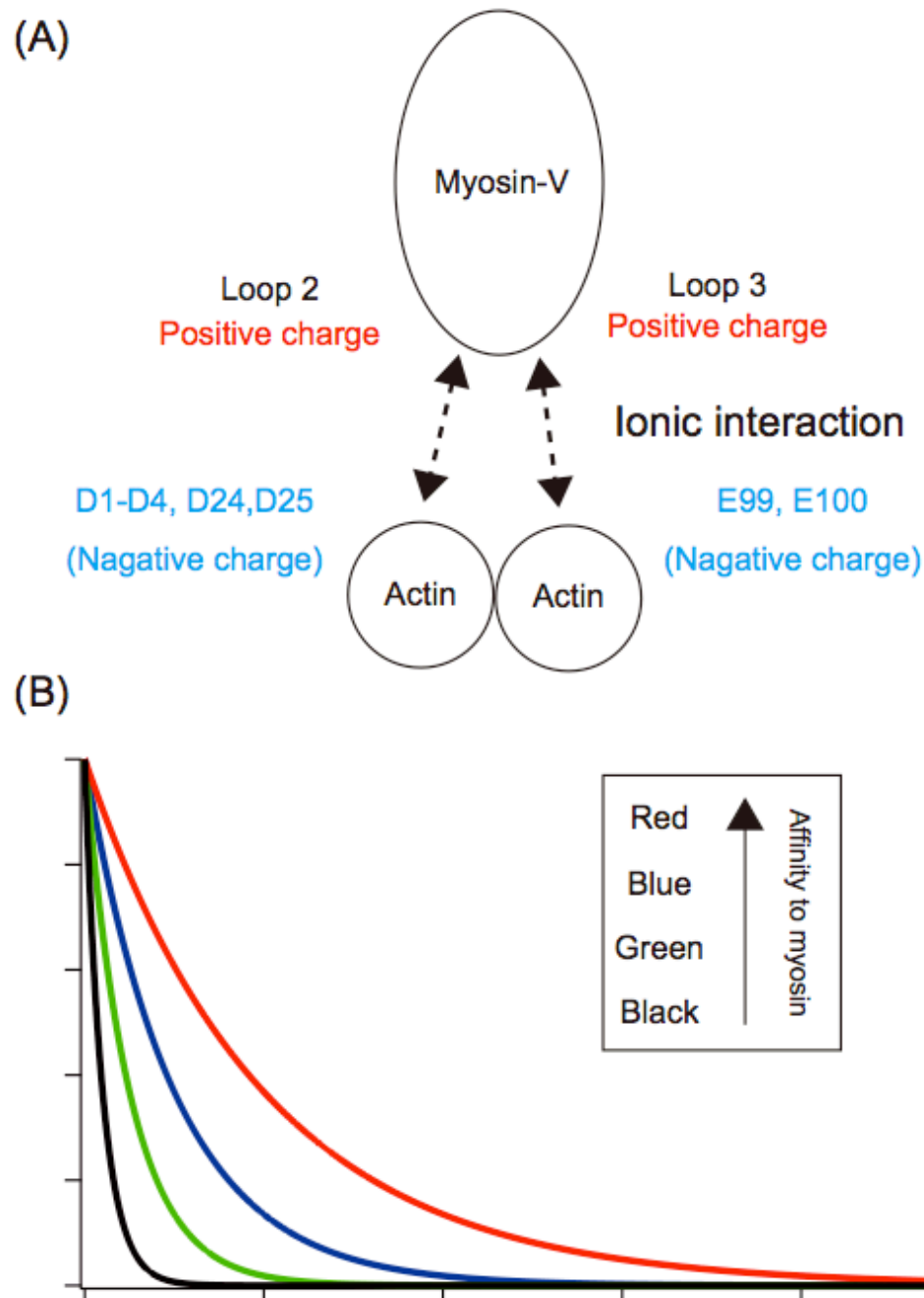
Figure S4.1 (A) candidates of actin mutant. Actomyosin interaction is stabilized by ionic interaction between positive charge of myosin head and negative charge of actin. Then, actomyosin interaction can be weakened by exchanging positive residues of actin to neutral residue. **(B) the expected affinity decrease of actin mutants.** The horizontal axis indicates the relative run length of myosin-V on various actin filament, while the vertical axis indicates number.

(A)

(B)
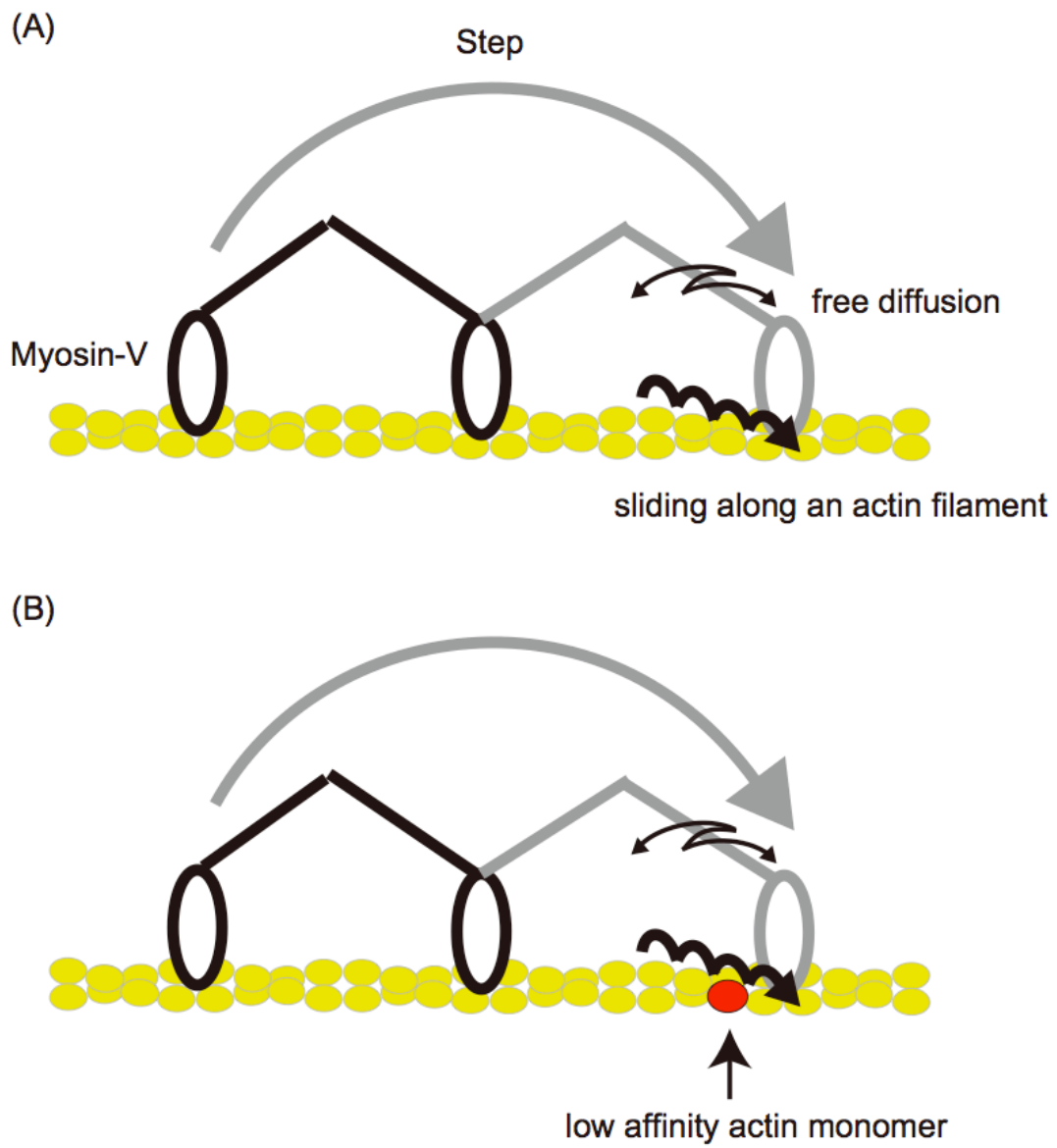
Figure S4.2 (A) the expected myosin motion on WT-actin filament without external load. (B) that on a chimera actin filament.

(A)

Step

F

free diffusion

Myosin-V

sliding along an actin filament

(B)

F

low affinity actin monomer
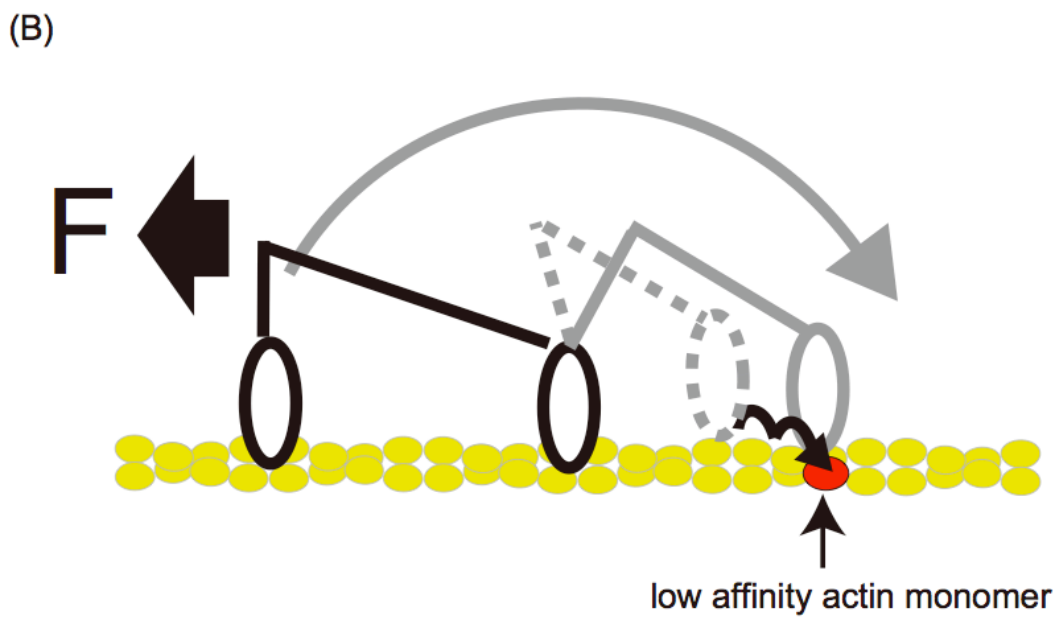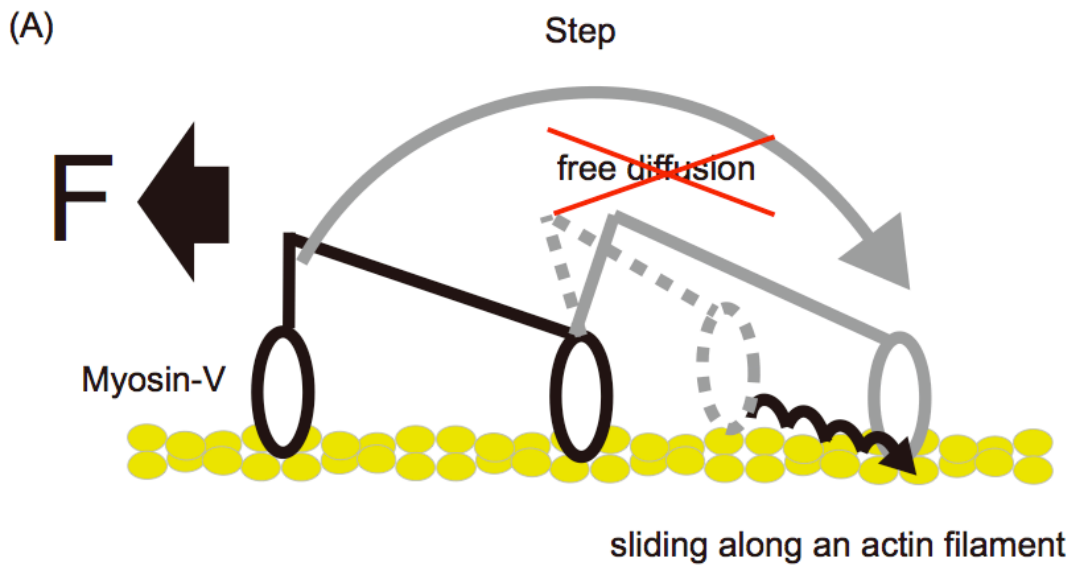
Figure S4.3 (A) the expected myosin motion on WT-actin filament with external load. (B) that on a chimera actin filament.
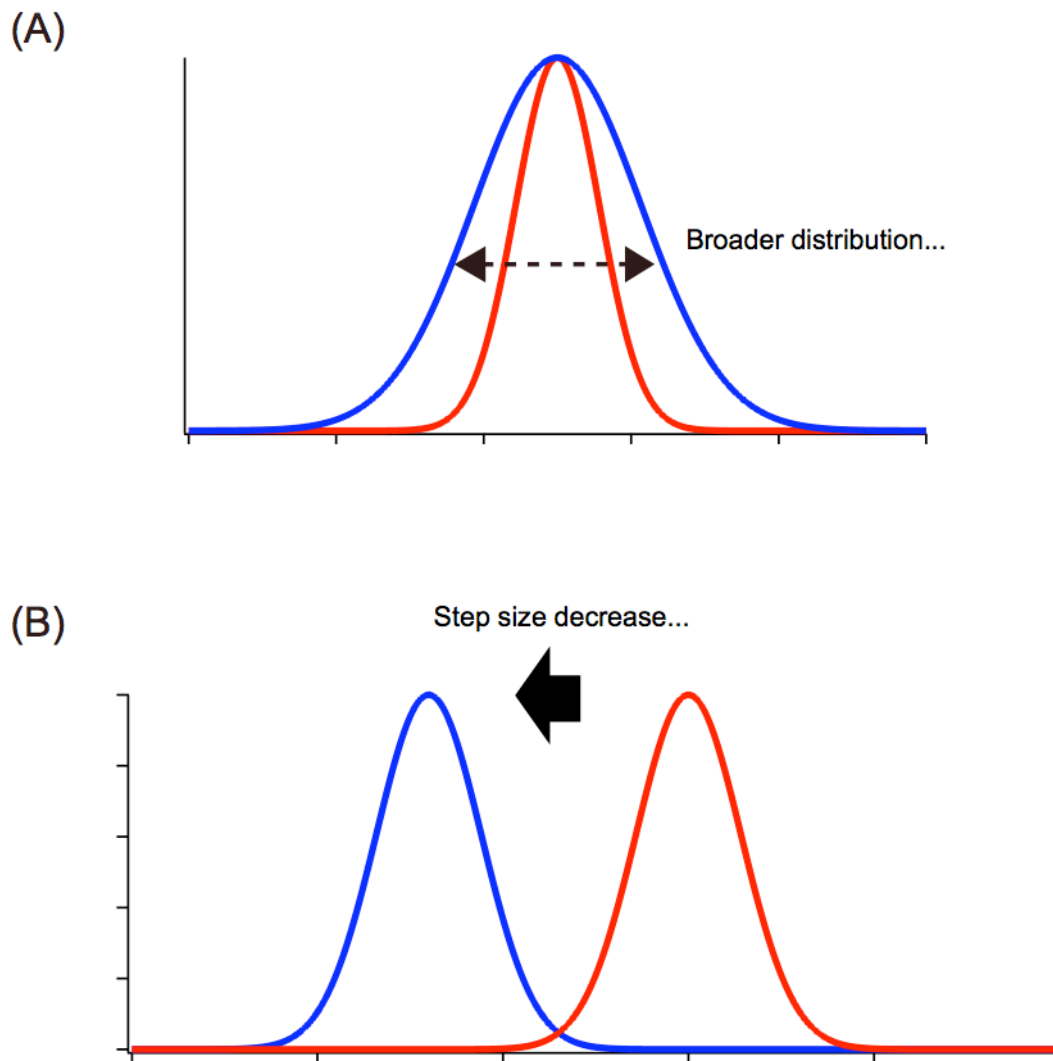
Figure S4.4 (A) the expected step size distribution without external load. the red line indicates a step size distribution on WT-actin filament, while a blue line for that on chimera actin filament. The standard deviation for chimera actin filament is estimated to increase compared with that for WT-actin filament. **(B) the expected step size distribution without external load.** Under high load condition, decrease of step size is expected.

Appendix 5: Future direction and outlook (the cooperative motility by multiple motors)

In general, multiple non-processive myosins work cooperatively and are responsible for various motile activities like large organelle transport or muscle contraction. Recently, Nishikawa et al. showed muscle type myosin-II can generate variable size steps by working cooperatively, whereas myosin-V truncated at Thr-1238 (refer Fig. 2.3) do not. Yet, I argue that full length myosin-V should work cooperatively and efficiently in physiological condition, since physiologically, 1-4 molecules transport single cargo simultaneously. In such a situation, each myosin-V attaches to the same vesicle and generates steps stochastically. If there is no mechanism to ensure cooperation during processive movement, these stochastic steps cause mutual friction and prevent motility. Therefore, the following portion to Thr-1238, which did not exist in truncated myosin-V of Nishikawa's experiment, may relate to this cooperative motion. I want to clarify the structural basis that ensures this cooperative manner.

At present, I am focusing on the unstructured portion of the myosin-V coiled-coil domain, located between the motor domain and GTD (Fig S5.1A). I suspect these unzipped regions provide a structural basis for the cooperative movement of myosin-V by elongating the coiled-coil region when myosin-V binds strongly to actin (Fig S5.1B). Recently, a similar assumption was made in kinesin (Bieling et al. 2008). If the coiled-coil region of myosin-V is too flexible, force generation by the motor domain cannot be transmitted to the vesicle attached to the C-terminus. If it is too strong, one

myosin may prevent the other myosins from moving because it strongly bound to actin. Therefore, the myosin-V coiled-coil region requires appropriate stiffness to achieve cooperative myosin-V movement.

(A)

Catalytic domain

Six light chains

Cargo-binding domains

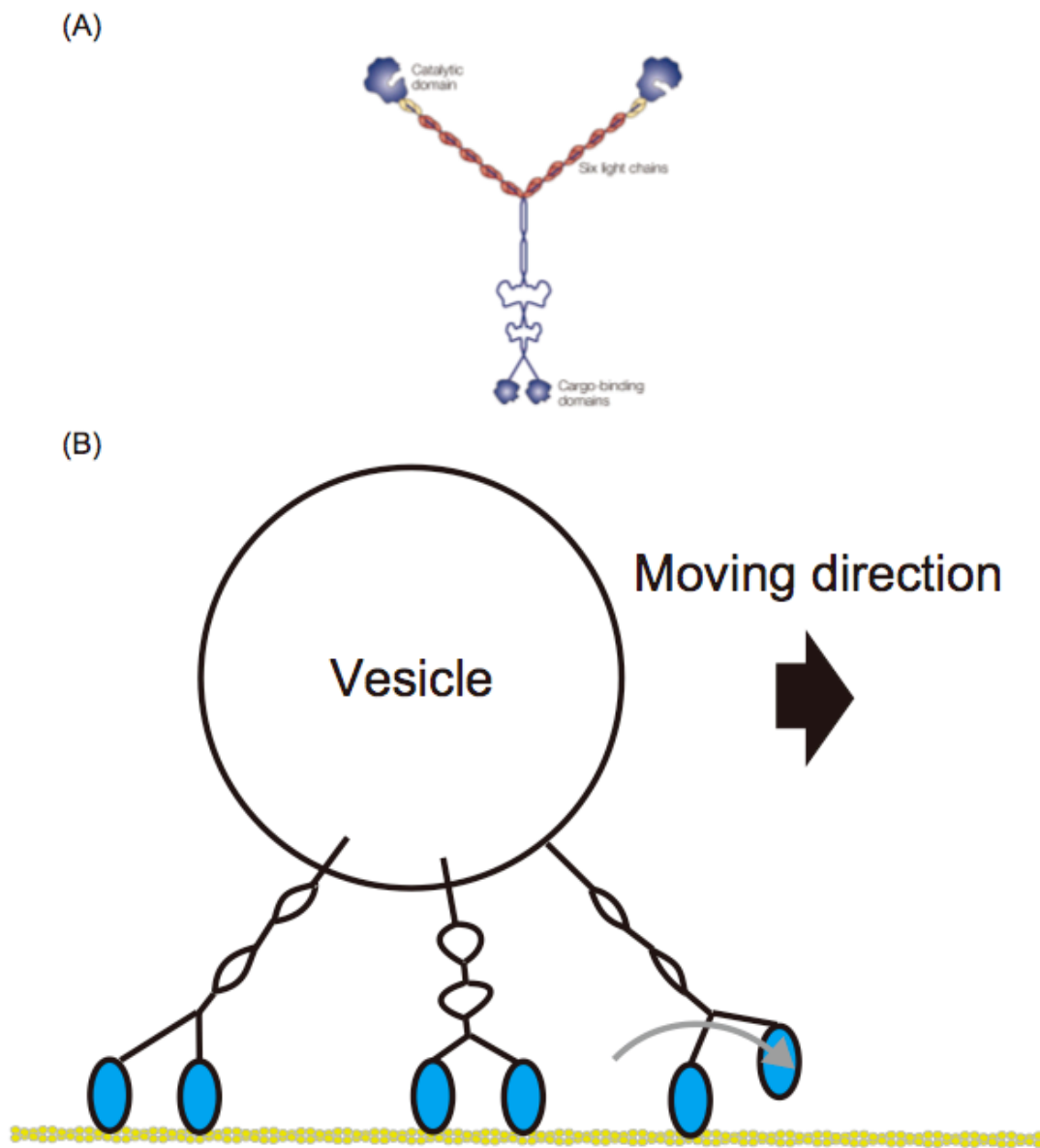(B)

Moving direction

Vesicle

Figure S5.1 Cooperative vesicle transport by multiple myosin-V.
(A) the structure of full length myosin-Va. (B) cartoon of vesicle transport by multiple full length myosin-Va.

Appendix 6: Future direction and outlook (simultaneous observation of muscle type myosin-II)

Previously, Ishijima et al. demonstrated that muscle type myosin-II generates force after ADP-release, which is kinetically different from myosin-V. However, they could not quantify this delay. In this thesis, I have improved their measurement system such that I could measure the ATP-turnover cycle and force generation at 100 nM Cy3-ATP. Ishijima et al. performed their experiments at 10 nM 2', 3' Cy3-ATP, which has a lower myosin affinity than Cy3-ATP (Oiwa et al., 2000). This increase in ATP concentration is expected to allow me to investigate myosin-II. This was not possible at 10 nM (Fig S6.1).

By collecting enough data, I hope to clarify how long myosin-II can generate force after ADP-release (Fig S6.2). This study has the potential to provide fundamental information regarding the time scale in which the structural relaxation after ligand dissociation from or binding to a protein.
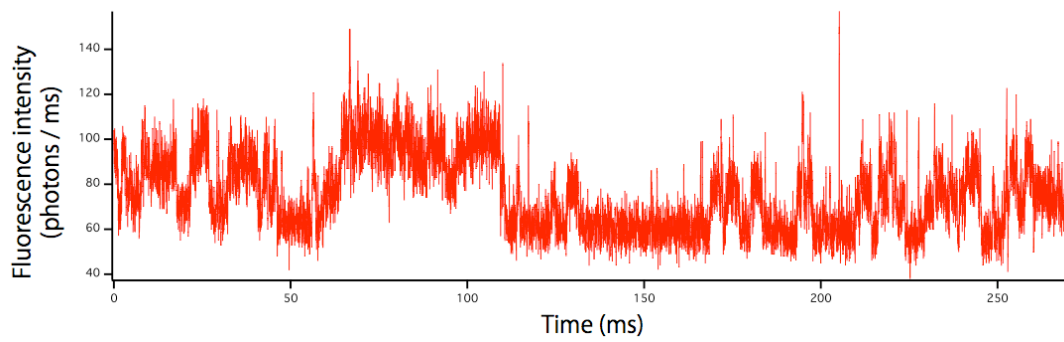
Figure S6.1 Cy3-ATP turnovers by muscle type myosin-II.

The trace shows single Cy3-ATP turnovers by muscle type myosin-II at 100 nM Cy3-ATP. The fluorescence intensity was detect using APD at 100 Hz sampling rate.
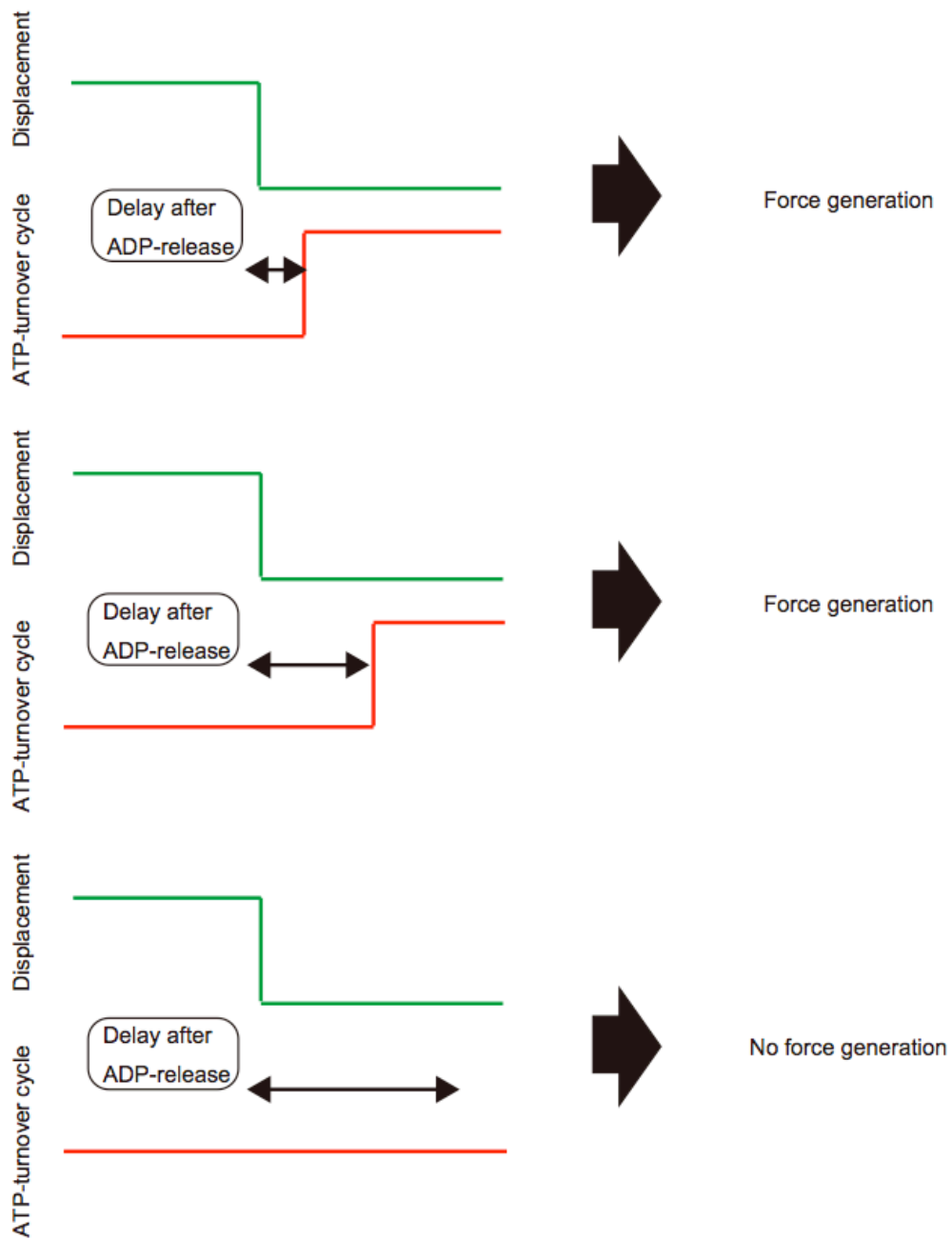
Figure S6.2 the cartoon of expected result of simultaneous observation of muscle type myosin-II.

Appendix 7: Future direction and outlook (mechanism of myosin-IX motility)

Myosin-IX is rather unique from other processive myosins, as to date it alone can move processively along an actin filament with only one head (Post et al. 2002, Inoue et al. 2002, Nishikawa et al. 2006). Currently, myosin-IX is poorly understood, although biochemical studies have proposed that myosin-IX has unique myosin kinetics (Nalavadi et al. 2005, Kambara et al 2006). The prevailing lever arm model cannot be applied to myosin-IX motility because the model depends on two heads. However, the actin filament sliding model can. Since the myosin family possesses well conserved structures at its motor domain, it is unlikely that myosin-IX uses a unique motility mechanism. Seeing that the actin filament sliding model and not the lever arm model holds for myosin-IX, it is reasonable to believe that all myosins follow this model when generating force.

Recently, it was postulated that an external and internal force applied to myosin is proposed can quicken ADP-release rate from myosin-I, -II, -V and –VI by several groups. Our group has proposed that external force to myosin-VI regulates the weak to strong binding state transition and this aids in the motile direction along an actin filament. Mechanically, the lever arm domain regulates these kinetics. The signal is transmitted through the myosins by a strain sensor at the motor domain C-terminus. However, as described in chapter I, force is never applied to myosin-IX via the lever arm during myosin-IX processive movement, meaning the strain sensor in myosin-IX

does not exist near the lever arm. Alternatively, I believe it is located near the acin binding region since only this region can detect the applied force. Future work will seek to investigate this hypothesis.

Recently, applied forece to myosin is proposed that regulate ADP-release rate from myosin-I, -II, -V and –VI by several groups. Furthermore, our group also proposed that applied force to myosin-VI regulate the weakly-to-strongly binding state in actomyosin-VI to find correct direction along an actin filament (Iwaki et al. in preparation). In these views, it is simply postulated that the applied force via lever arm domain regulate these kinetics and myosins have a strain sensor at its C-terminus of motor domain (an adjoining motor domain). However, as described in chapter I, force is never applied to myosin-IX via lever arm during myosin-IXb processive movement, meaning strain sensor in myosin-IXb does not exist near lever arm but near an acin binding region. Since in this situation, only actin binding region can detect applied force.

Reference

Bagshaw, J. W. (2007) Myosin mechanochemistry. Structure 15, 511-2.

Brau, R. R., Tarsa, P. B., Ferrer, J. M., Lee, P. and Lang, M. J. (2006). Interlaced optical force-fluorescence measurements for single molecule biophysics. Biophys J 91, 1069-77.

Bieling, P., Telley, I. A., Piehler, J. and Surrey, T. (2008). Processive kinesin require loose mechanical coupling for efficient collective motility. EMBO reports 9, 1121-7

Coluccio, L. M. (2008). Myosins A Superfamily of Molecular Motors. NetherLand: Springer.

Coureux, P. D., Sweeney, H. L. and Houdusse, A. (2004). Three myosin V structures delineate essential features of chemo-mechanical transduction. EMBO J 23, 4527-37.

Coureux, P. D., Wells, A. L., Menetrey, J., Yengo, C. M., Morris, C. A., Sweeney, H. L. and Houdusse, A. (2003). A structural state of the myosin V motor without bound nucleotide. Nature 425, 419-23.

De La Cruz, E. M., Wells, A. L., Rosenfeld, S. S., Ostap, E. M. and Sweeney, H. L. (1999). The kinetic mechanism of myosin V. Proc Natl Acad Sci U S A 96, 13726-31.

Dunn, A. R. and Spudich, J. A. (2007). Dyanmics of the unbound head during myosin V processive translocation. Nat. Struc. Mol. Bio. 14, 246-8

Espindola, F. S., Espreafico, E. M., Coelho, M. V., Martins, A. R., Costa, F. R. C., Mooseker, M. S. and Larson, R. E. (1992). Biochemical and immunological characterization of p 190-calmodulin complex from veretbrate brain: A novel calmodulin-binding myosin. J Cell Biol 118, 359-68.

Espreafico, E. M., Cheney, R. E., Matteoli, M., Nascimento, A. A. C., De Camilli, P. V., Larson, R. E. and Mooseker, M. S. (1992). Primary structure and cellulor localization of chiken brain myosin-V (p 190), an unconventional myosin with calmodulin light chains. J Cell Biol 119, 1541-57.

Finer, J. T., Simmons, R. M. and Spudich, J. A. (1994). Single myosin mechanics: piconewton forces and nanometre steps. Nature 368, 113-119.

Forgacs, E., Cartwright, S., Kovacs, M., Sakamoto, T., Sellers, J. R., Corrie, J. E., Webb, M. R. and White, H. D. (2006). Kinetic mechanism of myosinV-S1 using a new fluorescent ATP analogue. Biochemistry 45, 13035-45.

Forgacs, E., Cartwright, S., Sakamoto, T., Sellers, J. R., Corrie, J. E. and Webb, M. R. (2008). Kinetics of ADP Dissociation from the Trail and Lead Heads of Actomyosin

V following the Power Stroke. J. Biol. Chem. 283, 766-773.

Foth, B. J., Goedecke, M. C. and Soldati, D. (2006). New insights into myosin evolution and classification. Proc Natl Acad Sci U S A 103, 3681-6.

Funatsu, T., Harada, Y., Tokunaga, M., Saito, K. and Yanagida, T. (1995). Imaging of single fluorescent molecules and individual ATP turnovers by single myosin molecules in aqueous solution. Nature 374, 555-9.

Goodno, C. C. (1979). Inhibition of myosin ATPase by vanadate ion. Proc Natl Acad Sci U S A 76, 2620-4.

Harada, Y., Noguchi, A., Kishino, A. and Yanagida, T. (1987). Sliding movement of single actin filaments on one-headed myosin filaments. Nature 326, 805-8.

Ikebe, M., Kambara, T., Stafford, W. F., Sata, M., Katayama, E. and Ikebe, R. (1998). A Hinge at the Central Helix of the Regulatory Light Chain of Myosin Is Critical for Phosphorylation-dependent Regulation of Smooth Muscle Myosin Motor Activity. J Biol Chem 273, 17702-07.

Ishijima, A., Doi, T., Sakurada, K. and Yanagida, T. (1991). Subpiconewton force fluctuations of actomyosin in vitro. Nature 352, 301-306.

77

Ishijima, A., Kojima, H., Funatsu, T., Tokunaga, M., Higuchi, H., Tanaka, H. and Yanagida, T. (1998). Simultaneous observation of individual ATPase and mechanical events by a single myosin molecule during interaction with actin. Cell 92, 161-71.

Iwane, A. H., Funatsu, T., Harada, Y., Tokunaga, M., Ohara, O., Morimoto, S. and Yanagida, T. (1997). Single molecular assay of individual ATP turnover by a myosin-GFP fusion protein expressed in vitro. FEBS Lett 407, 235-8.

Jameson, D. M. and Eccleston, J. F. (1997). Fluorescent nucleotide analogs: synthesis and applications. Methods Enzymol. 278, 363-390.

Kerssemakers, J. W., Munteanu, E. L., Laan, L., Noetzel, T. L., Janson, M. E. and Dogterom, M. (2006). Assembly dynamics of microtutules at molecular resolution. Nature 442, 709-12.

Kishino, A. and Yanagida, T. (1988). Force measurements by micronanipulation of a single actin filament by glass needles. Nature 334, 74-76.

Kitamura, K., Tokunaga, M., Iwane, A. H. and Yanagida, T. (1999). A single myosin head moves along an actin filament with regular steps of 5.3 nanometres. Nature 397, 129-34.

Komori, T., Nishikawa, S., Ariga, T., Iwane, A. H. and Yanagida, T. (2008). Measurement system for simultaneous observation of myosin V chemical and mechanical events. Biosystems 93, 48-57.

Komori, Y., Iwane, A. H. and Yanagida, T. (2007). Myosin-V makes two brownian 90° rotations per 36-nm step. Nat Struct Mol Biol 14, 968-973.

Kron, S. J. and Spudich, J. A. (1986). Fluorescent actin filaments move on myosin fixed to a glass surface. Proc Natl Acad Sci U S A 83, 6272-6.

Larson, R. E., Espindola, F. S. and Espreafico, E. M. (1990). Calmodulin-binding proteins and calcium/calmodulin-regulated enzyme activities associated with brain actomyosin. J Neurochem 54, 1288-94.

Mehta, A. D., Rock, R. S., Rief, M., Spudich, J. A., Mooseker, M. S. and Cheney, R. E. (1999). Myosin-V is a processive actin-based motor. Nature 400, 590-3.

Moller-Jensen, J., Jensen, R. B., Lowe, J. and Gerdes, K. (2002). Prokaryotic DNA segregation by an actin-like filament. EMBO J. 21, 3119-27

Molloy, J. E., Burns, J. E., Kendrick-Jones, J., Tregear, R. T. and White, D. C.

(1995). Movement and force produced by a single myosin head. Nature 378, 209-12.

Nishikawa, M., Nishikawa, S., Inoue, A., Iwane, A. H., Yanagida, T. and Ikebe, M. (2006). A unique mechanism for the processive movement of single-headed myosin-IX. Biochem Biophys Res Commun 343, 1159-64.

Nishikawa, M., Takagi, H., Iwane, A. H. and Yanagida, T. (2008). Fluctuation Analysis of Mechanochemical Coupling Depending on the Type of Biomolecular Motors. PHYSICAL REVIEW LETTERS 101, 128103.

Nishizaka, T., Oiwa, K., Noji, H., Kimura, S., Muneyuki, E., Yoshida, M. and Kinosita. (2004). Chemomechanical coupling in F1-ATPase revealed by simultaneous observation of nucleotide kinetics and rotation. Nat Struct Mol Biol 11, 142-8.

O'Connell, C. B., Tyska, M. J. and Mooseker, M. S. (2007). Myosin at work: Motor adaptations for a variety of cellular functions. Biochem Biophys Acta 1773, 615-30.

Oguchi, Y., Mikhailenko, S. V., Ohki, T., Olivares, A. O., De La Cruz, E. M. and Ishiwata, S. (2008). Load-dependent ADP-binding to myosins V and VI: Implications for subunit coordination and function. Proc Natl Acad Sci U S A 105, 7714-9.

Oiwa, K., Eccleston, J. F., Anson, M., Kikumoto, M., Davis, C. T., Reid, G. P.,

Ferenczi, M. A., Corrie, J. E., Yamada, A., Nakayama, H. et al. (2000). Comparative single-molecule and ensemble myosin enzymology: sulfoindocyanine ATP and ADP derivatives. Biophys J 78, 3048-71.

Oiwa, K., Jameson, D. M., Croney, J. C., Davis, C. T., Eccleston, J. F. and Anson, M. (2003). The 2'-O- and 3'-O-Cy3-EDA-ATP(ADP) complexes with myosin subfragment-1 are spectroscopically distinct. Biophys J 84, 634-42.

Okada, T., Tanaka, H., Iwane, A. H., Kitamura, K., Ikebe, M. and Yanagida, T. (2007). The diffusive search mechanism of processive myosin class-V motor involves directional steps along actin subunits. Biochem Biophys Res Commun 354, 379-84.

Pal, P., Lesoine, J. F., Lieb, M. A., Novotny, L. and Knauf, P. A. (2005). A novel immobilization method for single protein spFRET studies. Biophys J 89, L11-3.

Post, P. L., Tyska, M. J., O'Connell, C. B., Johung, K., Hayward, A. and Mooseker, M. S. (2002). Myosin-IXb is a single-headed and processive motor. J Biol Chem 277, 11679-83.

Purcell, T. J., Morris, C., Spudich, J. A. and Sweeney, H. L. (2002). Role of the lever arm in the processive stepping of myosin V. Proc Natl Acad Sci U S A 99, 14159-64.

Purcell, T. J., Sweeney, H. L. and Spudich, J. A. (2005). A force-dependent state controls the coordination of processive myosin V. Proc Natl Acad Sci U S A 102, 13873-8.

Rief, M., Rock, R. S., Mehta, A. D., Mooseker, M. S., Cheney, R. E. and Spudich, J. A. (2000). Myosin-V stepping kinetics: a molecular model for processivity. Proc Natl Acad Sci U S A 97, 9482-6.

Rosenfeld, S. S. and Sweeney, H. L. (2004). A model of myosin V processivity. J Biol Chem 279, 40100-11.

Sakamoto, T., Amitani, I., Yokota, E. and Ando, T. (2000). Direct observation of processive movement by individual myosin V molecules. Biochem Biophys Res Commun 272, 586-90.

Sakamoto, T., Webb, M. R., Forgacs, E., White, H. D. and Sellers, J. R. (2008). Direct Observation of the mechanochemical coupling in myosin Va during provessive movement. Nature 455, 128-32.

Sellers, J. R. (1999). Myosins Second Edition. Oxford: Oxford University Press.

Spudich, J. A. and Watt, S. (1971). The regulation of rabbit skeletal muscle

concentration. I. Biochemical studies of the interaction of the tropomyosin-troponin complex with actin and the proteolytic fragments of myosin. J. Biol. Chem. 246, 4866-4871.

Tanaka, H., Homma, K., Iwane, A. H., Katayama, E., Ikebe, R., Saito, J., Yanagida, T. and Ikebe, M. (2002). The motor domain determines the large step of myosin-V. Nature 415, 192-5.

Tanaka, H., Ishijima, A., Honda, M., Saito, K. and Yanagida, T. (1998). Orientation dependence of displacements by a single one-headed myosin relative to the actin filament. Biophys J 75, 1886-94.

Thirumurugan, K., Sakamoto, T., Hammer III, J. A., Sellers, J. R. and Knight, P. J. (2006). The cargo-binding domain regulates structure and activity of myosin 5. Nature 442, 212-5.

Tokunaga, M., Kitamura, K., Saito, K., Iwane, A. H. and Yanagida, T. (1997). Single molecule imaging of fluorophores and enzymatic reactions achieved by objective-type total internal reflection fluorescence microscopy. Biochem Biophys Res Commun 235, 47-53.

Trybus, K. M., Krementsova, E. and Freyzon, Y. (1999). Kinetic Characterization of

a Monomeric Unconventional Myosin V Construct. J Biol Chem 274, 27448-456.

Uemura, S., Higuchi, H., Olivares, A. O., De La Cruz, E. M. and Ishiwata, S. (2004). Mechanochemical coupling of two substeps in a single myosin V motor. Nat Struct Mol Biol 11, 877-83.

Vale, R. D., Funatsu, T., Pierce, D. W., Romberg, L., Harada, Y. and Yanagida, T. (1996). Direct observation of single kinesin molecules moving along microtubules. Nature 380, 451-453.

van Dijk, M. A., Kapitein, L. C., van Mameren, J., Schmidt, C. F. and Peterman, E. J. G. (2004). Combining Optical Trapping and Single-Molecule Fluorescence Spectroscopy: Enhanced Photobleaching of Fluorophores. J. Phys. Chem B 108, 6479-6484.

Veigel, C., Schmitz, S., Wang, F. and Sellers, J. R. (2005). Load-dependent kinetics of myosin-V can explain its high processivity. Nat Cell Biol 7, 861-9.

Veigel, C., Wang, F., Bartoo, M. L., Sellers, J. R. and Molloy, J. E. (2002). The gated gait of the processive molecular motor, myosin V. Nat Cell Biol 4, 59-65.

Volkmann, N., Liu, H., Hazelwood, L., Krementsova, E. B., Lowey, S., Trybus, K.

M. and Hanein, D. (2005). The structural basis of myosin V processive movement as revealed by electron cryomicroscopy. Mol Cell 19, 595-605.

Yildiz, A., Forkey, J. N., McKinney, S. A., Ha, T., Goldman, Y. E. and Selvin, P. R. (2003). Myosin V walks hand-over-hand: single fluorophore imaging with 1.5-nm localization. Science 300, 2061-5.

Publication list

Publication list

<u>学術雑誌又は商業誌における論文</u>

[1] S. Ueki, M. Nakamura, **T. Komori** and T. Arata "Site-Directed Spin Labeling Electron Paramagnetic Resonance Study of the Calcium-Induced Structural Transition in the N-Domain of Human Cardiac Troponin C Complexed with Troponin I" **Biochemistry**, 44, pp.411-6 (2005)

[2] **T. Komori**, S. Nishikawa, T. Ariga, A. H. Iwane and T. Yanagida "Measurement system for the simultaneous observation of myosin V" **BioSystems**, 93, pp.48-57 (2008)

[3] **T. Komori**, S. Nishikawa, T. Ariga, A. H. Iwane and T. Yanagida "Simultaneous measurement of nucleotide occupancy and mechanical displacement in myosin-V, a processive molecular motor" **Biophysical J.**, 96(1), pp. L04-6 (2009)

<u>学術雑誌又は商業誌における解説、総説</u>

[1] S. Nishikawa, **T. Komori**, T. Ariga, T. Okada, M. Morimatsu, Y. Ishii and T. Yanagida "Imaging and manipulation of an actomyosin motor" **Single Molecule Technique**, pp.325-346 Cold Spring Harbor Laboratory Press (2007)

[2] S. Nishikawa, M. Sugawa, **T. Komori**, M. Morimatsu, A. H. Iwane and T. Yanagida "Single molecule detection of the two-legged nano-machine" 電気工学会紀要 (2008)

学会発表

国際会議（ポスター発表）

○T. Ariga, **T. Komori**, S. Nishikawa, A. H. Iwane and T. Yanagida "Development of a novel microscopy for simultaneous observation" **The 50th Biophysical Society**, USA (2006.3)

○**T. Komori**, S. Nishikawa, T. Ariga, A. H. Iwane and T. Yanagida "The construction of the measurement system for ATP hydrolysis and displacement of myosin V" **5th EABS& 44th BSJ**, Okinawa(2006.11)

○**T. Komori**, S. Nishikawa, T. Ariga, A. H. Iwane and T. Yanagida "The construction of the measurement system for ATP hydrolysis and displacement of myosin V" **The 51st Biophysical Society**, USA (2007.3)

○T. Ariga, **T. Komori**, A. H. Iwane and T. Yanagida "Coiled-coil domain of myosin V" **The 51st Biophysical Society**, USA (2007.3)

○**T. Komori**, S. Nishikawa, T. Ariga, A. H. Iwane and T. Yanagida "Simultaneous observation of ATPase and Displacement by Myosin V" **The 42nd Fujihara Seminar**, Tomakomai (2007.8)

○**T. Komori**, S. Nishikawa, T. Ariga, A. H. Iwane and T. Yanagida "Simultaneous observation of ATPase and Displacement by Myosin V" **Biocomp2008**, Italy (2007.9)

○T. Ariga, **T. Komori**, S. Nishikawa, A. H. Iwane and T. Yanagida "Measurement

System for Mechano-Chemical Coupling: Combining Optical Tweezers and Fluorescent Microscopy." **Biocomp2008**, Italy (2007.9)

○**T. Komori**, S. Nishikawa, T. Ariga, A. H. Iwane and T. Yanagida "Direct observation of chemo-mechanical coupling in single headed myosin V" **The 52nd Biophysical Society Annual Meeting & The 16th International Biophysics congress**, USA (2008.2)

○A. H. Iwane, T. M. Ichinose, M. Nishikawa, **T. Komori**, and T. Yanagida "Relationship between Myosin Va ATPase activity and motility." **The 52nd Biophysical Society Annual Meeting & The 16th International Biophysics congress**, USA (2008.2)

国内会議（口頭発表）

○小森智貴、中村志芳、植木正二、荒田敏昭「筋繊維におけるトロポニンCの ESR動的構造解析」生体運動班合同会議、東京（2004, 1）

○小森智貴、西川宗、有賀隆行、岩根敦子、柳田敏雄「ミオシン5のATP加水分解と変位の同時計測」生体運動班合同会議、金沢（2007, 1）

○小森智貴、西川宗、有賀隆行、岩根敦子、柳田敏雄「単頭ミオシンVの化学−力学反応カップリングの直接計測」第45回日本生物物理学会、横浜（2007, 12）

国内会議（ポスター発表）

○<u>小森智貴</u>、西川宗、有賀隆行、岩根敦子、柳田敏雄「ミオシン V の ATP 加水分解の１分子計測」第 **43** 回日本生物物理学会、北海道(2005,10)

○<u>小森智貴</u>、西川宗、有賀隆行、岩根敦子、柳田敏雄「単頭ミオシン V の化学-力学反応カップリングの直接計測」理論と実験の研究会、広島(2007,10)

○<u>小森智貴</u>、西川宗、有賀隆行、岩根敦子、柳田敏雄「単頭ミオシン V の化学-力学反応カップリングの直接計測」第 **45** 回日本生物物理学会、横浜 (2007,12)

○<u>小森智貴</u>、西川宗、有賀隆行、岩根敦子、柳田敏雄「単頭ミオシン V の化学-力学反応カップリングの直接計測」分子情報生命科学シンポジウム 2008

○**T. Komori**, S. Nishikawa, T. Ariga, A. H. Iwane and T. Yanagida "Simultaneous measurement of nucleotide occupancy and mechanical displacement in myosin-V, a processive molecular motor" 第４６回日本生物物理学会, 福岡 (2008.12)

○T.Q.P. Noguchi, **T. Komori**, H. Ueno, T. Yanagida, K. Hirose and T.Q.P. Uyeda "Mutation at Gly 146 of actin causes class-specific motility defect of myosin." 第４６回日本生物物理学会, 福岡 (2008.12)